

UNIVERSITÀ
DEGLI STUDI
DI PADOVA

UNIVERSITA' DEGLI STUDI DI PADOVA

Dipartimento di Ingegneria Industriale DII

Corso di Laurea Magistrale in Ingegneria Aerospaziale

Designing and Optimization of Pressurizing Gas Diffusers in Cryogenic Methane Tanks: A Technical Approach

Relatore : Prof. Daniele Pavarin

Tutor Aziendale : Alessandro Mogavero

Deputy Tutor: Luca Anzidei

Studente con matricola

Riccardo Casara 2062921

Anno Accademico 2023/2024

"To give anything less than your best, is to sacrifice the gift"

Steve Prefontaine

Summary

In the thesis work reported here, a sizing process of a key component for the operation of the pressurization system of a cryogenic liquid propellant engine will be presented. The intended component is the gas injector or diffuser. An essential element for the distribution of pressurant in tanks, over the years, it has been subjected to other attempts aimed at better determining its operation while always remaining relegated to a secondary component and designed with the simple aim of functioning. In this work, however, we want to try to take a step further, in addition to understanding how it works, also to make its way through the countless variables that distinguish its work and trace a possible path for a sizing methodology, in particular of geometries.

The specific case presented here is the one applied to cryogenic engines for space applications, in particular, that of launchers, given the activity carried out as an internship by the author in AVIO S.p.A, a leading company in the launcher sector in Europe; an activity that has made it possible to develop the work presented here.

The work will present the use of cryogenic methane as a propellant and inert gas, He, as a pressurizer, a choice dictated by the increasing use of methane as a propellant alternative. At the same time, helium is currently the most common choice as a chemical species.

The methodology that will be represented here will consist of two parts, the first a preliminary sizing by code and then a subsequent development of a fluid dynamics analysis campaign with special software. The whole procedure will be explained in detail, and an example case will be shown step-by-step. At the end, a brief mention will be made of the optimization of geometries, with related analyses and conclusions.

The work presented here is only an introduction to a vast topic that will also be extremely intricate. The author has tried as much as possible to make everything linear and understandable, limiting himself to the case in question here. In addition, the limited time for the drafting of the paper and the means used limited the breadth of the procedure, which could be developed much more deeply, leading to the omission of some secondary parts. Despite this, the author has tried to make everything as exhaustive as possible.

As will be repeated later, this is not an endpoint but just the beginning.

Contents

1	Introduction	1
1.1	Thesis Objectives	1
1.1.1	Report of the activities	1
1.1.2	AVIO Spa	2
1.2	Background and Motivation	6
1.2.1	Why Improve Diffusers?	6
1.2.2	Why for the LCH4 engine?	8
1.3	Research Methodology	11
1.3.1	Define a Methodology for Diffuser Sizing	11
1.4	Processes in Liquid Propellant Tank ullage	13
1.5	Analytic Research	17
2	State of the art and literature review	35
2.1	Case Studies and Known Operational Regimes of Diffusers	35
2.1.1	Pressurization Systems	35
2.1.2	Diffusers	41
2.2	Existing Design Methods	51
2.2.1	Previous Studies	51
2.2.2	Reference to NASA Studies and test	52
2.2.3	Reference to CFD Studies	57
2.2.4	Thesis on Diffuser for High-Altitude Rockets	60
2.3	Identified Criticalities	63
3	Design Methodology	65
3.1	Description of the Proposed Method	65
3.1.1	Core-hours evaluation for fluid-dynamics analysis	66
3.1.2	Preliminary Code	69
3.1.3	CFD ANALYSIS	84

3.1.4	Post Processing	94
4	Sizing Example	99
4.1	Analyzed Cases	100
4.2	Calculations and Simulations	105
4.2.1	Python Code Interpretation	105
4.2.2	CFD Cases Used for Verification	111
5	Optimization	133
5.1	Objectives of optimization	133
5.1.1	Possible solutions	134
5.1.2	CFD Analysis	136
5.1.3	CFD Results	137
5.1.4	Post Processing	141
5.2	Conclusions	146
6	Conclusions	149
6.1	Resume of the activities	149
6.2	Results from the processes	150
6.2.1	CODE	150
6.2.2	CFD simulations-Axial vs Radial	151
6.2.3	CDF Analysis GRID vs RAD	152
6.3	insights for the reader	153
A	Detailed tables and graphs	155
B	Code	157
C	Studies	159
Bibliography		175
	Entry conditions in tank	

Chapter 1

Introduction

1.1 Thesis Objectives

The objectives of the present thesis are multiple. First, it introduces the work implemented during the AVIO Spa, Colleferro (RM), Italy internship. The work introduces the possibility of sizing a key pressurization system element, the pressurant gas injector, also known as the diffuser. The diffuser introduces the chemical species used in an LRE to pressurize the propellant tanks. The following section will present a pressurization system model and the injector/diffuser element in more depth. The activities reported here aim to first study and better understand the physics behind such a component in the motor and, with this knowledge, try to define a methodology to size and optimize the component. In the history of spaceflight, the diffuser has been under similar investigation for different and sometimes common purposes, such as saving pressurant mass and simplifying the geometries. The state of the art of this component, an exposition of the pressurization system and the description of past studies will be presented in Chapter 2. This work will show all the processes, from the diffuser concept to the optimization, for cryogenic propellant, using first a code simulation and then fluid dynamics analysis. Chapter 3 describes all the procedures step by step. In Chapter 4, a case study will be presented. This work was previously implemented for the technologies designed and developed in AVIO Spa. But for different reasons, and above all because the author desires to test the method in other contexts, it will be proposed again on different geometries. Chapter 5 and 6 will focus on discussing effective design optimisation and conclusions related to work.

1.1.1 Report of the activities

The six-month internship at AVIO Spa, during which the work presented here was developed, allowed the author to experience working in one of the largest space companies in the world,

develop new skills, and consolidate others. The activities carried out, always related to what is discussed in this thesis, began with a presentation by the company tutor and colleagues of the problem, **‘to develop a better knowledge of the diffuser, as an active element of the pressurisation system’**.

The first step was to collect all past studies relating precisely to the diffuser, focusing particularly on those that had conducted advanced analyses of system influencing factors. During this phase, over 50 papers related to the field, 10 related books, and 9 NASA documents were collected. For a summary of the studies and considerations drawn from this initial research, refer to Chapter 2. From these studies and books, it was possible to lay the foundations for all the work presented here, making this step, although quite challenging, absolutely essential.

A second step was to define the operational field in which to focus the sizing, identifying the pressurisation technology using inert gas and cryogenic propellants such as liquid oxygen and liquid methane as the best applicable conditions.

Once the problem was identified, gathered all the materials and defined the principal influence factors, the sizing processes began. The first version of the code was written, starting from the implementation of the pressurization. Several versions were developed, transforming the code from a few hundred lines and a handful of functions into a thousand lines for the main code alone and about ten functions.

The code’s development took almost four months, resulting in significant findings and initial conclusions on some geometries considered by AVIO Spa.

In the remaining months, models obtained from the code were analysed using more specific tools. An intense campaign of fluid dynamics analysis began, initially to verify that if the results were consistent with the next step. Subsequently, the diffuser’s performance was evaluated and optimized through considerations made with the company tutor.

The activities carried out during these months of internship allowed the author and the company figures who accompanied him to deepen their knowledge of gas injectors.

This knowledge will then be used by AVIO for the technologies under their development.

1.1.2 AVIO Spa

This section’s sole purpose is to introduce the reader to the company’s activities, quickly presenting its technologies and some quantitative data. All information has been gathered from public domain sources, including its website[1].

AVIO Spa is a renowned aerospace company specializing in designing, developing, and producing propulsion systems for space launch vehicles. With a rich history and a commitment to innovation, AVIO has established itself as a leader in the aerospace industry. The company’s expertise encompasses solid, liquid, and cryogenic propulsion, enabling it to provide compre-

hensive solutions for various space missions. AVIO's dedication to research and development ensures that it remains at the forefront of technological advancements, contributing to the success of numerous international space endeavours. Through strategic partnerships and a focus on sustainability, AVIO continues to drive progress in space exploration and transportation. For this reason, AVIO represents one of the most important realities in the European aerospace sector and one of the few capable of guaranteeing a launch service to orbit with some continuity. Today, AVIO is a leader in the aerospace and defence sector and has multiple products and several open projects.



(a) AVIO's logo

VEGA Vega is ESA's satellite launcher designed to deliver light payloads into low Earth orbit (LEO). It provides great flexibility at a reasonable cost. Vega has the capability to carry multiple payloads simultaneously into different orbits up to an altitude of 1,500 kilometers. The typical mission involves launching 1,500 kilograms into a circular polar orbit at 700 kilometers altitude. Vega is a four-stage rocket, primarily powered by solid propellant the P80 engine, Zefiro 23 and Zefiro 9). One last liquid stage, responsible for the orbital manoeuvre instead, is the AVUM (Attitude and Vernier Upper Module). The AVUM is a 2.45kN of thrust motor, using Asymmetric dimethylhydrazine (UDMH), and Dinitrogen tetroxide as an oxidizer.

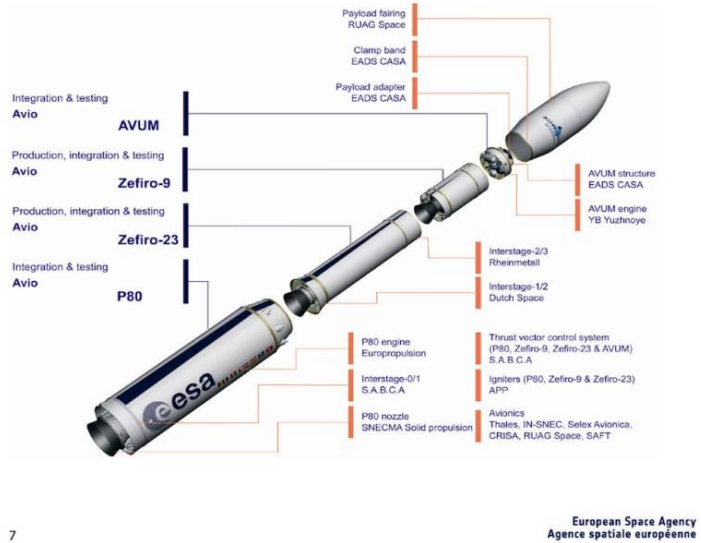
VEGA C The new Vega rocket configuration is called Vega C (Consolidation) and guarantees higher performance. The new launcher can carry up to 2,300 kg into low Earth orbit, a 60% increase compared to Vega.

Vega C fully exploits the capabilities of the new SSMS (Small Spacecraft Mission Service) payload adapter for transporting dozens of microsatellites into low Earth orbit. Moreover, it is the rocket chosen for the first launch of the European experimental space vehicle Space Rider.

The new Vega C will be more flexible and versatile than its predecessor. It is capable of carrying 90% of the low-Earth-orbit satellite market, compared to 50% for Vega. A substantial part of these can be launched using its capability to carry multiple payloads.



(a) VEGA launcher ready for the liftoff-credit for the figure [2]



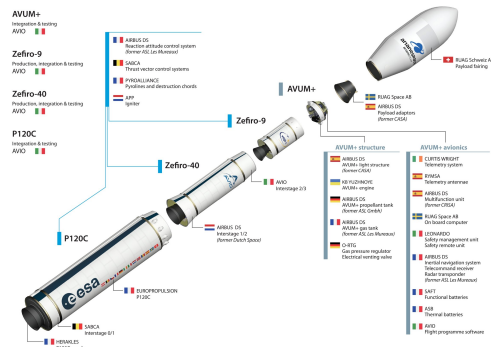
(b) VEGA SCHEME STAGES, figure from [3]

Figure 1.2: Comparison of VEGA launcher and its stages

The configuration of Vega C is based on that of Vega. In particular, like its predecessor, Vega C will have three stages with solid propellant, P120C, Zefiro 40 and Zefiro 9 engines and one stage with a liquid propellant engine, the AVUM+ and evolution of the predecessor[4].



(a) VEGA C during launch, from [4]



(b) VEGA C SCHEME STAGES, image from [5]

Figure 1.3: Comparison of VEGA launcher and its stages

VEGA E The future of the Vega program is Vega E (Evolution), a new launcher currently in development. Vega E will be the ideal product for light satellites with a low launch cost. The launcher will have a three-stage configuration instead of the four stages of previous versions. The first and second stages will be the P120C and Z40 developed for Vega C. The third stage will

feature a new engine, called M10, with a reduced environmental impact, using liquid oxygen and methane as propellants.

Unlike Vega and Vega C, Vega E will have a three-stage configuration. The first two stages, P120C and Zefiro 40, will be the same as Vega C. The last stage will be equipped with the new liquid oxygen and methane engine, currently in testing in its DM2 version[1]. The rocket will be able to deploy multiple satellites into different orbits in a single mission.

Development goals:

- Increased operational flexibility and versatility for the low Earth orbit market segment
- Use of new-generation low environmental impact propellants



Figure 1.4: Three VEGA at comparison, credit for the figure [6]

Space Rider But the focus of AVIO is not only the launchers market, also the new space vehicle and technologies. Avio is directly involved in the European Space Agency's Space Rider project. It is an unmanned reusable spacecraft operating in low Earth orbit to perform various missions. For about two months, Space Rider will be fully integrated with Vega C to provide a space laboratory operating in the space environment for a variety of applications[1].

- Payload: Up to 800 kg
- Payload bay: 1,200 liters
- IOD/IOV/Microgravity



Figure 1.5: Space rider render from [7]

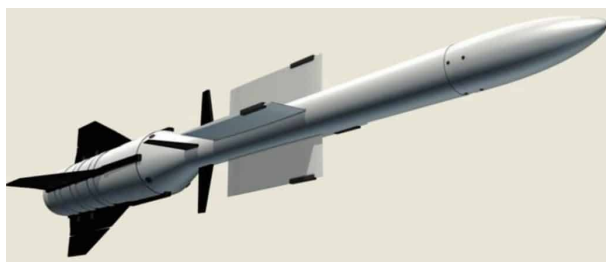


Figure 1.6: Aster-30 Sea Viper from [8]

Tactical/Military Tactical program is another sector for AVIO. The company is part of the joint program between Italy, France and the United Kingdom to produce the Aster 30, one of the best and most technologically advanced air defense missiles.

Avio collaborates with MBDA Italia to develop the CAMM-ER air defense missile, an extended-range variant of the CAMM surface-to-air missile[1].

There are also many other projects that a multi-sectoral entity such as AVIO is currently developing, testing, or even already on the markets.

1.2 Background and Motivation

1.2.1 Why Improve Diffusers?

The newfound interest in the space world and related technologies has led to the revitalization of the industry, with the emergence of new realities and the renewal of others, the so-called *new space economy*. Such new realities have also changed the paradigm by which space technologies were realized, seeking a very driven optimization of design drives, such as cost and schedule, but especially mass, to ensure a greater share of available payload. The optimization of a component such as the injectors is precisely at this juncture, the optimization of mass. Mass value is not directly related to the component itself but to the amount of helium used. Proper pressurizer distribution would save several kilograms of inert gas in quantity over an entire mission. A

smaller pressurizer also means smaller tanks, thus saving additional mass. This mass value depends relatively little on the operating conditions, mainly the start and end pressures[9]. The most significant influence is on the dynamics of the fluid and its use during the mission period. As reported by previous studies, comparing three injectors based on different physical principles (dissipator, diffuser injector and straight pipe) under fixed conditions and the same operating profile, the mass that is saved is 30% of the total mass of pressurant (figure 8-[10]). This value tends to decrease with the increase in tank time¹ for the cycle.

A further study underlines this mass saving, as reported in [11] the shape of the injector greatly affects the amount of mass for pressurization. In fact, in this study it is reported that in the pre-pressurization phase (pressurization phase on the ground) there is a saving of about 46% of mass by using a straight pipe rather than a diffuser injector; this decreases to 16.7% when the propellant is emptied. On the other hand, the choice of a straight pipe has limitations since the mass saving on the pressurizer translates into an increase in the mass used in the propellant. The mass savings, as will be reported later, mainly refer to the distribution of temperatures in the ullage, a distribution driven first of all by the geometry of the diffuser.

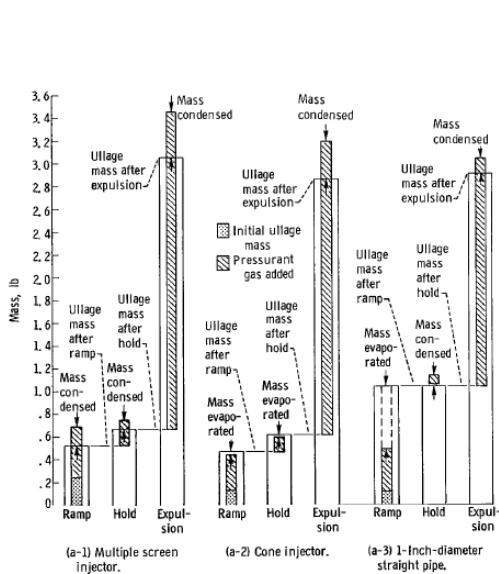


Figure 1.7: a) Tank Cycle 125s

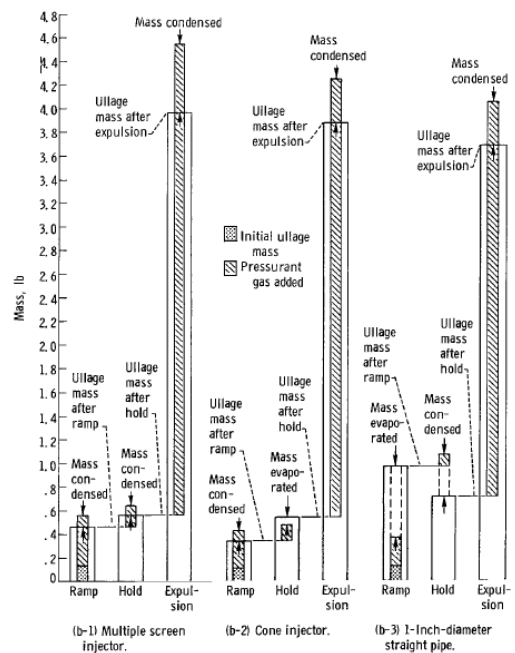


Figure 1.8: b) Tank Cycle 493s

Figure 1.9: Figure 8 pag 20[10]

In addition to mass savings, the diffuser is also the connecting element between the pressurization and propulsion systems. As seen above, pressurization is essential for the engine's

¹The tank time stands for the entire time necessary for the insertion of the pressurant, the pressurization hold and the expulsion time

proper functioning; it must guarantee a constant pressure level without fluctuations throughout the operating period, especially in the propellant escape phase. Therefore, in its modelling, it must be able to guarantee a flow that allows a certain degree of uniformity of the output velocities, an element to which a good degree of attention will be paid, especially in the CFD simulation phase. Therefore, the optimization of the pressurizer distribution becomes an important factor in the design of the component, especially during the ejection phase. This detail is then important in the final phase of emptying, the most expensive moment for the pressurizer, which enters a tank that is now emptied, in contact with most of the walls and the pressure level guaranteed only by the gas injected since the propellant column is now minimal. Based on the pressurization methodology, the final phase of emptying remains the most expensive phase, the one to which the pressurization system usually responds by often inserting more mass than necessary. In fact, as reported in the article [12] the pressure in the tanks undergoes a slight decline at the beginning, to drop linearly in the second phase to reduce drastically at the end. Optimization also involves studying the best approach to understanding the dynamics of the cryogenic fluids. their coexistence and the influence of one on the other. In particular, in this text we will deal with pressurization for LCH₄ reservoirs with more attention, for the main reason of want to add a degree of better understanding of the behaviour of this chemical species. This species is now receiving new attention thanks to some private companies that see in the use of LCH₄ an excellent compromise between LH₂, extremely efficient but not very handy, and RP-1, with a lot of literature, easily usable, but not very sustainable. LCH₄, as a propellant, has a much smaller number of studies than those for LH₂/LOX/hydrocarbon-based propellants. As reported in the study [13] where all the pressurization tests have been collected, about 80 tests have been reported in previous studies. Of these 80, over 50 were on hydrogen, and only 7 were about methane, a number which further decreased considering the use of Helium as a pressurant like the case reported here. This understanding is then translated into technical manufacturing knowledge useful for all the instrumentation necessary for the correct operation with this propellant, thus allowing the growth of technical notions. Therefore, a secondary effect of studying the sizing and optimization of a diffuser is to better deepen the knowledge of the use of this propellant.

1.2.2 Why for the LCH₄ engine?

As mentioned above, LCH₄ is becoming an important alternative in the world of bipropellant liquid propulsion compared to the more classic hydrogen (LH₂) and kerosene (RP-1), but knowledge of its behaviour in the cryogenic state is much more limited. Relatively abundant and low-cost hydrocarbon, if coupled with liquid oxygen (LOX), it has performance in terms of characteristic speed and Isp that are lower than LOX-LH₂, but compared to LH₂, presenting

clear advantages in management and transport since storage takes place at about -160°C unlike the -253°C required by LH2. In addition, LCH4 reservoirs are much smaller thanks to a density 6 times that of LH2 ($420 - 450\text{kg}/\text{m}^3$ at ambient pressure compared to $70\text{kg}/\text{m}^3$ for LH2), making it a propellant with a higher volumetric energy density. Compared to the LOX-RP-1 pair, it has less polluting emissions and superior performance, but in terms of volumetric energy density, RP-1 is better. In summary, therefore, the properties of this cryogenic propellant are positioned in an intermediate way between the two pairs. Some more specific and unique advantages, which have made it even more interesting for the new space economy, is the possibility of use in future missions to Mars, given the chance of production in, through water obtained from ice and carbon dioxide present in the Martian atmosphere.

Oxidizer (K)	Fuel (m/sec)	Temp. CC (kg/mol)	Chamber c^* (sec)	M (sec)	Shifting Is (sec)	Frozen Is (sec)	k
LOX	LCH4	3526	1835	20.3	-	296	1.20
			1853	-	311	-	-
LOX	RP-1	3571	1774	21.9	300	285.4	1.24
			1800	23.3	-	-	-
LOX	LH2	2959	2428	8.9	-	386	1.26
			2432	10.0	389.5	-	-

Table 1.1: Theoretical Chamber Performance of Liquid Rocket Propellant Combinations- Extracted from Table 5-5 pag 180[14]

Combustion chamber pressure—1000 psia ($6895\text{ kN}/\text{m}^2$); nozzle exit pressure—14.7 psia (1 atm); optimum expansion.

Adiabatic combustion and isentropic expansion of ideal gases.

The specific gravity at the boiling point has been used for those oxidizers or fuels that boil below 20°C at 1 atm pressure, see Eq. 7-1.

As reported in a study[15] Methane can be produced through well-understood processes such as natural gas reforming or carbon dioxide methanation, which can be applied in situ on Mars using local resources. This makes it a more sustainable option for long-term missions.

The technology related to the use of methane, in particular in combination with oxygen (MethaLox), to date has been used in flight by only 4 technologies:

- **Zhuque-2 (LandSpace-China):** first rocket to reach orbit with Metha-LOX engines in 2023. The engines, TQ-12, are gas-generator open-loop thrusters and were the first Chinese engines to be entirely privately developed.
- **Starship (SpaceX-USA):** SpaceX's Starship launch system, consisting of the Super Heavy rocket and the Starship shuttle, will use methane-oxygen Raptor engines. Starship carried out its first suborbital flight tests in 2022 and 2023. The Raptors are the most powerful LPREs in

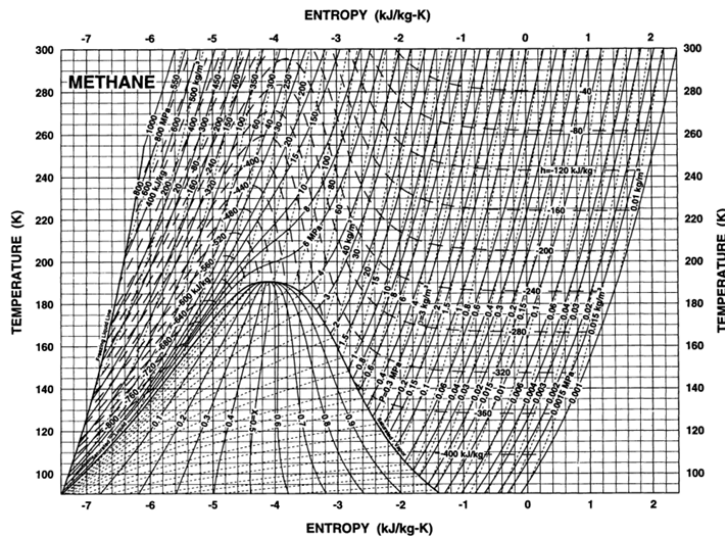


Figure 1.10: T-S diagram for methane (T= 90-300 K) -From page 201 Figure 5.23[16]

history, designed for precise use for space missions. They can achieve, to date (version 3)², 2.53 MN of thrust and a specific impulse of 380 s.

- **Terran 1 (Relativity Space-USA):** The Terran 1 rocket from the American startup Relativity Space, despite the failure in its first launch in 2022, is designed to use methane-oxygen engines, the AEON-R. The main peculiarity of these launchers and engines is the realization, which takes place by 3D printing.
- **Vulcan (Blue Origin-USA):** A rocket from the United Launch Alliance (ULA) uses Blue Origin's BE-4 engines to replace the Russian RD-180 engines previously used on the Atlas rockets. The engine, the first methane-oxygen completely developed by private individuals, currently has flown in the Vulcan rocket's first stage but will then be used for Blue Origin's new technology, the New Glenn.

In addition to these 4, two other engines under development use methane as a fuel, both from two European companies:

- **Ariane Next (ArianeGroup-Europe):** The European ArianeGroup is developing the Prometheus engine, a methane-oxygen engine, for the future Ariane Next rocket, scheduled for launch in 2030[17].
- **Vega E (Avio-Europe):** The European Vega E launcher, under development by Avio, will use a methane-oxygen engine called M10 scheduled for the first launch in 2026, and for the future a new version, the M60[18]

²At the date of writing this work, 2024



Figure 1.11: TQ-12 Engine[19]



Figure 1.12: Raptor Engine V2[20]



Figure 1.13: Aeon-R Engine [21]



Figure 1.14: BE-4 Engine [22]

arianeGROUP



Figure 1.15: Prometheus Engine[23]



Figure 1.16: M60-Engine [18]

1.3 Research Methodology

1.3.1 Define a Methodology for Diffuser Sizing

In the work proposed here, the methodology for the subsequent sizing and optimization will follow a procedure in successive steps by using tools such as the creation of Python[®] 0D code and subsequent fluid dynamics simulations using special software such as Ansys Fluent[®]. This is due to the large number of variables in the field, as will be seen in Chapter 3, which will be pre-

sented and which have an effect on the introduction of pressurizing. The countless unknowns of the case also make it necessary to study the importance of the phenomena inside the tank when the pressurization system is activated, whether it occurs in the pre-flight phase, therefore in the so-called on-ground (ONG) pressurization. Or when you have engines start. This last situation, as we will see, further increases the degree of complexity of the system itself. Since physical discharge tests cannot be performed, a simplified model and then a fluid dynamics analysis are necessary to give greater validity to both methods. The analyses that will be carried out will always involve certain simplifications. This is because fluid dynamics is a complex and relatively unexplored field, for which we have limited tools. Second, precisely because of the limited tools and time available for this kind of work, despite this, it still wants to be a technical study, useful more for business than for research. Third, to keep this paper's length congruent with its purpose, focusing on the main factors and data. It should also be noted that the models used in this paper are the composition and elaboration of other similar and previous studies, mainly for the code that will be used in the first-degree sizing, which makes use of part of knowledge taken from other studies that before today have tried to address the problem of the search for the optimal in pressurization. Still, on the other hand, it presents the implementation of the method, in this case, the author's work. The goal is also to obtain a complete and general work, a link between all the studies, so that once the most important parameters of the pressurization system have been defined, it can be used quickly to obtain the reference dimensions of the diffuser itself. The first step is represented by the 0D model of an on-ground pressurization (ONG) of the tank. Usually, this operation begins some minutes before the engine ignition phase, constantly monitoring the press up to T-0 and beyond; this operation is carried out for all stages of the launcher but at different times. In this first phase, therefore, ONG pressurization is simulated, by inserting the pressurizer from the diffuser, implementing the dynamics of entry into the tank and simulating the main phenomena that occur in the tank itself. To determine the value of the heat fluxes and the dimensionless numbers (Richardson, Reynolds, Stanton, Nusselt, etc.) that characterize the local phenomena and the chemical species that intervene. Interactions occur between specific points in the tank, exchanges are stationary and minor flows, such as conductive exchange through tank walls, are omitted. All this for a whole series of tank inlet sizes, and in parallel between the two most general configurations, that of axial injector (AX) and that of radial injector (RAD). The aim is to relate the heat flows that the pressurizer dissipates towards the fuel and the tank wall with the inlet dynamics, which are different for one or the other configuration. All this is through an efficiency relationship, which will therefore allow to obtain which geometry, with the same area, then has a better efficiency. Conversely, it is possible to obtain the minimum exit section that guarantees a certain level of efficiency for both configurations. The following step is carried out by fluid dynamic analysis with the FLUENT[®] software,

the aim is to verify the solidity of the code, through a transient simulation of the pressurization of the ullage only with inlet sections obtained previously. Also, in this case, the heat fluxes that the pressurizer loses are evaluated, as well as the temperature distribution. Therefore, only the areas of ullage are analyzed, considering the liquid as a simple exchange wall. This is followed by a post-processing phase to evaluate and confirm which of the two configurations is optimal. Once the size and configuration have been chosen, we move on to the detailed design of the same, looking for an optimization, again through this case, of the fluid dynamics simulations. The search for optimum, as will be seen later, will be based on modelling the geometry so that a distribution of speeds at the exit of the diffuser will be as uniform as possible while minimizing pressure drops. At the end, it is then necessary to carry out a subsequent fluid dynamic evaluation of the tank emptying, to verify the pressure profile during ignition.

Time (T-x)	Azione
T-13:00:00	RP-1 in S-I tank level check
T-09:00	Tanks purging with GN2
T-08:57:00	S-IC LOX tank Purge
T-08:34:00	S-II LOX Prepressurization S-II LH2 tank purge
T-07:42:00	Preconditioning S-II tank S-IVB LOX tank purge
T-07:31:00	S-IVB LH2 tank purge
T-07:28:00	S-IVB LOX Precool Fast Fill (5-96%), Slow Fill (96-99%)
T-07:04:00	S-II LOX Precool Fast Fill (5-40%) Fat Fill (40-96%) Slow Fill (96-99%)
T-06:30:00	Pre-cooling S-IC LOX
T-04:54:00	S-IVB LH2 Precool Fast Fill (5-98%), Slow Fill (96-100%)
T-04:11:00	S-IVB LH2 Precool Fast Fill (5-98%), Slow Fill (98-100%)
T \approx 04:00:00	S-I LOX tank pressurization with helium
T-01:00:00	S-IVB start GHe pressurization
T-00:34:30	S-IVB engine pressurization
T-00:03:07	S-II LOX pressurization
T-00:02:47	S-IVB LOX pressurization
T-00:01:37	S-IC RP1 pressurization S-II LH2 pressurization S-IVB LH2 pressurization
T-00:01:12	S-IC LOX pressurization

(a)

Time	Event
T-10:00:00	Falcon 9 to Vertical
T-08:30:00	Countdown Initiation
T-04:50:00	Precool for Propellant Loading
T-04:37:00	GO for Loading
T-04:20:00	Propellant 1 Loading
T-04:00:00	LOX Systems Setup
T-03:45:00	LOX Loading
T-01:30:00	LOX Replenish
T-00:30:00	Final LOX Topping
T-00:09:30	First Stage Merlin Engine Chilldown
T-00:07:30	Go/No Go for Launch
T-00:05:55	Pressurization for Strongback Retract
T-00:05:30	Strongback Cradles Opening
T-00:03:30	Strongback Retraction complete
T-00:03:00	LOX Topping Termination
T-00:02:45	Fuel Trim Valve to Flight Position
T-00:02:20	Propellant Tank Pre-Press
T-00:01:30	Final Engine Chilldown
T-00:01:00	Flight Computer to start-up
T-00:00:40	First Stage to Flight Pressure
T-00:00:20	All Tanks at Flight Pressure
T-00:00:03	Merlin Engine Ignition
T-00:00:00	LIFTOFF

(b)

Table 1.2: Some of the most important countdown events for NASA: Saturno V (a) from table 8-20 pag. 8-24 [24] and for SpaceX: Falcon 9 (b) from [25]

1.4 Processes in Liquid Propellant Tank ullage

Before defining and presenting the method for the design and sizing of the diffuser, it is necessary to explain the phenomena realized inside the LPRE tank. In fact, in this case, the phenomena

that are going to take place are very complex due to multiple factors, such as the paths of the gas particles, the exchanges of heat and mass by the gases at high temperatures with the propellant that could boil (for fuels such as UDMH, kerosene, NT) and evaporate (oxygen, hydrogen, methane), not considering the interaction between the vapour in the ullage and the propellant gases. Here, the different phenomena that are involved in pressurization methods are presented:

Pressurization The main phenomenon is characterized by the inflow of gas in a closed volume and depends on several factors, such as the shape and size of the diffuser, the output dynamics of the pressurizer and propellant, the operating conditions of both temperature and pressure, and the Archimedean forces caused by the significant differences in density between pressurizer and propellant.

Heat exchange between pressurizer and tank wall One of the main dissipative phenomena depends on the pressurizer inlet path, speed and temperature. In addition, the heat exchanges that are most present are those of the convective type and can range from forced to free. The first form occurs when the introduced flows have a high velocity, temperature and turbulence coefficient. On the other hand, free convective flows arise when dealing with flows at a much more limited and contained temperature and velocity. The predominance of one over the other also determines how the co-presence of gases in the ullage is achieved.

Evaporation of propellant The evaporation of propellant occurs in the presence of cryogenic propellant when it is placed in a closed volume due to the high volatility capacity of the elements in the cryogenic state. The introduction of inert gas further helps this behaviour. Evaporation is carried out using bubbles that form at the bottom of the tank and then rise to the surface, increasing the pressure in the ullage.

Under normal storage conditions in a tank, as reported in [26], the evaporation of cryogenic propellants can occur in several ways; the four main ones are:

1. Evaporation, uneven, from the surface
2. Steam explosion: due to a high surface evaporation in a transitory phase given by the bubbles that rise from the bottom of the tank.
3. Rollover: due to a continuous overturning due to the flows given by the buoyancy forces that bring heated liquid in contact with the walls to the interface area.
4. Boiling: from the central zone of liquid by homogeneous and non-homogeneous nucleation.

Also, in [26], evaporation is described as a complicated phenomenon that can be schematized in three different regions, starting from the interface with the vapour area and gradually moving away. The various evaporation phenomena converge on the free surface of the propellant, included in a layer of 1-2 μm , followed by an area where conduction is the master, with a thickness of 400 μm , characterized by a high-temperature gradient, and still below the intermittent convective recirculation zone, with a thickness that can range from 5000 μm to 5 mm with a lower thermal gradient.

Thermal stratification in the tank and circulation The arrangement of temperatures between the liquid and the upper dome of the tank also dictates the heat exchange inside the ullage. In a stationary configuration, the natural convection of the fuel in the vapour phase favours temperature stratification. On the other hand, when the pressurization system is activated to maintain a certain pressure level, the pressurizer flows mix the chemical species present, leading to greater uniformity of temperatures inside the ullage.

The propellants undergo thermal flows from the outside, even if only in preparation for launch. Through the walls, free convective flows are created and transferred to the surface of the fluid, helping to raise the total temperature in the tank and contributing to stratification.

Thermal stratification and its effect on the ullage of a cryogenic tank is presented in [12], where it is concluded that thermal stratification causes heat transfer from the ullage to the liquid generating condensation in the ullage and a gradual increase in the temperature of the liquid. Stratification, therefore, affects the temperature distribution and stability of the tank's thermal system, thus influencing the overall pressurization dynamics.

Conduction between the species present in the ullage and the propellant surface remains a phenomenon limited to the phase before the activation of the pressurization system and the one after its shutdown. In the analyses reported here, it will be used only as a starting condition, but the convective flows realized by the introduction of the pressurizer will be of greatest interest during the development phase of this study.

Condensation Fallout of propellant that has evaporated, in case the temperature is lowered below the vapor threshold, can also occur in the form of a liquid thin film right on the surface of the propellant.

Chemical reactions Reactions that can lead to a change in the composition of the gas in the ullage, with the reactions that can take place between propellant and pressurizing gas. This phenomenon is limited to systems characterized by a gas-generator cycle with pressurization of the tanks with the gas-generator discharge. Only inert gases will be considered in this study.

Tank emptying The propellant discharge is carried out using an outlet flow rate necessary for the operation of the motors, depending on various factors, such as the difference in pressures between the tank and the nozzle, the temperature of the propellant, the geometry of the tank and the total resistance that all piping and valve systems can create. The expulsion of the propellant lowers the tank pressure, affecting the stability of the flow itself, up to cavitation phenomena. Outflow remains one of the most challenging situations for the pressurization system and simultaneously the most difficult to simulate. The tank can be emptied constantly, the typical situation for a first and second stage of a launcher; in fact, the liquid level drops at a controlled rate to avoid unwanted fluctuations. On the other hand, emptying takes place more variably for third stages, kick stages or landers. Alternating between small corrections and long manoeuvres requires activations with interval times, and consequently, the liquid level lowers less linearly, thus creating situations of possible disturbances and oscillations. An example of this is NASA's Morpheus lander presented in [27], powered by oxygen and methane, pressurized by cryogenic helium but subsequently heated; it was tested with a wide thrust range (5:1 throttleable ratio) generating ever-changing emptying profiles and consequently requiring the pressurization system to have ample capacity for adaptation.

Buoyancy forces The thermal gradient within the liquid creates areas where the difference in density causes the hot fluid to move upwards, while the cold fluid moves downwards. Thus creating a stratification condition in the propellant as well, very similar to that described in the previous points. Some external phenomena take part and affect the correct pressurization, such as:

Thermal environment

During the ascent phase for a spacecraft, there is a reduction in both the pressure and the density of the air; as the height increases, this leads to very important thermal flows:

Aerodynamic heating The primary source of heat flows during ascent into the atmosphere passes through the layers of insulation of the tank and the walls. As concluded in [12], this heat flow is the main one influencing the pressure in the tank.

Space radiation Composed of four components that, once the Kármán line is crossed, take the place of the main heat flow. The components, as presented in [12], are:

1. Solar incident radiation:

$$q_1 = \phi_1 \cdot S \cdot \frac{A_{tp}}{A_t}$$

$$\phi_1 = \cos \beta_s$$

2. Albedo radiation:

$$\varphi_2 = \begin{cases} k^2 \cos \beta, & \text{if } 0 \leq \beta \leq \arccos k, \\ k^2 \cos \beta + \frac{1}{\pi} \left\{ \frac{\pi}{2} - (1 - k^2)^{1/2} (k^2 - \cos^2 \beta)^{1/2} - \arcsin \left[\frac{(k^2 - 1)^{1/2}}{\sin \beta} \right] - k^2 \cos \beta \cdot \arccos \left[\frac{(1 - k^2)^{1/2}}{k \tan \beta} \right] \right\}, & \text{if } \arccos k < \beta < (\pi - \arccos k), \\ 0, & \text{if } (\pi - \arccos k) \leq \beta \leq \pi \end{cases}$$

3. Infrared earth radiation:

$$q_3 = \phi_3 \left[\frac{(1 - \rho)}{4} \right] \frac{SA_{tp}}{A_t}$$

$$\phi_3 = \phi_2 \cos \psi$$

4. Deep space infrared:

$$q_n = \alpha q_{k(t)} - q_r = \alpha q_{k(t)} - \epsilon \sigma (T_w^4 - T_e^4)$$

These four components together, however, do not generate obvious changes in the operating conditions of the tank in terms of pressure [12]; in fact, their overall impact is mitigated by the rapid loss of heat through the drainage of the liquid.

Sloshing This can lead to uncontrolled depressurizations in the tank. The oscillations of the liquid, in fact, as reported in [28], can cause rapid pressure drops inside the tank until the cavitation condition is achieved. The oscillations attached to sloshing, in fact, create disturbances in the interface area between liquid and vapour that shift its position (creating a sloshing angle), increasing the contact surface between the two regions. These oscillations lead to a cooling of the ullage and relative pressure reduction. The study shows that adequate pressurization limits the negative effects of sloshing.

1.5 Analytic Research

Factores of Influences of Pressurization System

After seeing the multitude of phenomena involving the pressurization of a cryogenic tank, it is, therefore, necessary to focus on the main variables that influence the operation of the pressurization system, particularly the introduction of the pressurizer through the injector. In this section, all the variables involved will be briefly presented, and the previous studies on which this study was based will be recalled to show the complexity of the pressurization process. For each variable, how it is treated in the current study will be briefly reported and if it is considered.

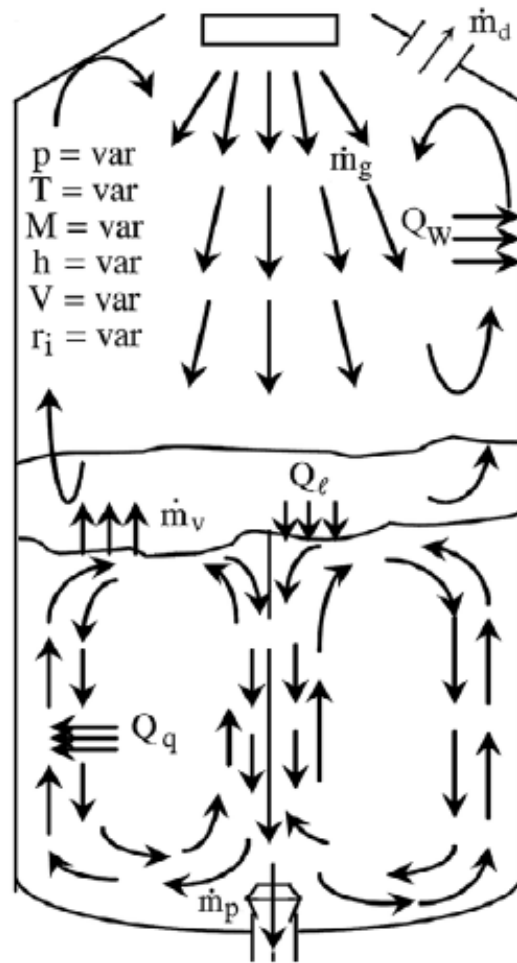


Figure 1.17: Schematic of a tank with aerothermal phenomena[29]

Pressurizing gas conditions:

Pressurant Temperature: The temperature of the incoming gas is the main factor, especially concerning the temperature of the liquid. The value of the temperature of the inlet gas is reported in several studies; the goal is to pressurize the ullage, and the level of pressurization strongly depends on the inlet temperature of the chemical species, so solutions involving the use of heated gases have been evaluated as in [30] in which the impact of helium at 600K in the distribution of energies was studied, which will be discussed below. The higher pressurizing temperature, the study reports, obviously improves pressurization capabilities but, at the same time, significantly increases the intensity of heat exchanges, relegating the share of valuable energy for pressurization to only 22-24%. Therefore, a future process of optimization of the injector geometry is necessary to increase this altitude, an activity carried out within the paper. Other studies [31] have instead carried out tests on the use of pressurizer, first stored at cryogenic temperatures

(-184°C) and then brought into contact with heat exchangers placed on the nozzle to heat it up to about 2°C and then introduced into cryogenic tanks. In this case, the study concludes that helium at room temperature offers advantages in terms of efficiency, weight savings (up to 130kg) and performance stability. The study indicates, in the end, that the main control variables for future improvements of the system will be:

- Minimize helium storage temperature.
- Maximize the heat capacity of the pressurization system.
- Design effective diffusers to minimize pressurizer energy loss.



(a) Integrated helium system



(b) Steady state of heat exchanger

Figure 1.18: Figure 7 -(a) and 10 (b) from [31]

These findings further underscore the crucial role of temperatures and the geometry of the diffuser in the pressurization process. Another study, [32], confirms these conclusions; also, in this case, the helium is kept in cryogenic conditions in the tanks at very low temperatures (-150°C) and then passed through a heat exchanger and introduced into the tank with room temperatures. This strategy, concludes the study, improves operational efficiency and reduces hardware complexity, but thermal interaction with cryogenic propellant can reduce overall system efficiency. The tests, the study continues, showed that the temperature of the inlet gas is crucial to determine the collapse factor³, and, therefore, the efficiency of the pressurization system. The results suggest that accurate control of the inlet gas temperature is essential to optimize the performance of pressurization systems. In the models reported in this study, the pressurizer temperature (T_{press}) reflects this importance and is directly related to the dynamics of the flow

³Coefficient that is presented later in this work and represents the difference between the effective mass of helium used for pressurization and the calculated mass

itself. The temperature of the pressurant is often linked to the liquid temperature value of the propellant, according to the definition:

$$\theta = \frac{T_{\text{press}}}{T_l} \quad (1.1)$$

This value is then used precisely in the determination of dimensionless velocities

$$u_m = \frac{U_{\text{press}}}{U_{\text{press_entry}}} \quad (1.2)$$

with U_{press} the local velocity of the liquid while $U_{\text{press_entry}}$ the velocity at the inlet of the pressurizer. In fact, according to the reports (9-57)-(9-58) of [29]:

$$u_{m1} = \frac{1.0226 - 0.0618\theta}{0.0805(\bar{x} - \bar{x}_{\text{entr}})\sqrt{\theta} + 1.0226 - 0.0618\theta}, \quad (1.3)$$

$$u_{m2} = \sqrt{\frac{0.9966 - 0.0087\theta}{0.0695(\bar{x} - \bar{x}_{\text{entr}})\theta + 0.9966 - 0.0087\theta}}, \quad (1.4)$$

where $(\bar{x} - \bar{x}_{\text{entr}})$ represents the distance of the entry point to the evaluation point in the axial direction to the tank. These two relationships are the same ones that are used and implemented in Python code for the determination of heat flows. As reported in [29], the increase of the temperature of the pressurant raises both the pressure and the temperature in the ullage, helping the pressurization processes. For example, an increase of 30% of the mean tank pressure can be achieved by an increase of 10% of temperature. On the other hand, the pressurant temperature growth can increase the amount of heat dissipated. At this point, the study concludes, the diffuser should be designed to mix the gas in the ullage as much as possible.

Pressurant direction: The direction of intake, as presented above, in the direction of the free surface propellant can generate significant evaporation, which, in a certain amount, helps the pressurization process. It is not always the best strategy because evaporation limits are often introduced in the propellant as a mission requirement; therefore, those who use this methodology usually have to verify that they can stay within the evaporation budget. To ensure limited mixing to preserve stratification, the introduction towards the tank walls or even in reverse configuration can represent a valid alternative; all possible configurations have been explained above. This study will implement the two dynamics by exploiting the analytical relationships in chapter 9 of [29].

The different dynamics are the central pivot of this study; in fact, the comparison between the axial and radial configurations shown in the table above underlines the empirical character with which they were obtained. The determination of l_s thickness, rather than l_k , therefore, rep-

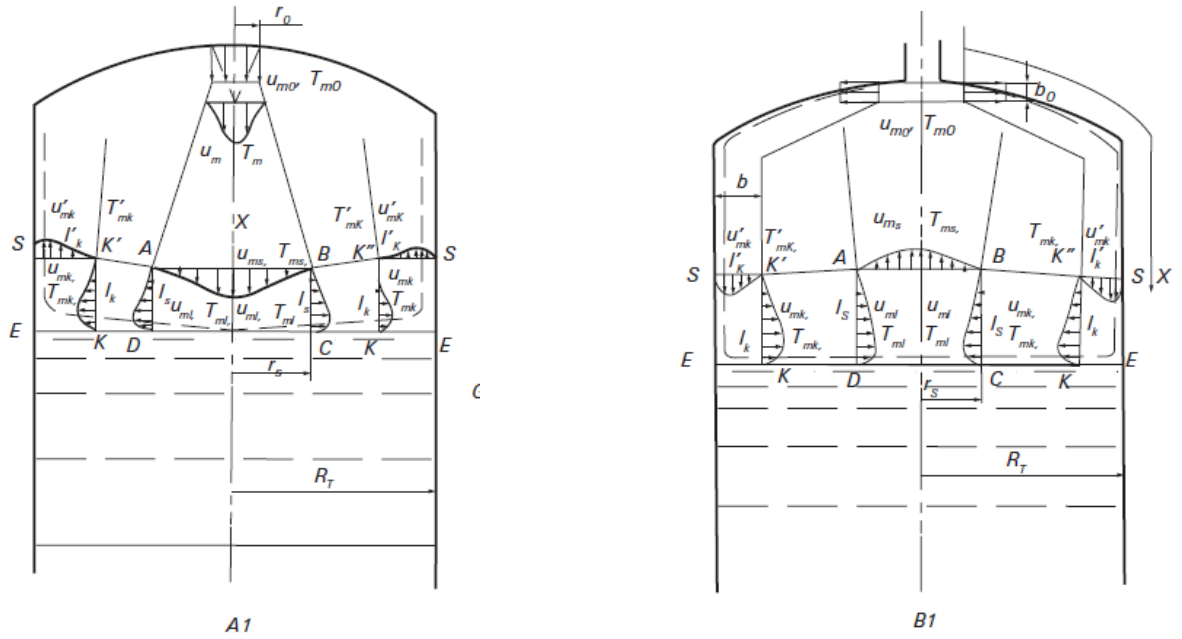


Figure 1.19: Scheme of the tank with the injection(left) and injection (right) -from figure 9-5 [29]

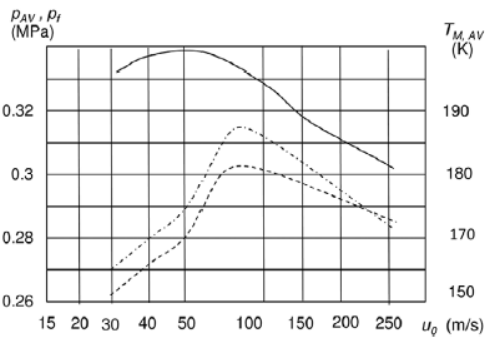
resents one of the main points for the beginning of the study presented here. The dimensionless velocities presented above will, in fact, be used for the local calculation of the velocity at that point and, therefore, will be useful for heat exchange. Meanwhile, the lengths l_s , l_k , and l'_k , which represent the thickness of the local flows, will be handy when evaluating dimensionless numbers.

Local Velocity	$u_{m2} = \sqrt{\frac{0.9966 - 0.0087\theta}{0.0695(\bar{x} - \bar{x}_{entr})\theta + 0.9966 - 0.0087\theta}}$	$u_{m1} = \frac{1.0226 - 0.0618\theta}{0.0805(\bar{x} - \bar{x}_{entr})\sqrt{\theta} + 1.0226 - 0.0618\theta}$
Local Dimension	$r_s = 0.8042 \cdot R_T, l_s = l_s \frac{2 \cdot r_s}{7}$	$l_s = \frac{f(\alpha) \cdot 2 \cdot r_s}{7}, l_k = \frac{l'_k (R_T - 0.2857 l'_k)}{R_T - l'_k}$

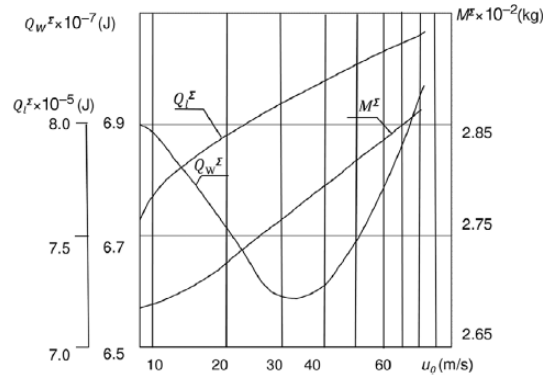
Table 1.3: Table of local velocities and local dimensions - Relations from [29]

Inlet speed: The speed of the pressurant is linked to the inlet section and the pressurizing flow rate and will characterize the nature of the phenomena that will take place inside the tank itself. The velocity of the flow will, in fact, first influence the character of the thermal flows; determining whether free or forced convection will be more important. The outgoing flow will also define the regime of the flow itself, laminar or turbulent. As reported in "Kinematic Combustion", the injection rate is important in maximizing cryogenic propellants' average and final pressure in the pressurization process. This speed minimizes the amount of heat lost on walls and propellant. For lower speed values, there is a tendency to stratify the ullage with consequent

overheating; at higher speeds, however, forced convective phenomena intensify excessively. These studies have been carried out for oxygen and nitrogen; no studies are related to cryogenic methane, although the same principle may apply. In this study, the optimal velocity will not be directly determined, but using the flow rate defined by the case study, comparing different possible geometries and outlet dimensions of the pressurizer, the configuration for which there is less dispersion to the walls will be determined. By managing, in the initial code, the pressurizing gas is incompressible.



(a) Variation of time-averaged pressures (solid line) and final pressures (dotted line) and mass-averaged final temperatures (dot-and-dash line) at oxygen tank pressurization by helium.



(b) Variation of heat for the heating up the tank walls Q_W^Σ , and consumed for the heating up of propellant Q_f^Σ , and total mass of the evaporated propellant M^Σ at pressurization of tank with oxygen

Figure 1.20: Figure 9-21 and 9-23 from Cap.9 [29]

- **Chemical species:** The chemical species used represents another essential element; as discussed above, the possibility of using one pressurization methodology rather than another, with attached chemical species, determines the presence or absence of some phenomena that participate in the total balance in the ullage. To understand the importance of the pressurizing element, for example, consider the possibility of replacing the gas, while keeping its operating parameters constant. This hypothesis can be applied only to systems that use evaporated or stored gas. Such a level of modification requires a complex degree of analysis and considering the different thermodynamic models that characterize each species. To carry out this change, one of the main conditions, as reported in [29], is that the volumetric flows for different gases are equal.

$$\frac{\dot{m}_x}{\rho_x} = \frac{\dot{m}_y}{\rho_y}$$

Using equations of state, it becomes:

$$\frac{\dot{m}_x}{\dot{m}_y} = \frac{\mu_x}{\mu_y} = \eta_{\text{ideal}}$$

This condition often does not occur due to the different thermodynamic properties, leading to values of η_{ideal} different from the values η_{real} , thus requiring changes to the operating conditions and to the system itself.

Propellant Conditions

Propellant temperature and specie: The condition of the fuels is another factor influencing heat exchanges and fluxes with walls and pressurizing chemical species. In the typical phase of sizing or optimizing a component such as a diffuser, the propellants and their conditions are already defined, together with the pressurization system. This study is based on and applicable to cryogenic propellants. No tests with storable fuels have been carried out for this methodology, but in principle, there should be no problems; as will be seen below, the methodology is very flexible, allowing a switch only with a modification of the chemical species involved. The type of chemical species used affect different aspect on the designing of pressurization system, like the type of the pressurant. For storable propellants (RP-1, nitric tetroxide, Asymmetric Dimethylhydrazine), reference made to specific studies, such as [33] in which the comparison is made between different pressurization technologies, such as stored gas or gas generated for storable propellants, by pressurizing agents such as helium, nitrogen or neon. Again, it is concluded that helium is the best pressurizer, given its low molecular mass and chemical incompatibility.

Tank operating pressure: Tank pressure levels determine the threshold to which the condition must be brought for the propellant to operate. A higher threshold means a greater quantity of pressurizer or longer times required for pressurization with the same propellant temperature. Operating pressure remains a constraint related to the design of the tanks and the chemical species used.

Net Positive Suction Head - NPSH: The threshold level must not be reached to avoid cavitation phenomena at the entrance of the turbopumps. Depending on other factors, such as the size of the tank, a larger propellant column allows a lower NPSH, the temperature and density of the liquid, and the pressure drop present downstream from the tank emptying system. As an influencing factor, this threshold level depends on and can be assessed using a series of simulations that require the tank to be empty entirely, increasing its complexity.

Internal and external heat flows

The heat flows that intervene in ullage are among the main factors that influence the operation and distribution of the pressurizer, among the phenomena underlined above, both of a dissipative nature such as the heat lost to the wall or to the propellant, but also for the external flows to the tank. The temperature of the liquid and ullage is essential in determining the operating

conditions of the pressurization system; their modification due to unexpected flows can cause major changes to the system's operation. The ullage can be seen as a closed system, with only one inlet flow rate (when the ON pressurization condition is achieved). The system, from first at rest with a certain level of energy, undergoes the entry of a flow rate of a chemical species; this raises the system's energy level by carrying out pressurization. However, contact with cryogenic liquid and with the walls, which in any case remain at a much lower temperature than the incoming gas, removes energy in the form of a thermal flow, cooling it and lowering the total temperature of the ullage. Thus requiring a new pressurizer. Writing the balance of the ullage, we can see that:

$$\underbrace{\int_2^3 \delta m_a h_a}_{\text{Enthalpy input by pressurant gas}} - \underbrace{\int_2^3 \delta m_T h_T}_{\text{Enthalpy of mass leaving through mass transfer}} = \underbrace{\int_2^3 \delta Q_l}_{\text{Heat leaving system}} + \underbrace{\int_2^3 dH}_{\text{Total change in ullage enthalpy}} \quad (1.5)$$

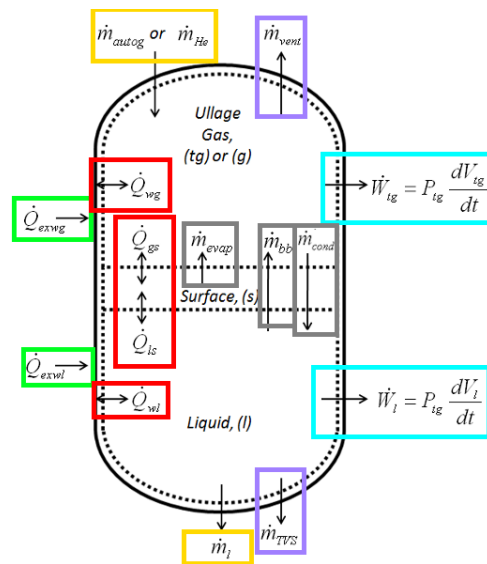


Figure 1.21: Scheme of the main flow in the entire tank

Green: Environmental fluxes

Red: Internal tank fluxes

Orange: Inlet and outlet flow rates

Gray: Mass transfers

Aqua green: Work done by the pressurizer

Lilac: Outgoing vapor flow rates

Therefore, in this case, the thermal flows leaving the system represent a significant loss that modifies the system's internal energy and, consequently, its partial pressure.

Heat fluxes can be conductive and convective, with the latter type divided into forced or natural convection. We can define forced convection when the fluid is moved by an external source, in this case the pressure jump. Natural convection means all phenomena that achieve

exchange for a difference in density without any intervention of external elements. Conductive heat flows linked to external sources are not considered here given the limited entity compared to convective flows and since our interest is focused on ullage as a separate element.

$$Q = \lambda \cdot A \cdot (\Delta T), \quad (1.6)$$

where λ is the conductive exchange coefficient [W/(m K)], which is part of the materials' properties or determined by electrical analogy. For convective flows, on the other hand, it is necessary to determine their magnitude using the Newton relation:

$$Q_{\text{conv}} = h_{sc} \cdot A \cdot (\Delta T) \quad (1.7)$$

Since it is not possible to define a priori which component is the dominant one and since one of the secondary objectives of the study is precisely to classify the phenomena that occur and calculate the total exchange coefficient, as:

$$h_{sc} = h_{sc \text{ forced}} + h_{sc \text{ free}} \quad (1.8)$$

The determination of this constant represents one of the main challenges in the simulations of the phenomena seen. This is done through correlations of experimental origin and is applicable for certain intervals and ranges of dimensionless numbers.

For the case of forced convection:

$$h_{sc} = f(Re, St) \quad (1.9)$$

For the case of natural convection:

$$h_{sc} = f(Nu, Pr) \quad (1.10)$$

Several texts and studies report multiple correlations for the most diverse and possible configurations, defining the ranges of applicability. Several previous studies have empirically determined the possible correlations functional for the situation reported in this study. The correlations used in this elaboration are taken from two distinct sources ([29] and [34]). After a careful dimensional study to verify their compatibility, they have been implemented by dividing by the possible cases that can occur inside the tank.

Dimensionless Numbers The main distinction between the convection cases that will be reported here is the Richardson number (Ri), which represents the ratio between potential energy and the kinetic energy of a flow. In general, a flow with a high Ri means that the flow is stable

in the direction normal to the average direction and has a certain degree of stratification. If Ri is low, then we are dealing with less stable and chaotic flows, which are easily associated with forced convection.

$$Ri = \frac{Gr}{Re^2} = \frac{g \cdot L \cdot \Delta\rho}{\rho_0 \cdot U_0^2} \quad (1.11)$$

Where g is the gravitational acceleration, $\Delta\rho$ is the density difference, L is a characteristic length, ρ_0 is the reference density, and U_0 is a characteristic velocity. Here, the Richardson number will take on a meaning linked to the typology of local phenomena, i.e. whether they are free or forced. Applicability ranges are then defined, namely:

- $Ri < 0.1$: Free Convection
- $0.1 < Ri < 10$: Mix Convection
- $Ri > 10$: Forced Convection

However, the Richardson number is made up of 2 other significant numbers, the Grashof and Reynolds numbers. Starting from the second, Reynolds is the best-known and most-used dimensionless number. It represents the ratio between inertial and viscous forces in a fluid. Based on some ranges, it allows to define whether a flow is in a laminar regime, turbulent, or a mix.

$$Re = \frac{\rho u L}{\mu},$$

where ρ is the density of the fluid, u is the velocity of the fluid, L is a characteristic length, and μ is the dynamic viscosity. In this study, the ranges applied to determine the flow regime are:

- $Re < 10^4$: Laminar Flow
- $10^4 < Re < 10^5$: Mixed
- $Re > 10^5$: Turbulent

The second number is the Grashof number, a dimensionless value that quantifies the importance of buoyancy forces compared to viscous forces in a fluid and is mainly used to represent natural convection.

$$Gr = \frac{g \cdot \beta \cdot \Delta T \cdot L^3}{\nu^2}, \quad (1.12)$$

where g is the gravitational acceleration, β is the coefficient of thermal expansion, ΔT is the temperature difference, L is a characteristic length, and ν is the kinematic viscosity of the fluid.

Finally, another number used in this work for calculating the heat transfer coefficients h_{sc} is the Prandtl number, defined as a parameter that links kinetic diffusivity with thermal diffusivity.

$$Pr = \frac{\nu}{\alpha}, \quad (1.13)$$

where ν is the kinematic viscosity and α the thermal diffusivity. The Prandtl number is significant for predicting heat flow and transfer.

Through the combination of these parameters, it is possible to define the range and characteristics of the flow under study. Moving now on to the correlations that quantify heat flows, it is first necessary to present the necessary dimensionless numbers.

Dividing then by the different configurations.

Ullage Gas Transfer to Tank Surface The heat transfer from the fluid to the inner surface of the tank from the gas in ullage per unit of area, can be obtained using the relation (1.7) :

$$\dot{Q}_w = h_{sc}(T - T_w) \quad (1.14)$$

With the overall convective heat transfer coefficient being determined by the sum of the two contributions to the exponential damping factor which is a function of the level of liquid in the tank, as reported in the expression (9-43/9-45) in [34].

$$h_{w,J} = h_{free} + h_{forc}e^{-\beta z} \quad (1.15)$$

$$\beta_w = \min(\beta_{w,a}, \beta_{w,max}) \quad (1.16)$$

$$\beta_{w,a} = (0.0137 + 0.00808z_w)(r_z - r_a)^2 \quad (1.17)$$

$$\beta_{w,max} = 0.00117(r_z - r_a)^2 - \left(\left(\frac{1}{z_w} \right) \ln \left| \frac{0.06}{4b_1} \right| \right) \quad (1.18)$$

With z_w be the vertical distance from the tank wall location being evaluated to the closest point of pressurant gas entry into ullage and the r_a radius of standard inlet diffuser, r_z the radius at z_w height, and $b_1 = 0.54$ as a constant determined by empirical way.

Studying case by case, in the case of heat transfer in forced conditions, both for laminar and turbulent regimes, the relationship is as reported in [29] (9.80):

$$St_x = \frac{0.485}{2 \times \text{Pr}_x^{0.75} (\text{Re}_T^{**})_x^{0.556}} \quad (1.19)$$

$$h_{sc} = St \cdot u \cdot \rho_m \cdot c_{p,m} \quad (1.20)$$

Like all the others presented here, the report is empirical in nature. It is based on previous works but without defining a range or hypotheses of applicability. Precisely, these relations are obtained through the application of the non-equilibrium kinetic method and the reactor method, i.e. the former is used in combustion processes under extreme conditions when the system in which the distribution of energies between the degrees of freedom is disturbed, e.g. in the passage of events such as a shock wave. The second, on the other hand, uses the chemical kinetics equations by means of zero-dimensional equations that integrate the classical kinetics equations; less precise than the first, it is simpler. However, as these topics are complementary to the work presented here, it is left to the reader to expand on them in Sections 1-4 and 1-5 of [29]. The Staton number (St) is another dimensionless parameter used in this study; it measures a fluid's heat transfer, defined as the ratio of the heat transfer coefficient to the heat capacity product times the fluid's velocity. The correlation practically represents the combination of Grashof, mentioned above, and the local Reynolds number squared.

$$Ri = \frac{Gr}{Re_{loc}^2}$$

By reversing the definition, the value of the heat transfer coefficient of the phenomenon h_{sc} can then be determined.

If we deal with heat transfer in the free condition, a new correlation and a high dimensional number take over. As reported, in this case in [34] (2-11)

$$Nu = c_1 \cdot [(Gr_L) \cdot (Pr)]^{c_4} \quad (1.21)$$

The constants $c_1 = 0.13$ and $c_4 = 1$ are always defined according to (2-1) expression in [34] after a long empirical work. With the heat transfer coefficient h_{sc} , which can also be calculated in this case from the inverse of its definition:

$$Nu_L = \frac{h_L \cdot L}{k} \quad (1.22)$$

Where h [W/m² K] is the heat transfer coefficient, L [m] is a characteristic length and k [W/m K] is the thermal conductivity of the fluid. The Nusselt number is the equivalent of the Staton number but for natural heat exchanges. It is defined by the ratio of convective heat transfer through the fluid to the conductive capacity of the fluid itself.

Ullage Gas Transfer to Propellant: For the heat exchange between the pressurizer and the propellant, correlations are different in the case of laminar rather than turbulent regime, i.e., in the case of forced convection $Ri < 0.10$:

Laminar:

$$St = \frac{0.332 \cdot Pr^{-2/3}}{\sqrt{Re_{loc}}} \quad (1.23)$$

Instead, Blasius's expression relates to the forced heat transfer by 2-D laminar flow on a surface with constant properties and temperature, as reported in [35] Chapter 6.

Turbulent:

$$h_{so} = \left(\frac{d_1 k_J}{r_i} \right) \left(\frac{r_i \dot{m}_{PG}}{A_d \mu_J} \right)^{d_2} (Pr_J)^{d_3} \quad (1.24)$$

Where: $d_1 = 0.06$, $d_2 = 0.8$, $d_3 = 0.33$, other constants determined in experimental way in [34] (3-50) and other previous works. While r_i represents the radius of the tank, \dot{m}_{PG} [kg/s] the pressurizing flow rate, A_d [m²] the diffuser inlet area, μ_J [Pa s] the dynamic viscosity of the fluid, while k_J the thermal conductivity [W/m K].

For the free exchange condition, the same relation is used as for the wall exchange:

$$Nu = c_1 \cdot (Gr_L \cdot Pr)^{c_4} \quad (1.25)$$

The evaluation of energy loss through heat flows is also reported in other studies to underline how important these phenomena are for proper pressurization, such as in [30]. In this, we want to define the degree of energy dispersion within the ullage, therefore the percentage of energy lost on the liquid, the percentage lost on the walls and what remains in the ullage. In this study, it is concluded that in the radial configuration, almost 60% of the energy is absorbed by the wall (δU_W), with only 20% remaining in the ullage, while for the other configuration, anticone, the share lost on the liquid increases significantly, almost to 40%, equaling that lost on the wall and keeping the share preserved for pressurization constant.

A further evaluation, carried out with the aim of determining the heat contributions lost and gained by the system, is reported in [10], in which different geometric configurations for the injection of pressurizing gas are studied and it is concluded that most of the absorbed heat occurs through the walls, representing, among the different configurations, an average between 77% and 93% of the dissipated heat. While, the study continues, the thermal share lost in contact with the liquid increases as the size of the injector decreases.

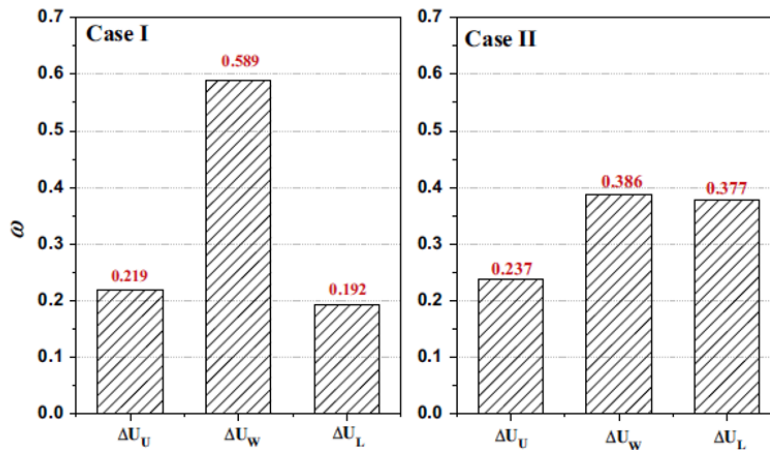


Figure 1.22: Comparison of energy distribution between radial diffuser case and anti-cone diffuser case -Figure 16 [30]

Dimensions, tank geometry and surface finish of the walls:

The size of the tank dramatically influences the degree of pressurization, the distribution of the pressurizing gas and the phenomena that occur inside it. Dimensions such as the radius and height of the tank are fundamental parameters to understand locally, through empirical correlations, the heat flows that are realized. Geometry, on the other hand, often influences the dynamics of the heat exchange rather than another; tanks for liquid engines can have different geometries, from elliptical tanks, therefore cylindrical body and convex spherical heads, commonly used as main launcher tanks, or cylindrical but with a concave head, a configuration called tandem, in which the convex head is in common between two. Or, for space applications, the tank becomes primarily spherical. The current paper focuses on the application on launchers, so the geometry that will be considered is that of a cylindrical body with spherical heads while the dimensions will be given by the case study.

An influencing factor related to the state of the tank is also the presence of ribs inside it, as reported in the study [36] where a tank with hydrogen is studied using "Volume of fluid" (VOF) with phase change, reports how the presence of these bodies in the tank help the pressurization of the tank, this help then increases with the decrease in the ratio between the spacing ($\frac{s}{p}$) and the height of the rib. On the other hand, however, the ribs have shown that at the beginning of the emptying phase, the surface exposed to heat flows increases, intensifying dissipative phenomena. In the same way, the flows are broken, creating pressurizer paths that mix the temperatures inside them more. Therefore, the internal state of the tank affects its operation in several respects, but in this thesis work, no type of internal structure of the tank is taken into consideration, given the increase in the degree of complication for the introduction.

Tank fill level: The filling of the tank is another important parameter for determining the

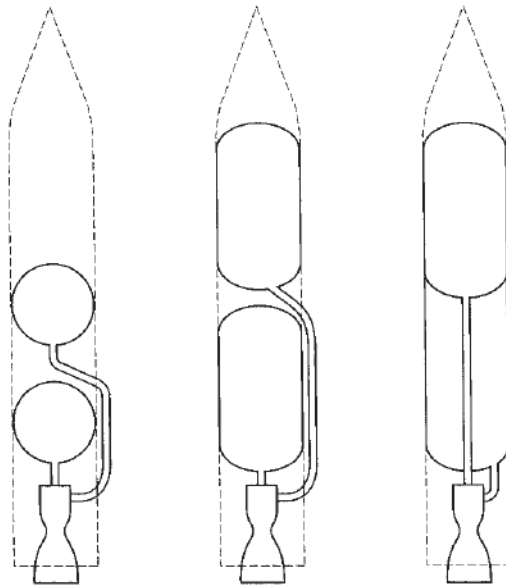


Figure 1.23: Some tank configurations reported in figure 6-2 [14]

operation of the pressurization system. The percentage of ullage in the tanks, often in this phase of development, is a defined and binding parameter. As reported in several studies, the fill level of the ullage influences the operation and the diffuser's positioning. As it is easy to guess, a small ullage, so a high liquid level, will allow rapid initial pressurization, with limited heat exchanges due to the small exposed tank wall.

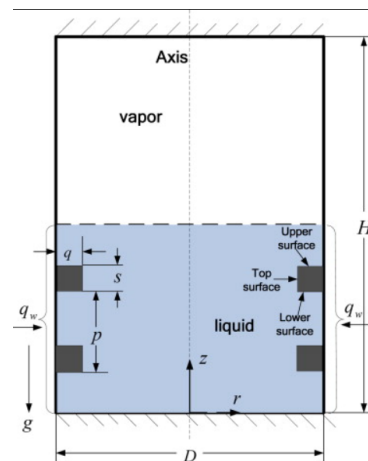


Figure 1.24: Scheme of ribs in cryogenic tanks

On the other hand, emptying, as already described, is a delicate phase because the walls involved in the exchange with the propellant increase, and the volume to be pressurized increases, which greatly engages the pressurization system. In this paper, the propellant level is given by the case study and maintained during the processing of the first analyses to simplify the study. A possible emptying will be carried out only later, through fluid dynamic software during the

verification of the chosen design to evaluate its performance throughout an operating cycle. On the other hand, however, as reported in [37] the propellant level also affects the positioning of the diffuser in the ullage. To avoid excessive pressurizer mixing and causing excessive propellant deflections, given the inlet size of the pressurizer and H_{fr} the deflection of the fluid, it is recommended that it should not be more than 10% of the inlet diameter of the diffuser. Given then the following correlation [9]:

$$\frac{H_{fr}}{D_e} = 61.32 \text{Fr} \left(\frac{H_{g,o}}{D_e} \right)^{-1.453} \quad (1.26)$$

$$\text{Fr} = \frac{\rho_g w_{g,o}^2}{D_e \rho_g g} \quad (1.27)$$

Where:

$$\text{Fr} = \left(\frac{\rho_{g,l} w_{g,l}^2}{D_e \rho_l g} \right) \quad (1.28)$$

The Froude number is another dimensionless parameter used mainly for free surface flows. In this case, it is used to evaluate the arrangement of the pressurizer on the propellant and the relative degree of dispersion of one on the other.

While:

- $\rho_{g,l}$: density of the pressurization gas
- $w_{g,l}$: Pressurization gas velocity
- D_e : equivalent diameter
- ρ_l : Propellant density
- g : gravitational acceleration
- n : gravitational loads
- $H_{g,0}$: distance from the injection device to the surface of the propellant

Report valid for:

$$0.1 < \text{Fr} < 0.52 \quad \text{and} \quad 23 < \frac{H_{g,0}}{D_e} < 65$$

In the code presented in this study, the above correlation will become very useful because, once the properties of the pressurizer and propellant, the inlet velocities and the inlet dimensions have been defined, the value of $H_{g,0}$ can be determined by turning the formula around, thus obtaining the minimum inlet height of the pressurizer assuming a maximum deflection.

Pressurization strategy, discharge times

The pressurization strategy and the time for emptying the tank also influence the operation of the pressurization system. As briefly presented with pressurization systems, strategies for achiev-

ing the operating pressure level can occur in several ways. From the classic pressurization, maintenance with level control and propellant discharge, to the addition of a pre-pressurization phase on the ground before the actual pressurization during operation, or the stepped pressurization, i.e., the achievement of a pressure level, the hold for a congruent interval, and then new pressurization strategy until the required level is reached. Or, for technologies that require multiple ignitions, pressurization must be guaranteed at each engine firing; therefore, a series of pressurizations, hold, and new helium injections.

In particular, the main factor influencing pressurization is the time relative to the different phases. Ramp time: i.e., shorter pressurization times correspond, with the same input geometries, to a greater amount of energy lost, mainly due to more intense forced phenomena. Hold time: the time required to maintain pressurization is another crucial factor. Longer pressurization periods result in more heat loss and, consequently, a higher demand for pressurizers.

Expulsion time: The time required for the tank's ejection is mostly at this design stage already defined and locked in for engine performance. As can be guessed, slower emptying, as for the previous phases, leaves less time for the pressurizer to come into contact with the dissipative elements, minimizing losses. On the other hand, a fast ejection often creates vorticity and mixing phenomena of the propellant and pressurizer that are difficult to simulate, as well as shortening the ejection time can lead to a significant increase in the pressure drop that occurs at the beginning of the ejection phase. The dropoff represents the pressure drop due to the beginning of the propellant expulsion phase. It is an annoying phenomenon because it creates dangerous oscillations in the pressure level, which, if excessive, could cause a reckless increase in the pressurizer demand until the nominal pressure is dragged below the minimum value threshold for the correct motor operation. The pressurization times will be given by the case study in this study, as this is not a factor influencing the first order.

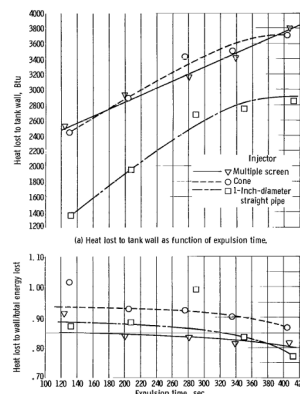


Figure 1.25: Heat flow to tank walls (a) and ratio between heat flows and the total energy lost- [10] figure 15

Chapter 2

State of the art and literature review

2.1 Case Studies and Known Operational Regimes of Dif-fusers

2.1.1 Pressurization Systems

Description of Pressurization Systems

The transfer of rocket propellants from the tanks to the thrust chamber at the needed flow rates and pressures requires a suitable feed system; this is the aim of a **pressurization system**. The pressurization system is usually all the hardware above the propellant tank (see figure 2.1), guaranteeing the right pressure level inside the tanks and avoiding various possible problems. Maintaining the right pressure level is crucial for the motors' feeding and constant propellant flow rate without instability events like bubbles. It is also important for structural integrity, avoiding the tank's collapse during the discharging processes (see figure 2.2¹).

As reported in [39], the selection of the right technologies will depend on the vehicle's accelerations, manoeuvres, and weight, the thrust level and duration, vibration levels, the available envelope, the type of propellants, reliability, and cost.

The two main methods are gas-pressurized and turbopump feed systems. Typically, small systems with a restrained propellant fraction prefer the gas-pressurized propellant because the complexity of a turbopump feed system is not justified. In contrast, in larger systems with downstream turbopumps, which increase the pressure, low-pressure propellant tanks are required, and weight considerations are crucial. With the progress in high-strength materials for propellant tanks and improvements in turbopump reliability, the upper limit for gas-pressurized tanks has increased. These improvements have led to a significant overlap in their practical applications.

¹The Agena rocket failed on the launch pad due to a gas bubble that developed in the pressurization system. As a result, the rocket's upper tank lost pressure, causing the tank to collapse and the Agena upper stage to fall.

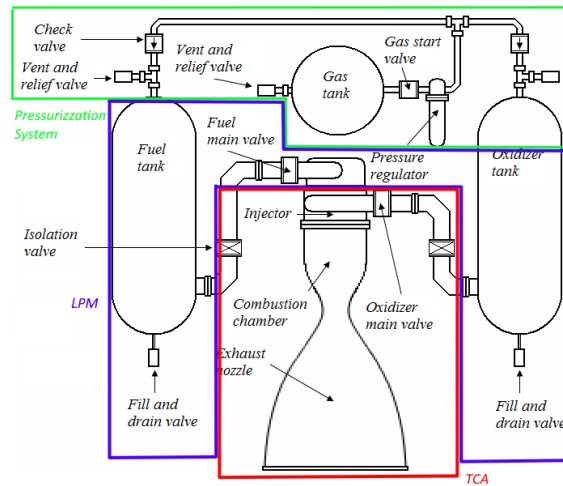


Figure 2.1: Generic Motor scheme from [14]

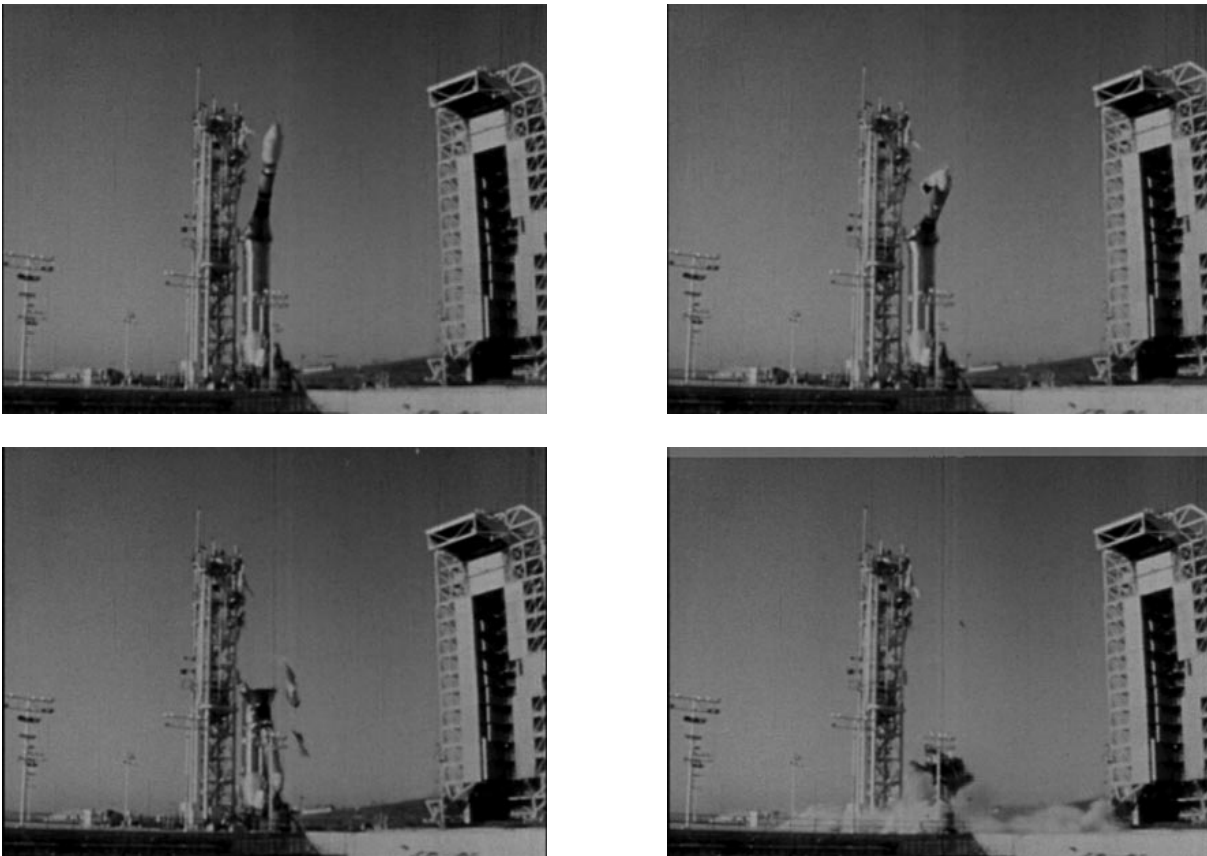


Figure 2.2: Four subsequent events during the ATLAS Agena D collapse, May 11, 1963[38]

However, even pump-fed systems usually require some low-level pressurization of the propellant tanks to minimize pump requirements and guarantee a constant level of inlet pressure; this is the case presented here.

Over sixty years of history in Liquid Propellant Rocket Engines (LPRE) have highlighted

key differences among the major types of pressurized feed systems. The classification can be made in two way, the first by the origin of the propellant for the pressurization, three main categories here:

- Exogenous: where the system is pressurized using another gas, different from the propellants
- Autogenous: Where the pressurant gas is the same pieces of the propellant like LH2 to LOX.
- Generators: Third and less common system, where the combustion gases are used.

Furthermore, this first classification, another can be achieved in the function of the typology. According with [39] Chapter 5,

Inert Gas	Evaporated Propellant^a	Combustion Products^a
Stored at ambient temperature under high pressure -Thor fuel -Saturn IB fuel -All spacecraft with pressure-regulated systems	Boiloff of saturated propellants in tank -Centaur fuel and oxidizer	Turbine exhaust gas -Titan II fuel tanks Separate solid-propellant gas generator -Lance fuel and oxidizer
Stored at cryogenic temperature and heated in heat exchanger -S-IVB oxidizer -LEM Descent fuel and oxidizer	Drawn from injector manifold -S-II fuel -S-IVB oxidizer	Separate liquid-propellant gas generator ^b Main tank injection ^b
Blowdown from pressurized condition -Titan II oxidizer -ERTS orbit-adjust ^c -Intelsat ^c	Evaporated in turbine-exhaust heat exchanger -S-II oxidizer Stored as a gas under pressure ^b	

Table 2.1: Description of propellants and inert gases stored under different conditions extracted from Table 1 of [40] a:Prepressurization on ground provide an initial pressure b:Not proven in flight vehicle c:Monopropellant

- **Stored gas**: Most simple one and widely used; the system is composed in a spherical tank, where the pressurant ranges up to $1e5 \text{ psi} (\approx 700\text{bar})$ and is supplied to the propellant tank by a regulator. The most common gas used is He; the pressurant must have a low molecular weight, high gas density at storage conditions, minimum residual gas weight, and a high allowable stress-to-density ratio of the pressurant-tank material. Different configurations are used: *Helium system without heating* (figure 2.3a), the most simple one where a high-pressure

storage tank, with a shutoff valve and pressure regulator. The downside is the relatively high weight for the low temperature and specific volume of the gas. *Helium system using heat exchangers* (figure 2.3b). Heating up the pressurant can be a good solution to increase the volume of the pressurant and consequently save the mass for the pressurization. The possibility of heating up the helium can be achieved with different methods, such as using a heat exchanger in the thrust chamber, like the one used in the A-4 motors. A cascade of the heat exchanger with the *cascade system* (figure 2.3c). Or through the heat exchanger inside the storage tank, commonly in the hydrogen propellant tank *He pressurization with heat exchanger in tank* (figure 2.3d).

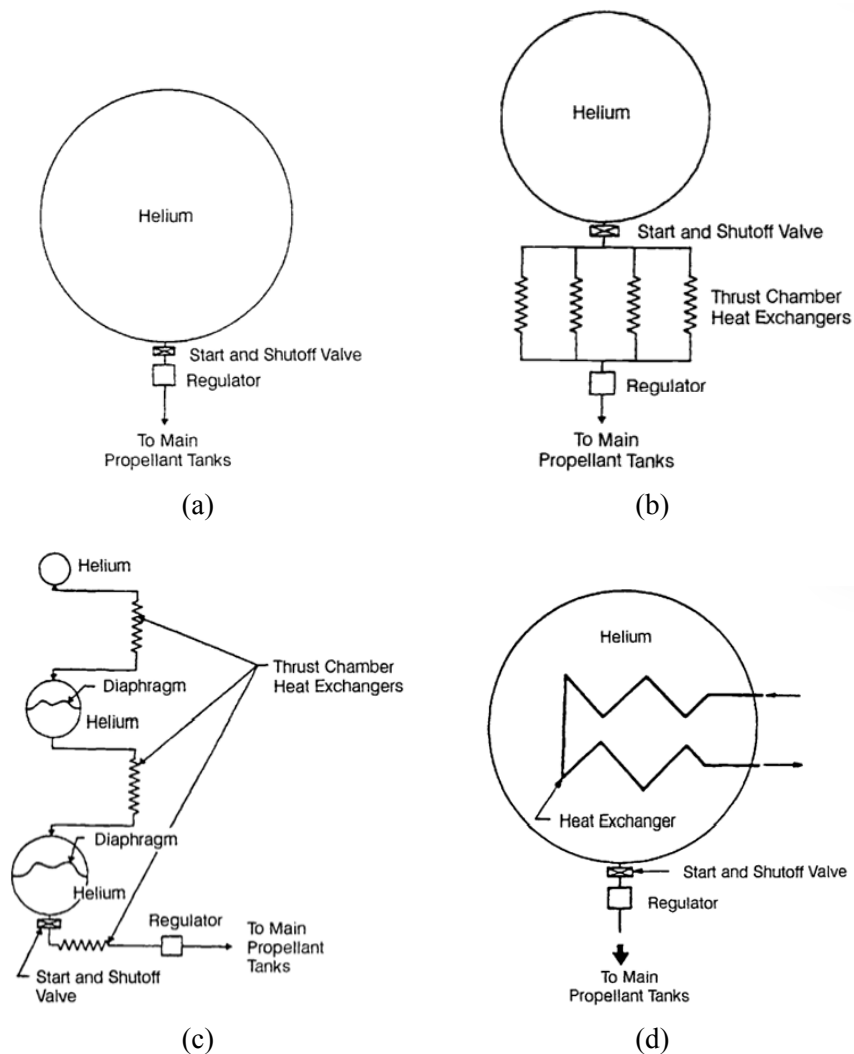


Figure 2.3: Illustration of helium pressurization systems: (a) HE pressure tank with no heat exchanger; (b) HE pressure with a heat exchanger in CC; (c) Cascade system; (d) HE exchanger inside the tank. (Adapted from [39].)

- **Propellant evaporation:** Useful only for thermally stable, low-normal-boiling point propel-

lants, such cryogenics. The possible configuration of this system could be: *Pump Fed Propellant Feed Systems* (figure 2.4), used in the pump-fed engines. Usually, the propellant is tapped off from the downstream of the pump, vaporized in the heat exchanger and then entered into the main tank. The heat is usually taken from the turbine exhaust gases. The configuration is typically for the RP-1/LOX pump-fed engines. The *Pump Fed Propellant Feed Systems* have limited application; in fact, the evaporation can lower pressurant-tank weight, as compared to stored-gas systems, because of higher storage densities and lower storage pressures at the same time, the advantage can be offset by the higher molecular weight of some propellants. Hydrogen, for example, has a low critical pressure (and low molecular weight), so to obtain reasonable volume increases, the tank pressure must be kept sufficiently below critical pressure. For all of these reasons, the propellant-vaporization will be used only for the fuel tank it is attractive for relatively low-pressure and low molecular weight

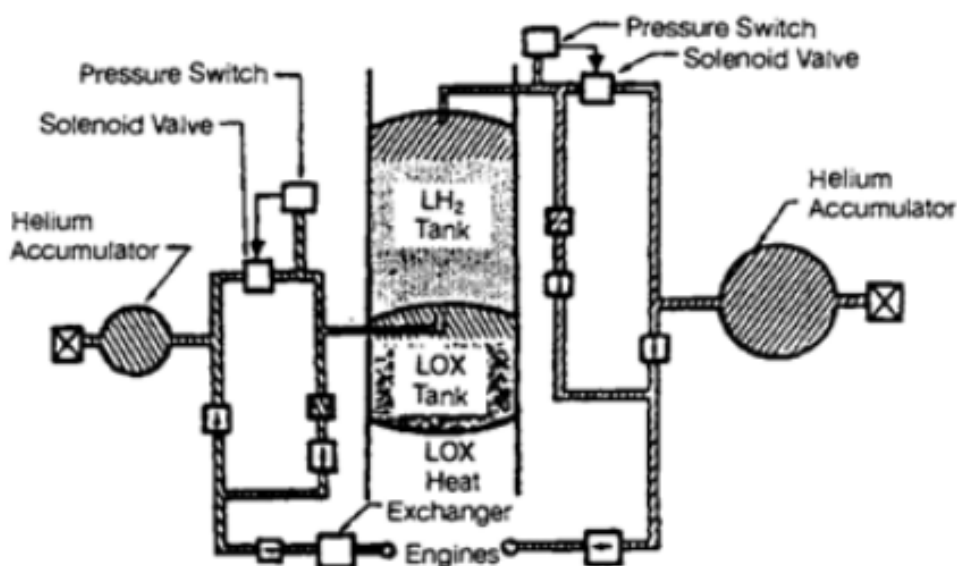


Figure 2.4: A-2 Evaporated propellant system figure 5-8 of [39]

- **Inert-gas-evaporation systems:** The principal configuration here presented and one of the most frequently used. As the name says, the pressurants are inert species, nitrogen and helium; the scheme is similar to one presented in a propellant-evaporation system because the evaporation is a side effect of this pressurization type. The pressurant gases are stored in high-pressure tanks at ambient temperature, but they could be heated in some cases[30]. The set-up usually consists of regulators to control the inlet flow, typically with closed-loop and reactive control to check the pressure level (solution common today also for the other systems).
- **Chemical reactions:** Pressurization using hot-gas products generated from propellant combustion or catalytic-reacted; not applicable to cryogenic propellant, typically for a storable

First stages	Propellant		Tanks					Feed line top tank	Tanks pressurization systems	
	Oxidizer	Fuel	Arrangement	Bulkheads	Shape	Material	Insulation		Oxidizer	Fuel
Space shuttle	LOX	LH ₂	LOX above	separated	LH ₂ cylindrical LOX ogive	Al – Li alloy	SOFI ¹ ablator phenolic ²	external	Autogenous GOX	Autogenous GH ₂
Ariane 5	LOX	LH ₂	LOX above	common	LH ₂ cylindrical LOX cylindrical	Al alloy	polyurethane	external	GHe	1) GHe 2) Autogenous GH ₂
Ariane 6	LOX	LH ₂	LOX above	separated	LH ₂ cylindrical LOX cylindrical	?	?	?	?	?
Falcon 9	LOX	RP-1	LOX above	Common (insulated)	LH ₂ cylindrical LOX cylindrical	Al – Li alloy	?	Crossing (insulated)	GHe (3-4bar)	GHe (3-4bar)
Starship	LOX	LCH ₄	LCH ₄ above	common	LH ₂ cylindrical LOX cylindrical	carbon fiber or stainless steel ³	?	crossing	Autogenous GOX	Autogenous GCH ₄
New Glenn	LOX	LNG ⁴	LNG above	common	LH ₂ cylindrical LOX cylindrical	Al	?	crossing	Autogenous GOX	Autogenous LNG

Figure 2.5: Common pressurization system from [40]

liquid-propellant system. Another possibility is the use of hypergolic injection in the tank and the pressurization provided by the products of reactions. The limitation with the cryogenic propellants is due to the undesirable rise in the bulk temperature. Still, in some case, the applicability with the cryo-prop is possible using directly the fuel-rich hot gases or oxidizer-rich hot gases into fuel or oxidizer tank as reported [40] that is the case for the *Starship-Space X pressurization system*. Compatibility and gas temperature are two critical points for the pressurization with the combustion product. The possibility to realise the hot gases can be: *Solid-propellant Gas Generators* usually for low production cost, long storability and relatively lightweight and compactness. The system is composed of electrically fired initiators and a solid propellant grain. *Liquid-Propellant Gas Generator* in the configuration of mono prop (e.g. hydrazine) and prop gas generators (nitrogen tetroxide and hydrazine or UDMH) have been used successfully with long operating times. The compatibility of the propellant is essential, as the temperature limits and molecular weight of the gas. The liquid gas generator is relatively complex, and its application is determined mainly by the time needed for the stars and the operating mission time.

As presented above, the pressurization system has to follow some requirements and data to chose which solution better fits, here are reported:

- **Operating Temperature Ranges:** Temperature limits for both feed-system components and the fluids they handle.
- **Propellant Properties:** Properties, weights, and volumes of propellants.

- **Tank Volumes and Dimensions:** To understand in which case it is operating.
- **Initial Ullage:** The empty space in the propellant tank at the start, not filled by the liquid.
- **Trapped Propellant:** The amount of propellant left in the tank after expulsion.
- **Operating Tank Pressure:** The standard pressure in the propellant tank and its potential fluctuations.
- **Mission Duration and Engine Firing Times:** The overall length of the mission and the specific times the engine is fired.

It is good to note that a lot of these aspects will be translated directly for the sizing diffuser procedures; in fact, all of these will be taken into consideration in the work presented here.

2.1.2 Diffusers

Description

The diffuser introduces the pressurant gas into the propellant tank as a critical component of the pressurization system in a liquid propulsion engine. Element present in both pressurization systems (self-pressurization and by inert gases), the diffuser makes the pressurant enter the propellant tank at a desired direction and velocity [39] to keep the pressure inside the tank at the design level during the pressurization activities without the engine working (on-ground operations or during coasting phase) and to avoid the creation of zones where the operating pressure falls below a threshold value of NPSH during engine firing. As mentioned earlier, a pressure level below the NPSH creates the conditions for cavitation of turbopumps located downstream of the reservoir or significant fluctuations in MEOP, leading to non-conformal engine operability. Diffuser is a generic term in the engineering field for the vast domain in which it can be found, from jet engines to perfume atomisers, from wind tunnels to refrigerators. The term diffuser is intended as a device that can manage energy in fluid dynamics, precisely designed to reduce the kinetic energy of moving fluid in favour of the pressure in an adiabatic process. Given the equation of conservation of energy, which defines the fact that energy in a closed system remains constant, applied for a moving fluid can be written as follows.

$$h + \frac{V^2}{2} = constant$$

Where h is the enthalpy of the system and V the velocity of the fluid. This equation can be written in an even better-known form by assuming an incompressible, inviscid fluid and steady-

state flow and reporting it for the fluid path:

$$p_1 + \frac{1}{2} \cdot \rho_1 \cdot V_1^2 = p_2 + \frac{1}{2} \cdot \rho_2 \cdot V_2^2$$

A diffuser, opposite a nozzle, slows down the velocity of the fluid in the inlet and raises the enthalpy. Ideally, the process would be isotropic and the efficiency could be written as:

$$\eta_{\text{isentropic, Diffuser}} = \frac{KE_{\text{exit, isentropic}}}{KE_{\text{exit, actual}}} = \frac{V_{2s}^2}{V_2^2}$$

[41]

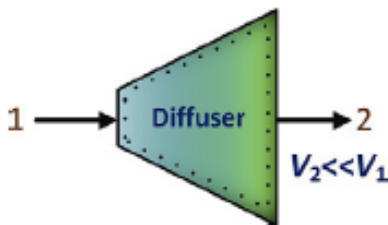


Figure 2.6: Diffuser schematic

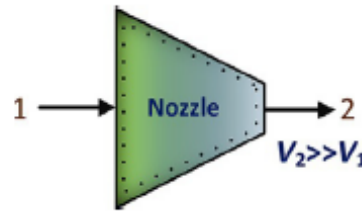


Figure 2.7: Nozzle schematic

For the different cases presented in this introduction, the term diffuser may not be the right choice; in fact, the different physics of some types of them will not fully reflect this definition. However, from this point on, we will use the terms “diffuser” and “injector” to refer to the element that performs the task of introducing the pressurizer into the reservoir without having to fully comply with the physics definition. Different types of diffusers can be located at different positions in the tank. The classical configuration of the gas injector is at the top of the propellant tank, positioned on the axis of the propellant tank(a). This is to allow a symmetrical introduction of the pressurizer species. However, non-symmetrical placements are also possible, thus presenting some angle to the axis of the tank itself(b). There are other possible configurations, such as the radial ring configuration, where the diffuser consists of a series of nozzles mounted internally to the reservoir that inject in a radial direction to the circumference, bringing the flows to collide and atomize and cooling the reservoir wall itself(c). A final possible configuration is placement at the bottom of the tank where the pressurizer is injected to create bubbles in the propellant (bubbler) that then move to the surface and pressurize(d). The inlet velocity of the pressurizer through the diffuser can vary from a few meters per second to tens of meters per second, depending on the size of the outlets, which in turn can be from a few centimetres up to tens of centimetres; consequently, the Reynolds number at the outlet can vary from 10000 to 200000[29].

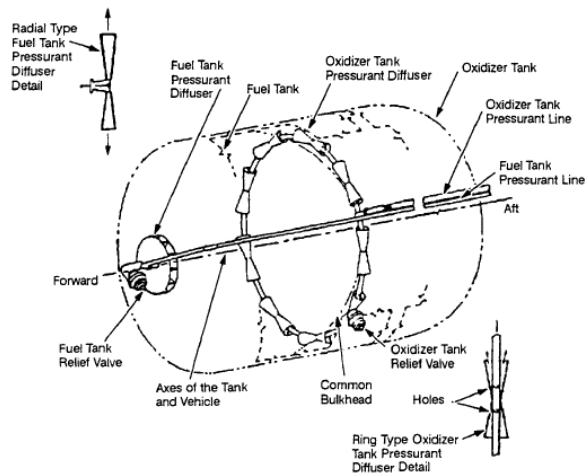


Figure 2.8: Axial (a) and Circunferential diffuser(c)[39]

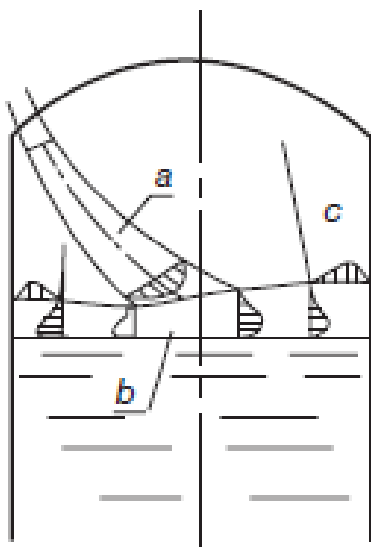


Figure 2.9: Lateral tank diffuser(b)[29]

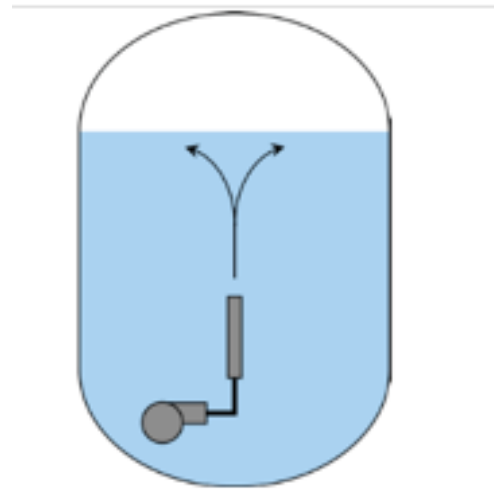


Figure 2.10: Submerged diffuser (d)[42]

Typology

Turning to the possible geometries of the component, the possible configurations adopted to date will be presented. This subdivision also outlines the operating physics that exploits the different types. The configurations can thus be divided into seven different categories:

- Diffuser injections
- Straight
- Dissipator
- Vortex
- Circumferential
- From the bottom
- Bubbler

As can be seen, this subdivision also echoes some of the configurations presented above when first defining a classification based on positioning. This emphasizes the strong link between the type and positioning of these technologies. The first category, diffuser injections, is the most conventional class, which this text will discuss most. Designed for uniform distribution of pressurizer in the ullage volume, they can come in different geometries, in turn, geometries dictated by the direction in which they inject pressurizer into the tank.

- **Radial:** Design that allows the pressurizer to be introduced in a direction radial to the tank axis.
- **Hemispherical:** Allows introduction at a specific angle to the axis.
- **Conical:** Designed to introduce gas at various angles from the tank axis to a precise angle.
- **Anti cone/Reverse cone:** Configuration quite similar to the hemispherical.
- **Reverse:** A screen is introduced at the outlet of a diffuser, usually radial, which inverts the direction of the flow.

The second category, on the other hand, represents a purely axial pressurizer injection method with one small exception. The main representative of the “straight” configuration is, in fact:

- **Straight Pipe:** In which the pressurizer inlet occurs coincident with the axis of the tank by means of a pipe that can have different sizes and which will influence downstream phenomena. The principle of pressurization, as will be seen below, differs significantly from the previous category. In fact, the pipe injects the pressurizer directly in the direction of the liquid surface, thus creating a separate category.
- **Straight Bar:** A slight variation, less common than the previous one, with an entirely similar principle, entry of the pressurizer in the direction towards the liquid but through often a perforated plate that would bring it very close to the category of Diffuser Injectors.

The third group is that of **Dissipators**, technologies that downstream of a diffuser injector have structures with bottlenecks (e.g., series of perforated plates) to slow down and thus equalize the inlet flow. Also part of this category is the so-called multiple screens, often placed as part of the first group, diffuser injectors. The **Multiple screens** constructed using the radial injector and a spreader screen mounted normal to the tank centerline. The fourth and final group for top-down injection technologies is the Vortex group. This configuration, which at the moment has only been evaluated on a student-sounding rocket, exploits the division of the pressurizer flow into two, one hot and one cold, to have a more controlled distribution of temperatures. The principle is based on the Hilsch Tube, a device consisting of a chamber with two openings,

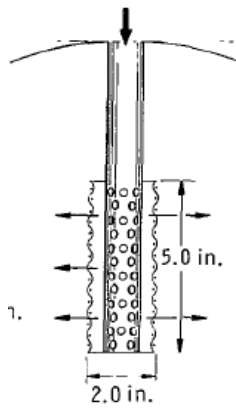
one at the mouth of the tube and one at the end. A jet of pressurized air is introduced into the chamber in a tangential direction, the flow then swirling through the chamber to the bottom, where a collision divides the flow into two directions, the hot one that comes out from the bottom of the chamber and the cold one that after the impact goes up the chamber and exits from the opposite end. Several attempts have been made to define the phenomenon mathematically, but an exhaustive explanation has not yet been provided, limiting its use, which in any case always requires an extensive test campaign to determine dimensions and operating conditions. Moving on to less conventional pressurization configurations, you can find the Circumferential type, already described above, which multiplies the number of diffusers, making them pass from a single component to a series of nozzles that shoot in unison in a defined direction. In addition to the one presented above, i.e. which shoots in the tangential direction, there is another configuration that instead injects the pressurizer in a radial direction; in this case, however, the geometries of the diffusive elements are not known. Another category, on the other hand, already briefly presented above, is that of the diffuser from the bottom up; the "From the bottom" category has as its common pivot the adduction from the bottom of the tank but inside it you can find different geometries. In fact, they incorporate configurations such as the axial/straight pipe and the shower head, similar to the geometries presented in the group of diffuser injectors. Characteristic is that of the Hoops, i.e. circular perforated coils in the ullage. The last group of possible configurations is that of bubblers, which are often defined among the indirect pressurization methods and just as often used in autogenous pressurization methods, exploit the principle of insertion of pressurizer/propellant (previously vaporized by heat exchanger) from the bottom of the tank, causing the formation of bubbles. The hot bubbles will rise towards the ullage allowing pressurization, but they will also have an effect in evaporating the propellant that comes into contact with these bubbles, helping the phenomenon. A classic configuration, which is often also used as a venting system, is that of the straight pipe but submerged often used for operations in microgravity such as landers and upper stages. Another configuration is that of the hoops, seen above, only in this case too submerged.

So, the diffuser is a key element in introducing gas pressurization, saving mass and enhancing performance. As will be presented in the next section, different previous studies identify the geometry of the injection as one of the main points for improving efficiency, especially the direction of the flow. But possible optimization processes are only a small piece of the puzzle. In fact, we are writing about a component that is located inside a system, so it has to respect different requirements. These requirements are usually already defined when the sizing processes for the gas injectors begin, so the room for maneuver is limited.

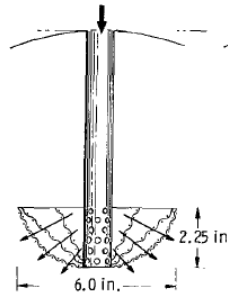
Table 2.2: All the geometries collected during the revision of the SOA

Category	Geometry	Use	System type	Pressurizer	References
Diffuser Injectors	Radial	1)-2)-3)S 4)Saturno V-S-II	1)-2)-3)I.G, 4)E.P	1)-3)He A.T, 2)He R, 4)GH2	1)[10] 2)[30] 3)[43] 4)[24]
	Hemispheric	1)-2)S	1)-2)I.G	1)He A.T	1)[10]
	Conical	1)S 2)Centaur	1)I.G	1)He A.T	1)[10], 2)[44]
	Anti-cone	1)S	1)I.G	1)He H.	1)[43]
	Reverse	1)S	1)I.G	1)He A.T	1)[10]
	Bulb-shaped	1)S,2)Saturno V IC STAGE	1)I.G	1)He A.T	1)[10]
	Multiscreen	1)S	1)I.G	1)He A.T	1)[10], 2)[24]
Straight	Pipe	1)-2)S	1)-2)I.G	1),2)He A.T	1)[10], 2)[43]
	Bar	1)Saturno V IVB Stage	1)I.G	1)He A.T	1)[24]
Dissipator	Splitter/Screens	1)Centaur U.P	1)I.G + E.P	1)He A.T +GH2	1)[44]
Vortex	Vortex	1)StratoS II	1)I.G	1)He A.T	1)[43]
Circumferential	Tangential	1)P	I.G	1)He A.T	1)[39]
	Radial				
From the bottom	Straight pipe	Centaur UP	1)I.G	1)LOX	1)[44]
	Shower Head	1)Saturno V S-II Stage	1)E.P	1)GOX	1)[24]
	Hoops	1)S	1)E.P + I.G	1)He	1)[42]
Bubbler	Straight pipe	1),2)S	1)E.P + I.G , 2)I.G	1)-2)He	1)[42], 2)[45]
	Hoops	1)Centaur	1)I.G	1)He	1)[44]

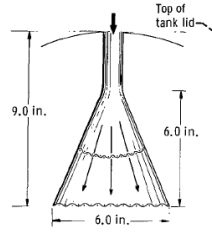
Legend: S: Study, application only in a study and test case, I.G: Inert GAS, E.P: Evaporated propellant, A.T: Ambient Temperature, H: Heated Up, U.P: Upper stage



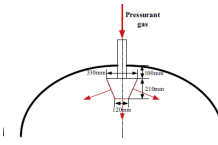
(a) Radial



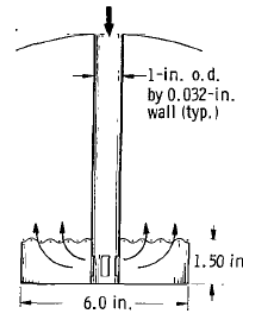
(b) Emispherical



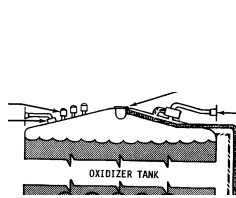
(c) Conical



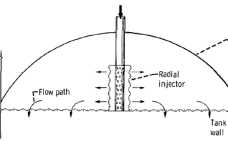
(d) Anticonical



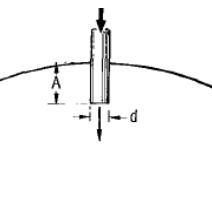
(e) Reverse



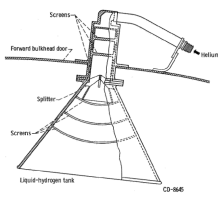
(f) Bulb-Shaped



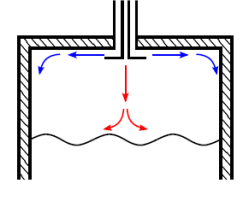
(g) Multiscreen



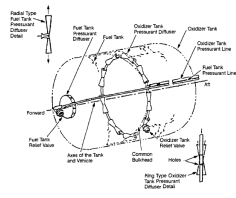
(h) Straight pipe



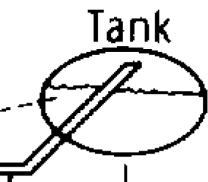
(i) Dissipator



(j) Vortex



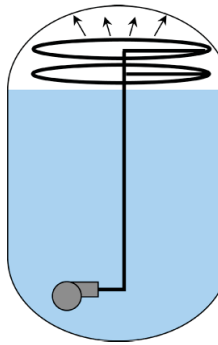
(k) Circumferential



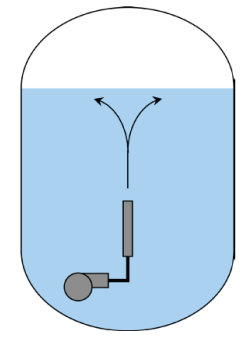
(l) From the bottom straight pipe



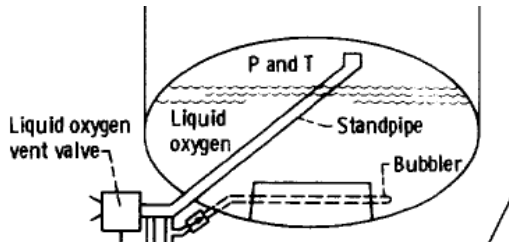
(m) From the bottom reverse



(n) From the bottom hoops



(o) Submerged



(p) Submerged hoops

Requirements for diffusers

The requirements are the translation in a quantitative way of the objectives set for a given space mission. The high degree of engineering complexity, and not only of a space project, requires that the objective for a given one, usually composed in one sentence and of a qualitative type, be translated into quantitative terms and then separated and specified for all the systems and subsystems that will be used in that particular mission. These requirements represent Ariadne's thread: all those involved in the mission must remain faithful to obtain the predetermined results. The structure of the requirements is hierarchical, starting from a limited and high-level group for each system; other requirements are then developed in a cascade, which in turn are pitted for the subsystems and components of that system. The requirements allow a parapet and an indication to proceed in the correct direction and safely to the target. For a component such as a diffuser, the requirements are a consequence of the system and subsystem to which they are part and their performance. However, it is also a function of the mission profile and the interface elements present.

The entire process which wants to present a certain degree of similarity with that of a space mission, is therefore defined as a fixed and immutable objective for the whole process and the requirements from which they derive.

Since this work wants to present a more technical imprint, after analyzing and studying the SOA, the second step was to put together and partly deduce the requirements that a system such as a diffuser must meet. These requirements are reported below in Tables 2.3-2.7.

Mission objectives: Design and optimize a diffuser for a pressurization system of a liquid technology.

Formulation: Develop a sizing methodology to obtain a technological configuration for the diffusion of pressurant in the propellant tanks for a launch vehicle, aimed at minimizing the pressurant required during all operational phases.

Mission Requirements	<i>They answer the question "What shall be done to reach the objectives?"</i>
M.1	The diffuser shall be capable of injecting the required flow rate of pressurant to ensure the correct thrust profile.
M.2	The diffuser shall be capable of injecting without interruptions or malfunctions throughout the entire operational profile.
M.3	The diffuser shall operate with the highest possible degree of optimization in all mission phases.

Table 2.3: Mission Requirements

System Requirements	Re-	<i>They answer the question “How shall the mission requirements be implemented?”</i>	Ref
Functional requirements	Re-	<i>Define the requested functions and/or operations that shall be performed to reach the objectives.</i>	
F.1		The pressurant flow rate shall ensure an adequate pressure level in any condition for the respective operational phase.	
F.2		The diffuser shall distribute the mass flow rate of pressurant required by the system.	
F.3		The diffuser shall not cause a liquid deflection greater than 10% of the diffuser’s diameter.	[37]

Table 2.4: Functional Requirements

Performance requirements	Re-	<i>Quantify the performance levels that shall be met by the functions defined by Functional Requirements.</i>	Ref
P.1		The oxidizer shall not be kept in saturated conditions but in sub-saturated conditions to prevent cavitation in the pumps.	
P.2		The radial thermal gradient relative to the tank axis shall be accentuated axially, while at the walls it shall be limited and contained.	
P.4		The pressurant shall experience the minimum possible level of energy losses within the system.	
P.5		The diffuser shall ensure a continuous pressurant flow that continuously guarantees propellant expulsion.	
P.5.1		There shall be no fluctuations in pressurant flow that could influence engine performance.	<i>3% considered acceptable according to [30]</i>
P.6		The injected pressurant flow rate shall always be \geq the rate required to ensure the correct thrust profile of the engines.	
P.7		The diffuser shall not generate cavitation phenomena in the pressurant before and during entry into the tank.	
P.8		The diffuser shall achieve a distribution that keeps the pressurant temperature consistent with the engine duty cycle.	<i>Page 89 of [46]</i>

Table 2.5: Performance Requirements

Design Requirements	Requirements	<i>Define the constraints that shall be satisfied by the system design.</i>	Ref
D.1		The diffuser shall always ensure a pressure in the tanks that prevents wall collapse due to underpressurization.	[47]
D.2		The diffuser jet shall achieve a heat exchange with the liquid interface that evaporates a propellant mass below the limits imposed by the mission requirement.	
D.3		The diffuser shall ensure a distribution that minimizes the dissipative flows of the pressurizing gas.	
D.4		The diffuser shall have dimensions consistent with those of the tanks in which it is positioned.	
D.5		Any increase in the mass of the diffuser geometry shall not exceed the propellant mass savings values.	
D.6		The diffuser shall present a degree of complexity no greater than or equal to the state of the art.	
D.6.1		The diffuser shall not contain active elements (valves, etc.) that could interrupt the gas flow.	
D.7		The diffuser shall be able to withstand the expected internal structural loads.	
D.7.1		The diffuser shall withstand even sudden loads from impulsive pressurant discharges.	
D.7.2		After a test for impulsive discharges, the pressurant shall not show visible fractures upon inspection.	

Table 2.6: Design requirements

Operational Requirements	Re-	<i>Define the procedures to be satisfied to use the system in a safe and reliable mode.</i>	Ref
O.1		The diffuser shall introduce pressurant into the tank at a speed and direction that achieve the desired temperature distribution in the ullage.	[46]
O.2		The introduction through the diffuser shall not generate vibrations that could damage the structure.	[46]
O.3		The diffuser shall achieve pressurizations without generating pressure losses.	[46]
O.4		The diffuser shall not exhibit leakage phenomena when supply valves are closed.	
O.5		The diffuser shall be made of materials compatible with the chemical species used as pressurant.	
O.6		The diffuser shall be made of materials consistent with operational temperatures and pressures.	
O.7		The diffuser shall operate even in microgravity conditions.	

Table 2.7: Operational Requirements

The operational conditions are fixed, and the pressure level, the gas species, and the nominal and WCS mass flow are determined. All these limits are the starting point for the dimensional processes, as well presented in Chapter 3.

Note that this breakdown is purely illustrative, the result of research aimed at evaluating the SOA. It is, therefore, not to be understood with any official character, not least because the subdivision between two geometries is often very poorly delineated. It is only intended to provide the reader with a clear view of the geometries currently in use.

2.2 Existing Design Methods

Different studies have already targeted the diffuser since the early 1960s, wanting to understand the influences of the stratification inside the ullage [48]. But here, the diffuser was just nominated; instead, in the second half of the 1960s the first investigations on the diffuser effect were started[10]; the principal focus was on the existing interaction between LH2 and the pressurant gas. The principal author of this study, Richard L. DeWitt, produced in the same year a series of other very useful studies, like [49], which will be better presented in the next chapter for the operational conditions. From the end of the Apollo programme to this, only a few other studies[50] and technical reports[44] which involve partially diffuser have been published. A new interest in the subject began after 2000; after this year, almost all of the studies here reported are inferred by the author. Of these numerous studies, only a few concern the diffuser specifically, trying to understand the physics behind the pressure injectors and defining a design methodology or a pressurant evaluation.

2.2.1 Previous Studies

Various investigations have been conducted previously on this work to better understand the pressurization processes and all the influence factors involved. Here are reported brief presentations of related studies not directly used in this work. Thus, this section is not linked to the work but can help with possible research on the correlated topics.

Barsi and Kassemi (2013) performed experimental and numerical studies on tank pressurization and thermal stratification, providing a comprehensive understanding of the auto-pressurization process [51], [52]. Similarly, Liu et al. (2015) examined the evaporation and pressurization processes in on-orbit cryogenic liquid hydrogen storage tanks, as well as the development of thermal stratification in a rotating cryogenic liquid hydrogen tank [53], [54]. The influence of wall ribs on thermal stratification and self-pressurization was explored by Fu, Sunden, and Chen (2014), who later extended their research to the effects of phase changes under microgravity conditions (2015) [55], [56]. Roh et al. (2013) and Wang et al. (2013) utilized CFD

models to study transient natural convection in LNG tanks and the thermal and pressurization performance during LH2 tank discharge, respectively [57], [58]. Ludwig and Dreyer (2014) investigated the thermodynamic phenomena during the active-pressurization process in cryogenic propellant tanks [59]. Additionally, Liu, Li, Wang, and colleagues (2013-2015) focused on various aspects of cryogenic tank pressurization, including the influence of phase changes, thermal stratification, and pressurization performance during different operational stages [53], [54]. This extensive body of research provides valuable insights into the complexities of managing cryogenic storage tanks.

Speaking about the thermal fluxes, Chai and Wilthite (2014) presented a work about the sensitivity of the liquid propellant to the dissipative heat flow towards the external environment [60]. A heat flow from the wall during the auto-pressurization process of a spherical LH2 tank is presented in Ayedlott (1967) [61]. Investigation of the performances influenced by the aerothermal heat during ascent phase can be found in another Wang and Li (2013) study [62]. For the CFD models used to evaluate respectively the performances of pressurization with LHe cryogenic LH2 and LN2, or in an ellipsoidal LH2 tank with normal gravity, see Gary et al. (2007) or Alfredo et al. (2008) [63], [64].

In Appendix-C is reported a table with the collection of the studies relative not directly to this work but about the pressurization and the diffuser. The only scope of the table is to help the research.

2.2.2 Reference to NASA Studies and test

Chronologically speaking, the first evaluation on the diffuser has been discussed in [10], where six different geometries were tested during cryogenic hydrogen discharge from an 820-litre cylindrical tank. Two inlet temperatures, ambient gas ($282K$) and heated gas ($310K$), have been tested at a constant pressure of 1100 kPa. The pressurant species is the hydrogen taken from the tank. The study also confronts the analytical model with the test, concluding a good agreement for diffuser-type injectors but simultaneously indicating the need for a mixing theory for radial and axial temperature gradients in straight pipe gas requirements. One of the most important results of this test was the lower gas requirements for the straight configurations concerning the diffuser-type injectors. This is due to the significant contribution of the evaporation part in the ullage. Two different discharge times have been evaluated, and as the ramp increases, the evaporated fraction increases, which has the most impinging effect on the propellant surface. This effect could be emphasized by lowering the straight pipe dimension, but under the 1/2-inch-diameter entrance, the dropoff at the beginning of the expulsion time would become prevalent.

Methodology

In this first relevant study, a combination of numerical method and test evaluation has been implemented. The latter was conducted with a 8 mm 304 stainless steel plate tank. The tank, spherical with an inside diameter of 686 mm and a total length of 2080, managed the heat dissipated by a vacuum jacket. A series of heat exchangers with valves introduced GOX with 116 K and 389 K temperatures with a max mass flow of 0.018 kg/s. The activation profile for the pressurization system was a simple ramp-hold-expulsion, with the pressure in the tanks controlled by a closed-loop circuit. A turbine-type flowmeter regulated the out-flow from the tank, and an orifice in the pressurant supply line was used to determine the pressurant flow rates. Various thermocouples were allocated inside the tank along the main axis in combination to realize a thermopile. The gas temperature distribution in the ullage, one of the most important effects for evaluating performance, has been obtained by stacking different thermopiles with platinum resistor temperature sensors. Each level of the thermopiles was at 7.6 cm, except for 5 at the top of the structure, which has a distance of 5.1 cm. All these positions were made to minimize the error in the single channel for the measurement (figure 2.12).

The procedure was simple: first a purge with He, then a filling operation with LH2 to a height of 49.8 cm from the top of the tank. After the loading process, the tank was pressurized with a controlled speed at the operational pressure. Then, the pressure was maintained constant for 50 s to stabilize the inside temperature. Next was the expulsion of the pressurant, a phase in which initially, the pressure and the temperature suffered an instability for the dropoff, which ended around 10 – 15 s. The expulsion is ended when the propellant reaches 212.3 cm from the top of the tank.

Geometries

The six geometries presented in the studies were divided into two groups, the first five were diffuser injectors (i.e., cone 2.11c, hemisphere 2.11b, radial 2.11a, reverse 2.11e, and multiple screens 2.11g). Designated to diffuse the pressurant gas uniformly throughout the ullage volume, all with the same area, and the last of this category, *multiple-screen* geometry made by a radial one with a spreader screen mounted orthogonally to the tank centerline. Another category was the straight pipe, which concentrates the flow towards the liquid surface. Three dimensions for the straight pipe (2.11h) have been tested: 1, 3/4, and 1/2 inches, respectively.

Parameters

As reported above, the mass of the pressurant gas could be a parameter used to compare the performance of the six injector geometries. This study is the case where t_f mean final time, and

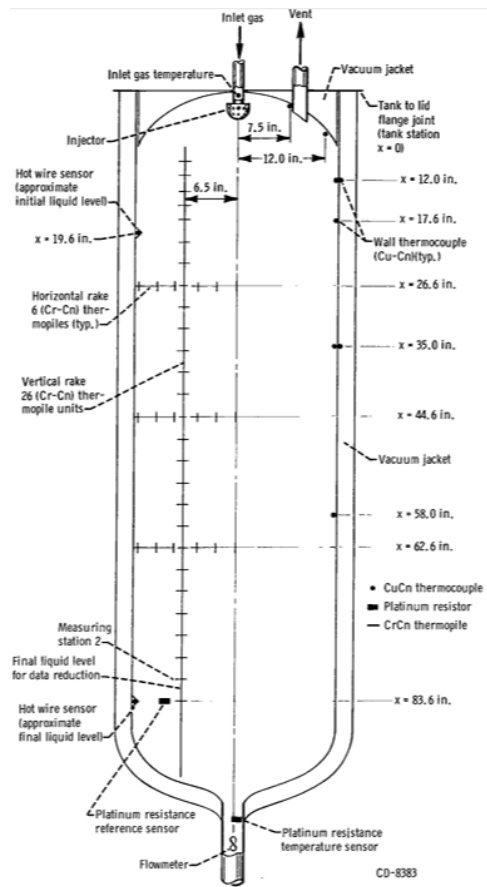


Figure 2.12: Instrumentation inside the tank[10] figure 4 page 8

t_i initial time in the numerical integration:

$$m_{a,i-f} = \int_{t_i}^{t_f} K \cdot y \cdot D^2 \cdot C \cdot \sqrt{\rho \cdot \Delta P} dt, \quad (2.1)$$

where:

- C orifice coefficient of discharge
- D orifice diameter, in.
- ρ : density, lb/cu ft
- y : net expansion factor for compressible flow through orifices
- ΔP : differential pressure, lb/sq in.
- y : net expansion factor for compressible flow through orifices

Focusing on the heat balance, the integration over the time of expulsion, with constant tank pressure, is reported as:

$$\int_2^3 \delta m_a \cdot h_a - \int_2^3 \delta m_T h_T = \int_2^3 \delta Q_l + \int_2^3 dH, \quad (2.2)$$

where the limits of the domain of the integral, respectively 2 and 3, correspond to the pressurization phase. The contributes are:

- $\int_2^3 \delta m_a \cdot h_a$: Energy introduced by pressurant gas
- $\int_2^3 \delta m_T h_T$: Energy leaving by the mass transfer between ullage and liquid
- $\int_2^3 \delta Q_l$: Heat dissipated
- $\int_2^3 dH$: Total change in enthalpy

The terms can be grouped into three categories in the study: enthalpy input by the pressurant, total change in the entropy and energy lost. Each term can be evaluated individually in the following manner:

Enthalpy input:

$$\int_2^3 \delta m_a \cdot h_a = m_{a,2-3} \cdot h_a, \quad (2.3)$$

with the enthalpy evaluated a time-weighted average inlet temperature and pressure.

Total ullage enthalpy:

$$\int_2^3 dH = \int_{V_3} \rho(T) \cdot h(T) \delta V - \int_{V_2} \rho(T) \cdot (T) \delta V, \quad (2.4)$$

with the density and enthalpy function of the temperature at constant pressure.

Energy loss:

$$Q_{L,2-3} = \int_2^3 \delta m_T \cdot h_T + \int_2^3 \delta Q_l. \quad (2.5)$$

The quantity $\int_2^3 \delta m_T \cdot h_T$ represent the mass transfer between liquid and ullage. Instead, the $\int_2^3 \delta Q_l$ represent the total heat dissipated, divided in two contributes, namely 1) the heat lost to the tank wall $\int_2^3 \delta Q_w$ and 2) the heat lost to the propellant surface $\int_2^3 \delta Q_b$:

$$\int_2^3 \delta Q_b = |(h_{fg} \cdot m_t) + Q_s. \quad (2.6)$$

At the same time, the heat towards the wall can be calculated for each transducer as follows:

$$\int_2^3 \delta Q_W = \sum_{i=1}^7 [\delta m_w \int_{T_2}^{T_3} c_w \cdot (T_w) dT_W]_i, \quad (2.7)$$

where:

- m_w stand for the tank mass
- $c_w(T_w)$: specific heat of wall
- T_w : wall temperature

The heat transferred to the propellant is composed of three parts:

$$\int_2^3 \delta Q_b = \int_{m_3} h_b \cdot \delta m_b - \int_{m_2} h_b \cdot \delta m_b + \int_2^3 h_b \cdot \delta m_{bl} - \int_2^3 \delta m_T \cdot h_T \quad (2.8)$$

The first two terms on the right part of the equation represent the final and the initial bulk liquid enthalpy. Furthermore, the $\int_2^3 h_b \cdot \delta m_{ml}$ and $\int_2^3 \delta m_T h_T$ terms represent, respectively, the enthalpy expelled and the enthalpy gained by propellant. But in this investigation, the direct value of Q_L could not be made, so the total energy lost was therefore evaluated by subtracting the change in enthalpy of gas between the initial and final state from the enthalpy added to the system during expulsion.

All these considerations were vital for defining the efficiency parameter and the models used in the current thesis. The considerations about efficiency were based on this study.

Conclusions

During the overall tank cycle as presented in [10], the total pressurant gas added in the ullage, which varies from the 17.5% and 21.6%, when using the diffuser-type injectors was greater than the one used in the straight pipe configurations, and this in both of the tank cycle time tested (215s and 493s). At the same time, the mass present in the ullage after the ramp time with the straight pipe was two times that for the diffuser type. Whereas for the latter the fractions were principally for condensation, for the straight pipe was evaporation. Again, during the expulsion period, the diffuser-type injectors were the most demanding for the gas pressurant, with mass transfer by condensations. Among the diffuser-type injectors, the multiple-screen version was the most gas-demanding; in contrast, the cone diffuser type was the least gas-demanding. In fact, from the multiple screen to the cone, the study reports that the pressurant gas saves 8.9% of the gas mass for the shortest tank cycle and 6.9% for the 400s gas cycle. For the straight pipe, the mass saved was the 29.7% for the shortest tank cycle and 16.8% for the 400s cycle. Another influential factor for the straight pipe injectors was the ramp time; in fact, a shorter ramp time means more mass evaporated from the propellant to the ullage. The reason is simply the more intense impingement on the liquid surface; the same result can be achieved with a decrease in the pipe's diameter. The reduction of the mass of pressurant is due to the high fraction of the vaporization during the expulsion. A decrease in the diameter (3/4in 1/2in) of the pipe can

amplify the effect of the gas required but at the same time can realize a pressure dropoff in the tank, causing instability of the pressure. This behaviour was noted with 1/2in diameter.

Temperature profiles were obtained right after the expulsion period to better understand the difference between the different injectors' gas requirements. Both vertical and radial temperature disposal where shown. For the diffuser type, the axial temperature is linear from the ullage diffuser exit section ($T \approx 277K$) to the liquid ($T \approx 41K$). The radial profile instead is constant for different heights, except for the series of transducers allocated at the diffuser height. In

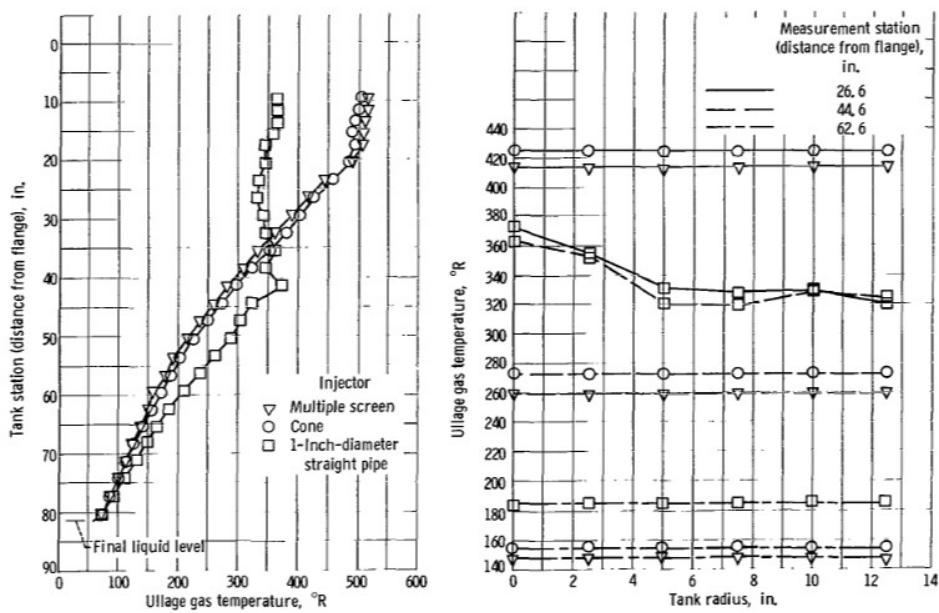
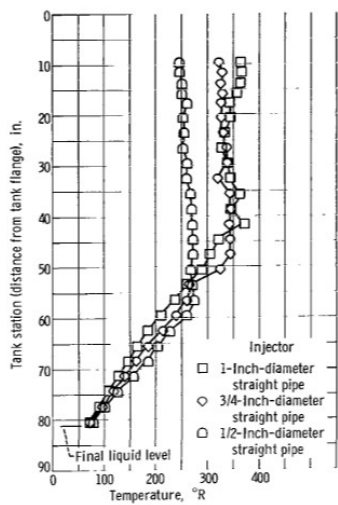


Figure 2.13: Temperature profile from [10] figure 12 pag 24

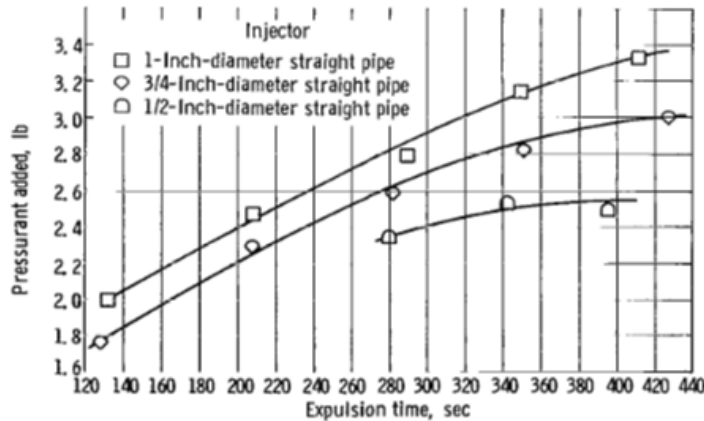
the straight pipe, in contrast, in the axial temperature, the first section is constant, then moving towards the liquid, the temperature decreases linearly. The radial profiles instead are lower near the tank wall and higher in the centre of the tank. The study's conclusions continue with the valuation of the heat input to the tank wall using a 1 – inch diameter straight pipe; for this configuration, the heat flow are 45% and 21% less compared with the heat flow for diffuser-type injectors, respectively, during 130 s and 400 s expulsion time. The differences between the two cases are the different ullage temperatures near the walls. The walls represent the larger part of the heat lost, so optimizing the distribution of the gas could mean better performance.

2.2.3 Reference to CFD Studies

Other studies have confronted the evaluation and the diffuser design processes using a modern approach, with the CFD, computational fluid dynamics. In [65] is presented the attempted study of pressurization performance during propellant ejection from a tank containing hydrogen by vaporized propellant or helium. Several influencing factors are addressed in this study, including:



(a) Axial temperature for different straight pipe dimensions figure 16 pag 27 [10]



(b) Gas required for different dimensions figure 17 pag 28 [10]

Figure 2.14: Comparison of axial temperature and gas required for different pipe dimensions

inlet gas temperature, wall thickness, outflow rate and injector structure.

As mentioned above, the study uses a modern approach by CFD model with FLUENT 6.3 software, employed to be able to simulate interface phenomena inside the reservoir by applying the fluid volume method (VOF)² with mass flow conditions for both gas inlet and outlet from the reservoir.

In this case, the tank was a 3.35m diameter tank, 10m height, and 3mm thickness. The external surface has an adiabatic condition to facilitate the analysis, and the gas properties in the ullage are a function of the temperature.

Methodology

The CFD model presented in [11] is comprehensive of the propellant's phase change when pressurized with the evaporated propellant. Furthermore, it is based on different hypotheses:

- **Ideal Gas Model:** Used to calculate the gas density.
- **Adiabatic Boundary Conditions:** Applied to the external surface of the tank.
- **Phase Change Model:** Used to account for mass and heat transfer associated with the phase change process.

²VOF, The Volume of Fluid (VOF) method is a modeling technique used in computational fluid dynamics (CFD) to track the interface between immiscible fluids. It is based on a conservative transport equation for the fluid volume fraction, allowing for efficient handling of free surfaces. Although simple and versatile, the VOF can exhibit interface smearing issues, requiring advanced advection schemes to maintain accuracy. It is particularly useful in simulations where the interface between two immiscible fluids needs to be determined and tracked accurately.

- **Boussinesq Approximation:** Used to account for changes in liquid density with temperature.
- **Two-Phase Mesh:** Adopted to describe fluid flow and heat transfer within the tank.
- **Low Reynolds Number Model:** Used to account for the effect of fluid-solid heat transfer.

The study takes advantage of the simulation in the axial symmetry of the tank's geometry. For this reason, a 2D axial-symmetry model is more convenient. The tank, furthermore, is divided into two regions, one with a structured grid, including the near wall region, and the internal tank, where unstructured grids are preferred. The structured part presents an increase in size to capture the steep gradient near the wall, with the distance from the near wall fluid and the tank wall small enough to ensure a complete resolution of the region. The unstructured one is made to lighten the simulation. A sensitivity analysis for this case results in $0.28E + 05$ cells sufficient to capture all the aspects of the simulations.

The validation of the CFD model presented in [11] is based on a discharge test conducted at Lewis Research Center. In the comparison between the CFD and the test, it can be noted that the gas required in the CFD model is always smaller than the corresponding experimental data, but the temperature profile is a little bit higher. The study indicates the cause of the deviation in the lack of consideration of the hardware inside the tank. In general, there is a good agreement.

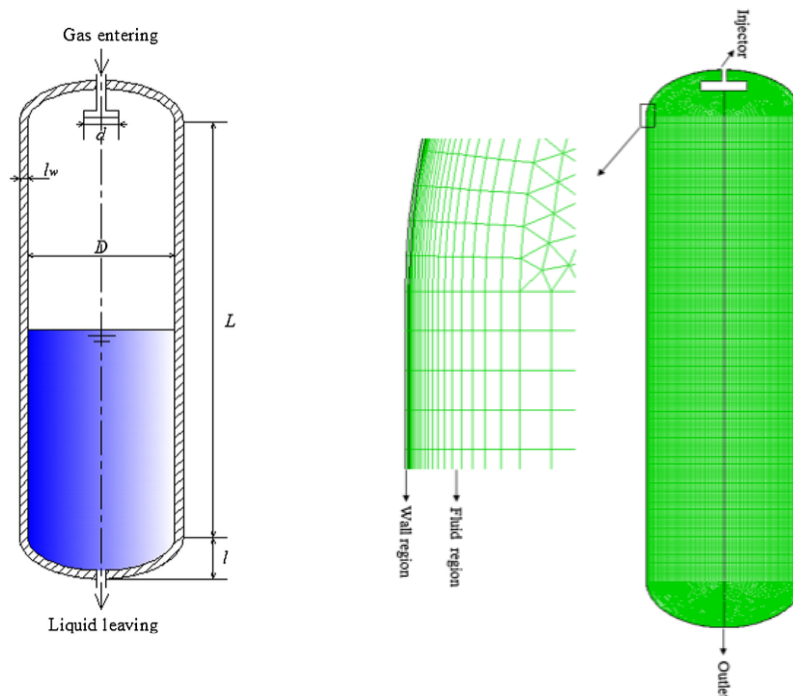


Figure 2.15: Schematic tank numerical investigation (Figure 1 in [11]) (left) and grid used for CFD simulation (figure 2 in [11] (right))

Conclusion

The results of this study provide valuable information for the design and optimization of diffuser injectors. Numerical implementation with the CFD model made it possible to analyze various factors' influence on a cryogenic tank's pressurisation performance, highlighting the importance of inlet gas temperature, injector structure, and liquid. Here briefly are reported the main conclusions, much of which reflect the study previously presented.

1. **Inlet Gas Temperature:** The temperature of the pressurant is a key parameter, increasing the inlet gas temperature, in fact, reduces the gas requirement, improving the efficiency of the pressurization system.
2. **Inlet Gas Temperature Ramp Time:** The ramp time is a factor of influence process, and a ramp-up time, using a straight tube injector, can cause excessive pressure drop at the beginning of the discharge.
3. **Wall Thickness:** A thin wall to construct the tank reduces the gas requirement. That is because a thicker wall means a bigger capacity for heat absorption, an absorption capacity that grows with the expulsion time. After all, it increases the surface exposed to the pressurant.
4. **Drain Rate:** Increasing the drain rate reduces the gas requirement. That is the opposite effect of a long expulsion, which means a longer heat dissipation to the tank wall, which represents the heat sinks.
5. **Injector Structure:** Using a straight tube injector can significantly reduce the gas requirement but leads to substantial loss of liquid propellant and high residual gas weight. Similarly to the previous study [10], this is thanks to the evaporation.

2.2.4 Thesis on Diffuser for High-Altitude Rockets

One of the most relevant work on the pressurization LPRE with the diffuser is from [66], here is presented a combination of lumped numerical simulation and test of a pressurization system in a cryogenic liquid propellant tank for a student sounding rocket.

The study presents the investigation to realize a simple and low-cost diffuser for a 30L oxygen cryogenic tank, realized for the student rocketry team DARE (Delft Aerospace Rocket Engineering) 2.16, to optimize the required pressurant mass. The study starts from the conclusion of the previous test, which observed more efficiency for the axial configuration. However, a better distribution of the pressurant in the tank could significantly improve performances. From this first step, the study presented a new geometry concept for the diffuser, the *Vortex* configuration, a geometry that uses the principle of the *Hilsch tube*.

The *Hilsch tube*, also known as *Ranque-Hilsch tube* or *vortex tube*, divides a compressed inlet gas in two flows, one hot and the other cold. That is obtained by an inlet gas which enters tangentially, creating a vortex inside; the circulating flow hits the bottom of the tube, dividing with the hot one exit from the lower part of the tube, and the cold travels through again the centre of the tube. The principle of sending the hot flow directly to the propellant and letting the cold one travel along the tank walls can be very useful for minimizing the heat dissipated.



Figure 2.16: Stratos II+ comparison and mission patch

Methodology

The study consists of two parts: numerical analysis and test, to compare the collapse factor calculated and the one obtained by testing. The first is a 1D numerical lumped simulation. The model comprises 8 different nodes, representing the different parts of the liquid inside the tank. The model calculates the energy and mass between the nodes at each time step. The tank's wall comprises two parts, the first for the ullage and the second for the propellant. The conduction heat is modelled by the use of the transfer law by Newton's law; instead, for the convection, the correlations used are made using standard correlations. The main problem was modelling the heat flow during the model's development. Focusing only on free convection eliminated the applicability. For the testing side, an entire hardware set-up was prepared. To avoid all the problems linked with oxygen, a 30 L tank designed to contain nitrogen was used

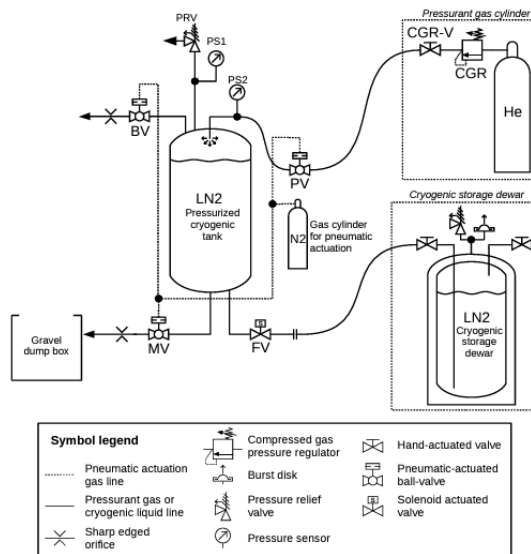


Figure 2.17: Scheme of feeding sounding rocket

as a propellant. To constantly monitor the conditions, a pressure regulator controls the helium adduction in the entry tank line, and the pressure/temperature is positioned at a strategic point inside the tank. Another pressure regulator realized the nitrogen exit and expelled, simulating the nominal mission profile for a sounding rocket. The pressurization test procedure comprised a traditional ramp-hold-expulsion profile and a depressurization phase. The conditions are here briefly reported:

Configuration	Geometry Details
	8 holes, 2 mm diameter
	No holes
VORTEX	1 mm holes, spaced 2 cm apart

Table 2.8: Operating conditions and geometry configurations.

The helium flow was measured using mass thermal flowmeters, which evaluated the mass flow by using the amount of heat required to maintain a constant temperature difference between two sensors. Level sensors were used to measure the mass inside the tank, which measured the change in electrical capacitance caused by the change in liquid level inside the tank. The tank was weighed for the initial and final mass, and the respective expelled mass was calculated by subtraction. In addition to the innovative vortex design, the axial and radial injectors were tested, but unfortunately, the vortex had problems during the test campaign.

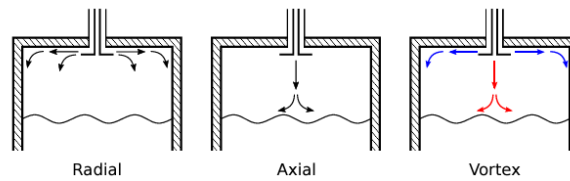


Figure 2.18: Axial, radial and vortex scheme

Conclusions

It is reiterated that the study's objective was to evaluate the pressurization efficiency of three possible injection configurations by comparing the collapse factor calculated by a numerical model and that obtained from emptying tests. At the end of the study, the authors report that the radial diffuser minimized the interaction with the tank wall but required a larger mass of pressurant. In contrast, the axial configuration requires less mass, so the efficiency is higher, but the interaction with the propellant is intense. The numerical models presented evaluated a collapse factor 10%–25% lower than the tested value, confirming the tendency to underestimate the collapse factor from the numerical model compared to the test. The temperature profile was, instead, quite in accordance with the numerical models, with the axial injectors creating a radial gradient and the radial creating a vertical one. Despite the precision, the numerical models need more accuracy to include all the aspects.

2.3 Identified Criticalities

All the studies above have been crucial for the activities reported in this work. The conclusions of the previous one were a starting point for the process presented here. The energy balance with the confront of the fractions dissipated towards propellant or walls was taken from the [10]; for setting the CFD model and the mesh realization, the [65] was an inspiration. The principles used for the computational model were similar to those presented in [66]. Looking at these studies, some common features jumped out at once. These included the large number of variables influencing the analysis process. A high number of unknowns to be taken into consideration often leads to the study of only a few well-defined sub-cases, thus relegating all previous work to specific applicability and presenting a high degree of rigidity. Rigidity was expressed through a lack of ability to test different combinations of pressurizer and operating conditions. Often the models were linked to tests conducted in a second phase, translating into many studies, each relating to a possible handful of cases. The lack of flexibility makes their use impractical, especially for possible industrial applications. This was because the studies were more oriented toward understanding the behaviour and efficiency of pressurization systems, thus being academic. Lacking an illustrative purpose for sizing. This thesis attempts to fill this lack

by applying a more practical approach by introducing the possibility of implementing different configurations, making the study more useful from a different point of view.

Another substantial limitation characteristic of previous studies is the simulation-test combination. This combination helps check the accuracy of numerical models but is impractical because it requires building an entire test set-up. Tests must be strongly related to the case at hand, thus requiring a fair degree of similarity with the operating configuration. The entire set-up must meet requirements and standards, including the presence of valves, flowmeters, transducers, and procedures. This is necessary for an entire test campaign, which becomes unavoidable during a Critical Design (CDR) phase, but a preliminary sizing phase could be unnecessarily onerous and of little benefit. The alternative to a test could be a campaign of CFD simulations, which is less demanding in terms of practical set-up and has no security requirements. However, as we will see in the next chapter, a series of computational fluid dynamics simulations without a pre-selection for dimensions or conditions could be even more time-consuming than a test campaign. So, the possibility of having a flexible and fast step before a more detailed study can be very helpful in the process.

One last critical issue is the discrepancy of the collapse factor and the difficulties in correctly predicting the value. Therefore, using the collapse factor as an efficiency parameter could be misleading. The most accurate test has a 10% discrepancy with the collapse factor obtained with numerical simulations, a good result but too approximate for an optimization phase but too approximate for a precise sizing process. From this initial consideration, the possibility of using dissipated heat as an evaluation element during this sizing phase is revisited.

Chapter 3

Design Methodology

3.1 Description of the Proposed Method

The current design methodology is based on the complementary work between a code script made by Python¹ and a series of CFD analyses, using Fluent² software. The approach is to define reference sizes in a wide range of dimensions and an evaluation between the and inlet geometries by code, then to verify making a more precise fluid dynamics analysis in different possible regimes. And the end of the work, with the dimension and configuration chosen, the optimization of the geometries is faced. The objective is to define step-by-step processes to evaluate and define the dimensions for pressurant gas injectors into cryogenic propellant tanks in LPRE. A methodology that must be as easy and general as possible to use in a major number of cases. Furthermore, the use of this process is thought to be used in, particularly for industrial applications, so needs to be clear and comprehensive, The author is conscious of the difficulties involved in such work. In fact, it took more than 8 months to complete, and despite all this time, the work presented different important limits. The thesis presented here should not be considered a concluded work but can be seen as a spark for further and future work.

As presented above, the diffuser is an element, part of a subsystem; for this reason, when its sizing process begins, the project is usually at a component level; when almost all of the system is defined, the requirements are implemented, and the operational conditions are determined. All these corners are the first step of the processes; the definitions of parameters such as pressurant gas temperature and mass flow rate, propellant temperature, species, and operational pressure are vital, as are the dimensions and geometry of the tanks. The current work will try to obtain the best possible configuration from all these parameters. The process here will be presented in

¹<https://www.python.org/> is a high-level programming language, widely used for its simplicity and versatility

²ANSYS Fluent, <https://www.ansys.com/products/fluids/ansys-fluent> is a computational fluid dynamics simulation software used to model fluid flow

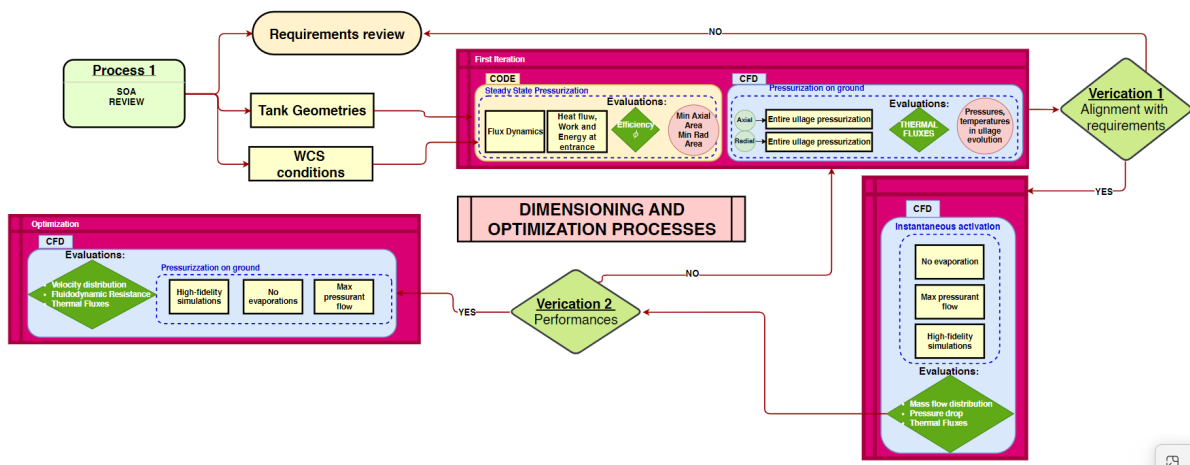


Figure 3.1: Methodology scheme

a study case, taken from literature and applied linearly, but the entire process can be repeated if some pressurization process requirements do not comply or if the performances are not as expected.

3.1.1 Core-hours evaluation for fluid-dynamics analysis

As presented in the previous sections, the process is divided into different sections, making them more flexible and allowing different variables to be assessed together, thus shortening the time required. In chapter one, a brief list of all influencing factors has been made, identifying those of the first-order. Obviously, the immediate use of CFD analysis would be the most logical solution once the operating conditions have been defined, but in this case, starting with this approach means spending a lot of time completing at least one simulation for each dimension. This brute force scenario would require extraordinary time and calculation effort. To estimate the total computation time required for all CFD simulations, we need to consider the following factors:

- Number of cells: Assuming a range from 400,000 to 1,000,000 cells³.
- Time step: 0.01 seconds.
- Pressurization processes duration: 30 seconds.
- Iterations per time step: 30 iterations (Default Fluent©value).
- 4 CORE for each analysis.

³Range defined from experience; the minimum ensures sufficient simulation results, the maximum reflects tool limitations.

The calculation of the Total number of time steps is:

$$\text{Tot.numb. time steps} = \frac{\text{Sim. duration}}{\text{Time step}} = \frac{30}{0.01} = 3000 \text{ time steps}$$

Fluent set the value of 30 iterations for each time step to reach the default residual threshold.

$$\text{Tot. numb. iterations} = \text{Tot time steps} \times \text{Iter. per time step} = 3000 \times 30 = 90,000 \text{ iter.}$$

The time required for a single iteration in a CFD simulation depends on various factors, including mesh complexity, boundary conditions, problem physics, and processor capabilities. However, we can make an estimate based on typical experiences.

For a typical processor of personal machine, and a mesh ranging from 400,000 to 1,000,000 cells, the time per iteration might vary significantly. Let's assume an estimated range for iteration time:

- For a mesh of 400,000 cells, the time per iteration could be approximately 1 second.
- For a mesh of 1,000,000 cells, the time per iteration could be approximately 2.5 seconds.

For the worst-case scenario (1,000,000 cells):

$$\text{Total simulation time} = 90,000 \text{ iterations} \times 2.5 \text{ seconds per iteration} = 225,000 \text{ seconds}$$

$$\text{Total time in hours} = \frac{225,000}{3600} \approx 62.5 \text{ hours}$$

For the best-case scenario (400,000 cells):

$$\text{Total simulation time} = 90,000 \text{ iterations} \times 1 \text{ seconds per iteration} = 90,000 \text{ seconds}$$

$$\text{Total time in hours} = \frac{90,000}{3600} \approx 25 \text{ hours}$$

These values refer to just a single analysis. Analyzing each possible entry dimension in a range of 16 (the value taken as an example) possible sizing and for both axial and radial configuration, we obtain a total of 32 analyses, which is the minimum required. So the total hours for a 30 possible analysis are:

Worst-case scenario (1,000,000 cells):

$$\text{Total time for all combinations} = 62.5 \text{ hours} \times 32 = 2000 \text{ hours}$$

Best-case scenario (400,000 cells):

$$\text{Total time for all combinations} = 25 \text{ hours} \times 32 = 800 \text{ hours}$$

Using 4 cores: For the worst-case scenario (1,000,000 cells):

$$\text{Total simulation time for all combinations with 4 cores} = \frac{2000 \text{ hours}}{4} = 500 \text{ hours}$$

For the best-case scenario (400,000 cells):

$$\text{Total simulation time for all combinations with 4 cores} = \frac{800 \text{ hours}}{4} = 200 \text{ hours}$$

Core-hours represent the product of the number of cores used and the execution time. While the execution time is reduced by dividing by the number of cores, the core-hours remain constant.

Worst-case scenario (1,000,000 cells):

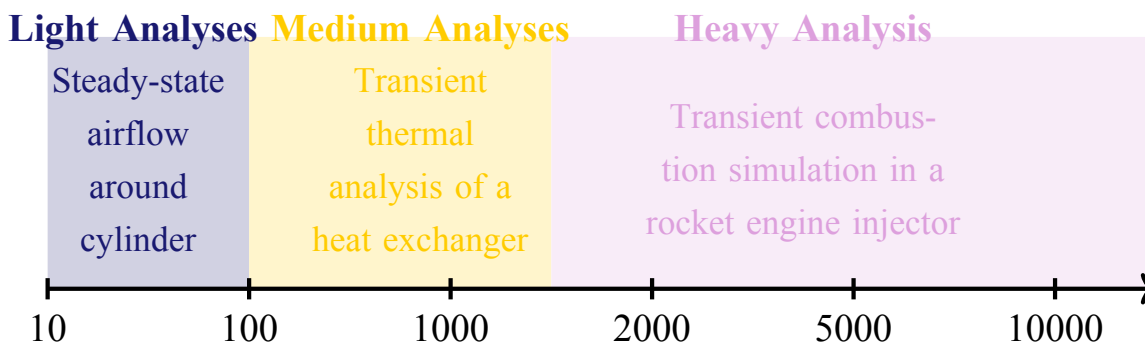
$$\text{Core-hours for all combinations} = 2000 \text{ hours} \times 1 \text{ core} = 2000 \text{ core-hours}$$

Best-case scenario (400,000 cells):

$$\text{Core-hours for all combinations} = 800 \text{ hours} \times 1 \text{ core} = 800 \text{ core-hours}$$

- Total time for all combinations:
 - Worst-case scenario (1,000,000 cells): 500 hours
 - Best-case scenario (400,000 cells): 200 hours
- Core-hours for all combinations:
 - Worst-case scenario (1,000,000 cells): 2000 core-hours
 - Best-case scenario (400,000 cells): 800 core-hours

This estimate may vary depending on the actual specifications of the laptop and the optimization of the CFD software.



This brute force approach would be expensive in computational and time terms, straddling the line between medium and high computing power simulations. So, using code to understand preliminary physics and phenomena is essential to save time and cost.

3.1.2 Preliminary Code

The code used for the first evaluation has been written using Python©, is based on a *main* code "Alg_DIFF_steady_state" containing different section:

SECTION 1: INPUT

SECTION 2: PRELIMINARY CALCULATIONS

- 2.1: Creation and Initialization of New Iterations
- 2.3: Ullage-tank surfaces and volumes
- 2.4: Calculation Chemical Properties for Pressurant and propellant
- 2.5: Ullage Mixing Properties

SECTION 3: FOR LOOP:HEAT CALCULATIONS

- 3.1: Calculation of Dimensionless Velocities with For Loop
- 3.2: Calculation of Dimensionless Parameters
- 3.4: Heat evaluation
- 3.4: Data Extraction from the Iteration Pools

SECTION 4: WORK, EFFICIENCY, AND NEW VARIABLES

- 4.1: Calculation of Diffuser Occupancy in the Ullage
- 4.2: Calculation of HEAT LOST to different surfaces[W]
- 4.3: Sum of Contributions (Q_{EVAP} [W] + Q_{WALL} [W]) for Both Configurations (Radial and Axial)
- 4.4: Calculation of Pressurization Work, energy entrance and Efficiency

SECTION 5: CREATION OF GRAPHS

SECTION 6: SAVE AND PLOT

The main code presents different links to files containing the functions to maintain the code as readable and flexible as possible.

Calc_chemical_species_propt

Molar_mass_fraction_ullage

calc_ullage_propt

calc_adimem_local_velocity

calc_local_lenght	calc_first_conf_func
calc_num_adm	plot_graph_only_V1
calc_AXIAL_DIFFUSER	new_variables_func
calc_RAD_DIFFUSER	penetration_verification
extract_from_dict_V1	calc_ullage_ingombro
calc_heat_dissipation	calc_ullage_volume

The sources from which all the information has been taken are:

1. *Chemical Kinetics in Combustion and Reactive Flows Modeling Tools and Applications*, Chapter 9: Pressurization of Liquid Propellant Rocket Engine Tanks[29].
2. *Experimental and Analytical Studies of Cryogenic Propellant Tank Pressurant Requirements*[67]
3. *The Way of Determining the Optimal Parameters of the Propellant Tank Pressurization Gas in the Feeding System for Liquid Rocket*[37].
4. *Analytic Modeling of Pressurization and Cryogenic Propellant Conditions for Liquid Rocket Based Vehicle Designs*[68].
5. *Multi-Node Modeling of Cryogenic Tank Pressurization System Using Generalized Fluid System Simulation Program*[69]

The code wants to represent a 0D dimensional steady state processes, during the pressurization of the tank by using the pressurant. The core of this code is the *for* cycle where given the operational conditions as `m_gas_dot`, `pressurant temperature`, `tank dimensions`, `propellant temperature` and a series of possible entrance dimensions, *for* each of them are evaluated the entry velocity, the local dimensional numbers (Re, Ri, Gr ecc). Defined the range, as presented in Chapter 1-Dimensionless Number 1.5, the type of dominant phenomena, between natural and forced, or the regime of the flow, laminar or turbulent, can be easily determinate. For the identified regime and convection type, for each case, there is a different correlation to evaluate first the heat flow coefficient, h_{sc} and then the heat flows with the relationship(1.14).

Assumptions

To simplify the work, the following assumptions were made given the high degree of physical complexity of many phenomena involved and the desire to focus on the influence of the pressurizer in the ullage rather than simulating the entire internal environment of the tank.

- The ullage is schematized by 4 main nodes.
 1. Pressurizing gas - N1
 2. Liquid propellant - N2
 3. Tank wall - N3
 4. Ullage mixing gas - N4

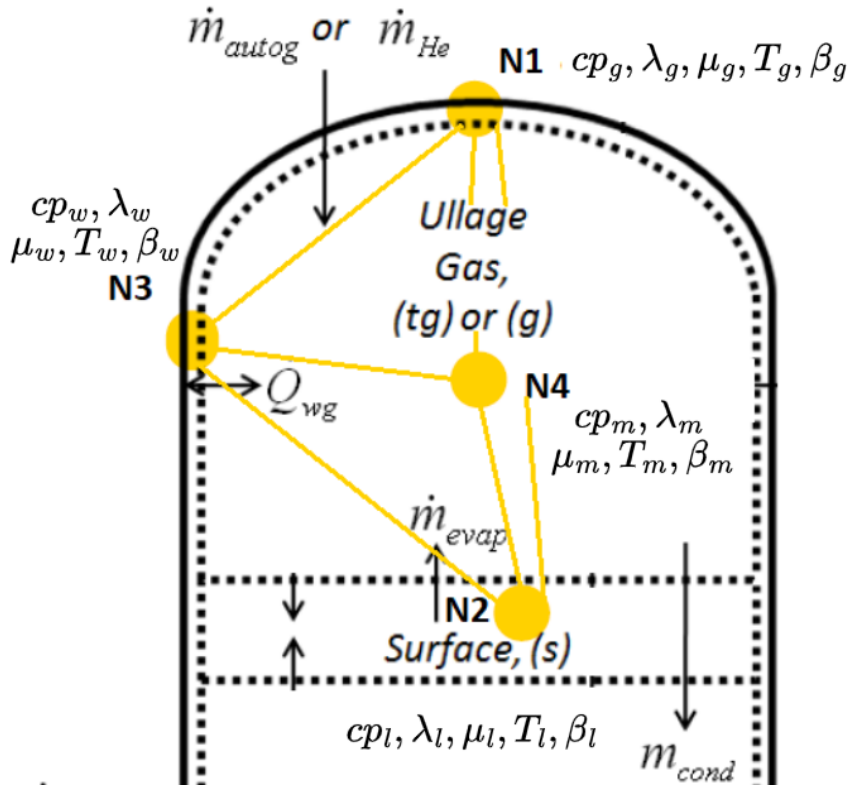


Figure 3.2: Schematic representation of the ullage nodes

- The properties of the chemical species are considered constant, so we will respectively have:

$$\begin{aligned} \rho_g, c_{pg}, \mu_g, T_g, \beta_g, \lambda_g &\Rightarrow \text{Pressurant} \\ \rho_l, c_{pl}, \mu_l, T_l, \beta_l, \lambda_l &\Rightarrow \text{Propellant} \\ \rho_w, c_{pw}, \mu_w, T_w, \beta_w, \lambda_w &\Rightarrow \text{Wall} \\ \rho_m, c_{pm}, \mu_m, T_m, \beta_m, \lambda_m &\Rightarrow \text{Ullage gas mix} \end{aligned}$$

- Conservation equations of mass and energy are used among the individual nodes
- In the first version, a linear model of the HEpercentage will be introduced; subsequently, other models can be implemented.
- Incompressible ideal gas is assumed
- A stratification of the pressurizing percentage in the ullage is assumed with a well-defined linear trend. With a pressurizing percentage of 100% at the gas inlet (and 0% of propellant),

conversely, 100% of the propellant on the free surface (and 0% of pressurant). This type of stratification is not entirely correct, but it is chosen as an initial

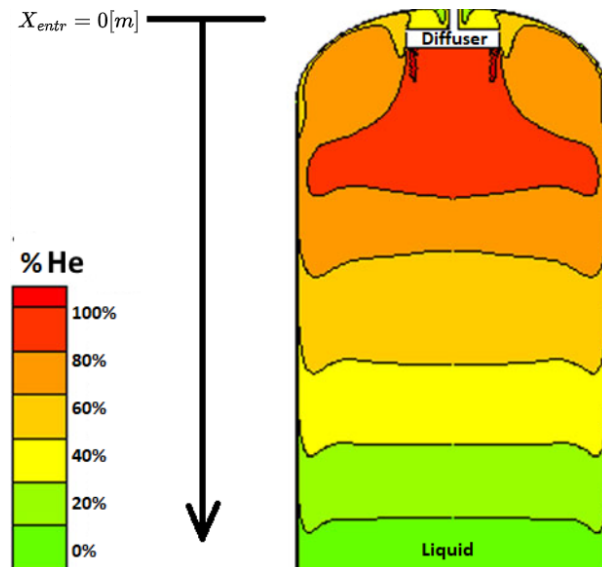


Figure 3.3: Pressurant percentage trend in the ullage zone

- The heat exchange at the wall occurs all localized at node N3 defined at a height that will coincide with the position entered in the program (x_{pos}). Whereas the evaporative flow occurs entirely at node N2, i.e., on the free surface of the propellant (x_{vapor}). The properties consistent with the position and distribution of the pressurizing percentage are used in both positions.
- Ullage properties at each level of filling are constant.
- Constant flow rate corresponding to the maximum value from the requirement.
- Tank approximated as a cylinder.
- Thermal conduction with the outside through the tank wall is not considered.
- The properties of the gas mix in the ullage are defined by a weighted average of helium and propellant vapour and the weight fraction is used.
- Temperature of the propellant (constant T_{liquid}) and also of the pressurizer (constant P).
- Evaporation not considered.
- No environmental or aerothermal heating.
- Inputs: For the correct functions of the code, some values must be known. At the typical dimensioning stage these values are already determined; the values are:

– **Propellant-Pressurant:**

* Options: He_LOX, He_LCH4⁴

⁴In this work, the pressurant choice is the HE because it represents the most common option. Other inert gas can be simply added

- **Gravitational Constant:** g * Diametro_tank[m]
- **Propellant & Pressurant Flow:** * Ullage_level %
 - * m_gas_dot [kg/s]
 - * t_scarica_press[s]
 - * t_scarica_prop[s]
- **Tank Dimensions:**
 - * R_dome [m]
 - * h_cilindric_bodm]
 - * Altezza_tank[m]
- **Diffuser Dimensions:**
 - * list_diff_dim⁵
- **Operative Conditions:**
 - * dati_tank_temp[K]
 - * Temp_ullage[K]
 - * Tank_Press_0[Pa]

Methodology

The code will represent on-ground pressurization, so the profile will be a constant steady-state pressurant mass flow rate in the tank. The system is based on determining the conditions, as it can be used for various operating requirements (Pressurization with gas at different temperatures, different tank sizes, etc.). Therefore, the data and geometries of the operational condition under study are collected.

1. **Sec 1: Input** Operational conditions, entered by the user of the code, some can be chosen from options such as whether to apply it to the He-CH₄ or the He-LOX pair. For reasons presented in Chapter 1 and for brevity, this work will focus on using liquid methane as a propellant and HE as a pressuriser. This does not deny the possibility of being able to use the same code for different chemical species, the implementation of the function in the relevant section would suffice.
2. **Sec 2.4/2.5/2.6:** From the conditions, the properties of each chemical species are derived, and through the stratification model, the combination of properties in the ullage is also obtained as a mix of propellant and pressurize. Once the evaluation positions have been defined, at the nodes' dimensions, the chemical species are evaluated using the library provided by Python©, CoolProp. CoolProp is an open-source Python library used for calculating of the thermodynamic and transport properties of pure fluids and mixtures. It offers various functions to determine density, enthalpy, entropy, heat capacity, viscosity, and thermal conductivity giving the temperature and pressure. It is particularly useful in chemical, mechanical, and thermodynamic engineering applications, where accurate knowledge of fluid properties is essential. In this case, the function Calc_chemical_species_propt allows the determination of helium, methane and oxygen properties. This function takes user-defined conditions

⁵Range of possible values[m]

such as the temperature of the chemical species and pressure as input and outputs a dictionary with all properties for the given position. The next step is the stratification model in the ullage, in this work, as presented in the previous section, for the first iteration a linear concentration of pressurant is considered. From a 100% of HE at the gas entry to a 0% at the propellant-free surface, implemented in the function `Molar_mass_fraction_ullage`, the output is the molar mass fraction of both pressurant and propellant vapour at the positions `x_pos`, and `x_vapor`. With the trend set and the chemical properties defined, as reported in [68] in the "Heat transfer" section, the mixture properties can be calculated in function of the molar (y_{vl}, y_{rg}) and mass fraction (Y_{vl}, Y_{vg}) at the defined position:

$$\rho_{tg} = \frac{m_{vl} + m_{rg}}{V_{tg}} \quad (3.1)$$

$$\beta_{mix} = \beta_{vl}Y_{vl} + \beta_{rg}Y_{rg} \quad (3.2)$$

$$\mu_{mix} = \frac{\mu_{vl}M_{vl}^{1/2}y_{vl} + \mu_{rg}M_{rg}^{1/2}y_{rg}}{M_{vl}^{1/2}y_{vl} + M_{rg}^{1/2}y_{rg}} \quad (3.3)$$

$$C_{p_{mix}} = C_{p_{vl}}Y_{vl} + C_{p_{rg}}Y_{rg} \quad (3.4)$$

$$k_{mix} = k_{vl}y_{vl} + k_{rg}y_{rg} \quad (3.5)$$

Recalling the subscript vl is for propellant vapour, and the subscript rg represents Helium gas.

3. **Sec 3/3.1/3.2:** For loop, for each diffuser inlet dimension (r_0 and b_0), the local velocities at the wall and on the free surface of the propellant are calculated, and from these, the non-dimensional numbers of the phenomenon are defined.

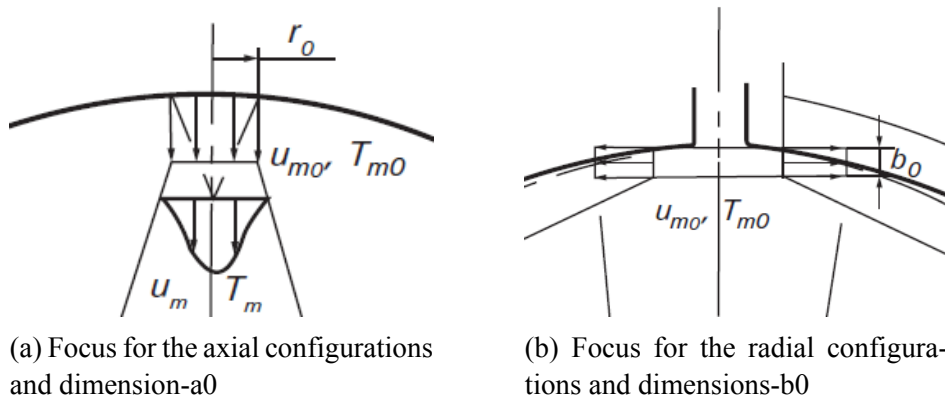


Figure 3.4: Image extracted from figure 9.5 Calculation schemes of pressurizing gas flows in the ullage pag 350 of [29]

$$\text{Re} = \frac{\rho \cdot V \cdot L^*}{\mu} = \frac{[\text{Inertial Forces}]}{[\text{Viscosity}]} \quad (3.6)$$

$$\text{Gr} = \frac{L^{*3} \cdot \rho^2 \cdot g \cdot \beta \cdot \Delta T}{\mu^2} = \frac{[\text{Buoyancy Forces}]}{[\text{Viscosity}]} \quad (3.7)$$

$$\text{Pr} = \frac{c_p \cdot \mu}{\lambda} = \frac{[\text{Kinematic diffusivity}]}{[\text{Thermal Diffusivity}]} \quad (3.8)$$

$$\text{Ra} = \frac{\beta \cdot g \cdot L^{*3} \cdot \Delta T}{\nu \cdot \alpha_0} = \frac{[\text{Buoyancy Forces}]}{[\text{Viscous friction}]} \quad (3.9)$$

The reported numbers serve to simplify the study of fluid mechanics; in fact, certain known ranges can be determined. The Reynolds number in this study is used in two separate definitions, the first relating to the definition of the value of the flow entering the tanks and locally respectively the definitions are:

Reynolds Number	Injector Type	Wall	Evap
$Re = \frac{\rho \cdot L^* \cdot u_m}{\mu}$ <p>Where L^* = local layer thickness and u_m = local velocities</p>		$L^* = l'_k \quad u_m = u'_{mk}$ $\rho = \rho_m \quad \mu = \mu_m$	$L^* = l_s \quad u_m = u_{ml}$ $\rho = \rho_l \quad \mu = \mu_l$
		$L^* = l'_k \quad u_m = u'_{mk}$ $\rho = \rho_m \quad \mu = \mu_m$	$L^* = l_s \quad u_m = u_{ml}$ $\rho = \rho_l \quad \mu = \mu_l$

Table 3.1: Reynolds Number Definitions for and Configurations

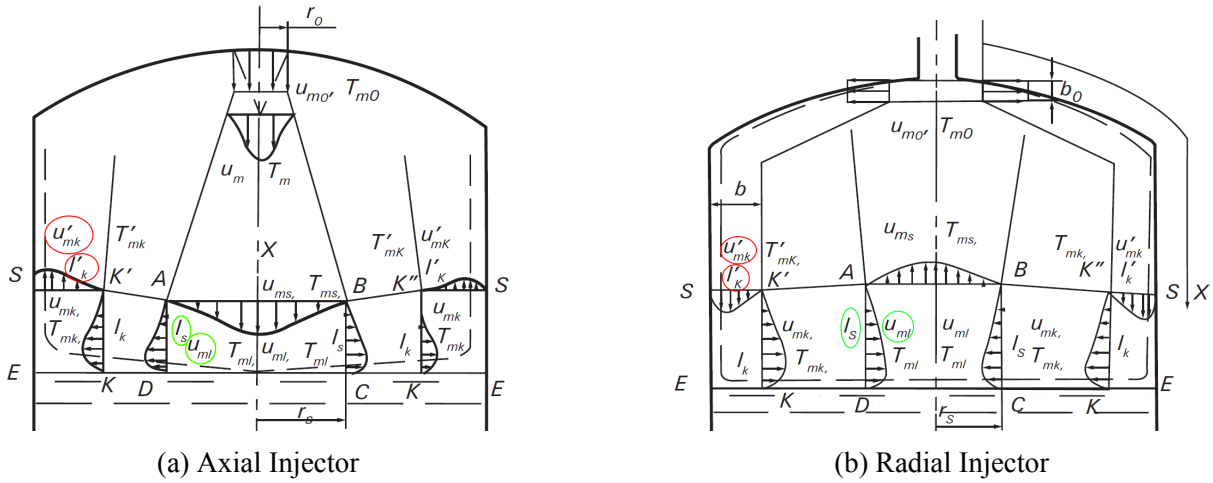


Figure 3.5: Zoom of Initial Emptying for Axial and Radial Injectors: Green circle for the Evaporation, Red for the wall

The subscript "m" stands for the ullage node N4 table-3.2, so properties of the ullage mixing, functions of the position of the node and the stratification model implemented. Instead, the subscript "l" stands for "liquid" node N1 table -3.2, function too of the stratification in the ullage and of the propellant species. For both wall and free surface phenomenons, the positions are fixed by the user (x_{pos}, x_{vapor}). For the local thickness, the values depend on the injection configuration of the radius of the tank R_t .

Each of these local velocities u_m is calculated in function of the θ (Ratio between pressurant and propellant temperature) and the distances from the entry ($x - x_{entr}$) of the HE species. For both, the relationships to evaluate them are presented in table 1.3, Chapter 1 As reported in [29], despite the different flows generated by the two different configurations, the flow path is similar to both of them. After the entry the pressurant flows free downside, along the wall for the radial, or direct to the propellant for the axial. But at this point the path changes, it makes a curvature and continues toward the center for the radial or to the tank's wall for the axial passing from free regions to a constricted one. This passage is important for evaluating the local velocities, in fact the transition change the formula used for the calculation. For the local dimensionless velocities in the axial configuration in the constricted area (\bar{u}_{avc1}), and for radial one (\bar{u}_{avc2}) [29] in equations (9 – 69, 9 – 70) reports that:

$$\bar{u}_{av1C}^2 = \sqrt[3]{\bar{u}_{av1G-G}^2 \left[\bar{u}_{av1G-G} - \frac{3}{2} K_1 (\bar{x} - \bar{x}_{1G-G}) \right]} \quad (3.10)$$

$$\bar{u}_{av2C}^2 = \sqrt[3]{\bar{u}_{av2G-G}^2 \left[\bar{u}_{av2G-G} - \frac{3}{2} K_2 (\bar{x} - \bar{x}_{2G-G}) \right]} \quad (3.11)$$

Where the \bar{u}_{aviG-G} and $(\bar{x} - \bar{x}_{iG-G})$ are respectively the velocity and the position from the entrance to the transition free flow to constricted flow. K_1 and k_2 are two constants:

$$K_1 = g \left(\frac{\rho}{\rho_0} - 1 \right) \frac{r_0}{u_{av0}^2} \quad ; \quad K_2 = g \left(\frac{\rho}{\rho_0} - 1 \right) \frac{b_0}{u_{av0}^2} \quad (3.12)$$

Whit ρ = density at the transition point [kg/m^3], ρ_0 = density at the gas entrance [kg/m^3], r_0 and b_0 dimensions of the diffuser entrance [m] and u_{av0}^2 velocity at the entrance [m/s]. In this work the transition is assumed to happen at the local thickness height from the liquid, so $(\bar{x} - \bar{x}_{iG-G}) = h_{liquid} - l_k$ for the axial configuration, and $(\bar{x} - \bar{x}_{iG-G}) = h_{liquid} - l_s$ for radial one. The dimensionless velocities for the transition from free-constrained zones and the local velocities for wall and propellant heat dissipation are calculated at specific positions $x = x_{pos}$ and $x = x_{vap}$, using equations (3.10) and (3.11).

For the Grashof number, the considerations are similar. The properties used to evaluate the heat to the walls are those from the mixing ullage at node N3, subscript "m". Instead of the flow through the propellant, the properties are those from the combination near the free surfaces of the propellant, nodes N2.

Grashof Number	Injector Type	Wall	Evap
$Gr = \frac{g \cdot \beta \cdot (T_s - T_\infty) \cdot L^*3}{\nu^2}$ <p>Where</p> <p>$L = \text{characteristic length}[m]$</p>		$L^* = l'_k, \beta = \beta_m$ $\nu = \nu_m$ $T_S = T_w, T_\infty = T_m$	$L^* = l'_k, \beta = \beta_l$ $\nu = \nu_l$ $T_S = T_l, T_\infty = T_m$
		$L^* = l'_s, \beta = \beta_m$ $\nu = \nu_m$ $T_S = T_{wa}, T_\infty = T_g$	$L^* = l'_s, \beta = \beta_l$ $\nu = \nu_l$ $T_S = T_l, T_\infty = T_m$

Table 3.2: Grashof Number Definitions for and Configurations

For the Prandtl number, used in the determination of the Stanton number for the forced convection flow, similar considerations are made:

Prandtl Number	Injector Type	Wall	Evap
$Pr = \frac{c_p \cdot \mu}{\lambda}$		$c_p = c_{pm}, \mu = \mu_m$ $\lambda = \lambda_m$	$c_p = c_{pl}, \mu = \mu_l$ $\lambda = \lambda_l$
		$c_p = c_{pm}, \mu = \mu_m$ $\lambda = \lambda_m$	$c_p = c_{pl}, \lambda = \lambda_l$ $\mu = \mu_l$

Table 3.3: Prandtl Number Definitions for and Configurations

Correlations are extremely useful tools for determining heat transfer in different flow regimes. Most empirical in origin, they are composed of dimensionless numbers, such as Re, Pr, Gr etc. They are often obtained by testing, for certain operating regimes, so it is also essential to define the range of applicability and the assumptions that apply when using them.

The author realises the extreme caution in using these relationships; an example of this is one of the main studies on which he relied [34], in fact in this case the heat transfer constant h_{sc} for the forced convection (non used here because out of the range applicability), evaluated using the correlation:

$$h_{sc,j} = \left(\frac{b_1 k_J}{r_z} \right) \left(\frac{r_z \dot{m}_{PG}}{A_d \mu_J} \right)^{b_2} (Pr_J)^{b_3} \quad (3.13)$$

reports that the constant b_1 , should be increased from 0.06 predicted by a previous study to 0.54, and this change is due, the study reports, for small different test operating conditions presented by one compared to the other.

The ones given here are a collection of different correlations, put together after a lengthy comparison phase.

Determining these correlations has been one of the most difficult tasks in this work, partly because it is difficult to recover the sources of the model presented in the bibliography, making the information usually incomplete. On the other hand, to verify if the cases presented were compatible and in the same range of the applications. To verify this last point, a long work of dimensions analysis has been made besides the different attempts with various other correlations. With the coefficient determinate, the last step in section 3 is the calculation of the heat flow $[W/(m^2 \cdot K)]$ with the equations 1.14. With the difference of the temperature

⁵Mixed correlations with β calculated with eqs (1.16), (1.17), and (1.18).

Correlation for $\frac{Gr}{Re_{fc}^2} < 0.1$ Forced heat exchange					
Heat flow type			Heat flow type		
Flow	WALL	EVAP	WALL	EVAP	Hp
Lam $Re < 10^5$	$St_x = \frac{0.485}{2 \times Pr_x^{0.75} (Re_T^{**})_x^{0.556}}$ $h_{sc} = St_x \cdot u \cdot \rho_m \cdot c_{p,m}$	$St = \frac{0.332 Pr^{-2/3}}{\sqrt{Re_x}}$ $h_{sc} = St \cdot u \cdot \rho_m \cdot c_{p,m}$	$St_x = \frac{0.485}{2 \times Pr_x^{0.75} (Re_T^{**})_x^{0.556}}$ $h_{sc} = St_x \cdot u \cdot \rho_m \cdot c_{p,m}$	$St = \frac{0.332 Pr^{-2/3}}{\sqrt{Re_x}}$ $h_{sc} = St \cdot u \cdot \rho_m \cdot c_{p,m}$	a) For natural or forced b) Equilibrium of heat and wall stresses c) 2D laminar boundary layer d) Constant prop fluid
Turbo $Re > 5 \cdot 10^5$	$h_{sc} = \left(\frac{b_x k}{r_i} \right) \left(\frac{r_i \dot{m}_{PG}}{A_j \mu_j} \right)^{b_x} (Pr_j)^{d_1}$	$h_{sc} = \left(\frac{d_x k}{r_i} \right) \left(\frac{r_i \dot{m}_{PG}}{A_j \mu_j} \right)^{d_2} (Pr_j)^{d_3}$	$h_{sc} = \left(\frac{b_x k}{r_i} \right) \left(\frac{r_i \dot{m}_{PG}}{A_j \mu_j} \right)^{b_x} (Pr_j)^{d_1}$	$h_{sc} = \left(\frac{d_x k}{r_i} \right) \left(\frac{r_i \dot{m}_{PG}}{A_j \mu_j} \right)^{d_2} (Pr_j)^{d_3}$	a) 2D turbulent boundary layer b) Mass transfer phenomenon c) Uniform fluid properties

Figure 3.6: Forced Correlations

Correlation $0.25 < \frac{Gr}{h_{sc}^2} < 10$ Mix convection					
Heat flow type			Heat flow type		
Flow	WALL	EVAP	WALL	EVAP	HP
Laminar or Turbo	$h_{sc} = h_{scforz} \cdot e^{-\beta_s \cdot z^2} + h_{scslib}$	$h_{sc} = h_{scforz} \cdot e^{-\beta_s \cdot z^2} + h_{scslib}$	$h_{sc} = h_{scforz} \cdot e^{-\beta_s \cdot z^2} + h_{scslib}$	$h_{sc} = h_{scforz} \cdot e^{-\beta_s \cdot z^2} + h_{scslib}$	

Figure 3.7: Mixed correlations

Correlations $\frac{Gr}{Re_{fc}} > 10$ Natural Convection					
Heat flow type			Heat flow type		
FLOW	WALL	EVAP	WALL	EVAP	Hp
LAM & TURBO	$Nu_L = \frac{h_x L}{k} = c_1 (Ra)^{c_2} = c_1 [(Gr_L)(Pr)]^{c_2}$ $h_{sc} = \frac{Nu_L k}{L}$	$Nu_L = \frac{h_x L}{k} = c_1 (Ra)^{c_2} = c_1 [(Gr_L)(Pr)]^{c_2}$ $h_{sc} = \frac{Nu_L k}{L}$	$Nu_L = \frac{h_x L}{k} = c_1 (Ra)^{c_2} = c_1 [(Gr_L)(Pr)]^{c_2}$ $h_{sc} = \frac{Nu_L k}{L}$	$Nu_L = \frac{h_x L}{k} = c_1 (Ra)^{c_2} = c_1 [(Gr_L)(Pr)]^{c_2}$ $h_{sc} = \frac{Nu_L k}{L}$	Natural Transfer c1 = 0.13 c2 = 0.33

Figure 3.8: Natural Correlations

$\Delta_T = T_m - T_{wall}$ for the wall heat dissipation, or a $\Delta_T = T_m - T_{liquid}$ for the propellant heat flow.

When the flow regime and the convection type have been defined, the code is routed into an ‘if’ structure where each possible Reynolds and Richardson configuration is defined, reporting the value of the heat transfer coefficient h_{sc} for each one. The correlations for each case have been presented already in Chapter 1, speaking about the influencing factors of the phenomena. Here is the report for each case.

- sec4: Calculation of the work, the energy entry and the efficiency** With the heat flow identified, the next step is determining the power dissipated through the wall and propellant surface. The propellant surface is the same dimension of the section of the tank $A_{prop} =$

$2 \cdot \pi \cdot R_{Tank}$. The wall, instead, is the inside surface of the tank, which is considered a cylinder with a spherical dome. So the the thermal power [W] is:

$$Q_{wall} = q_{wall} \cdot A_{wall} \quad (3.14)$$

$$Q_{evap} = q_{evap} \cdot A_{prop} \quad (3.15)$$

As presented in Chapter 1, the ullage, in this work, can be considered a close domain, with only a mass flow inlet. So balance of the system can be simplified as:

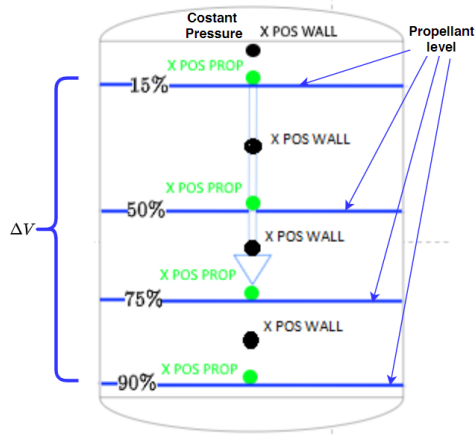
$$\Delta E = E_{entry} - (Q_{wall} + Q_{propellant}) + W_T \quad (3.16)$$

The input helium mass [kg/s] introduces energy to the system, so considered positive, with the species' enthalpy [J/kg] at the entry pressure and temperature.

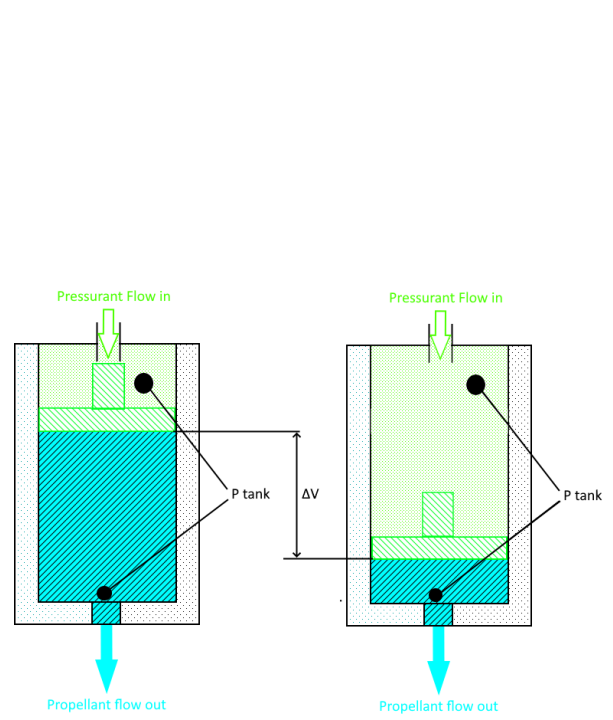
$$E_{entry} = \dot{m} \cdot h_{in}$$

The energy and the heat lost have been evaluated; the last term is the work done from the system to the outside, so it can be considered positive. The code is implemented not for simulating the emptying of the tank, but for a first valuation that can be calculated with some simplification. As presented in Chapter 2, the pressurant introduced by the diffuser makes the work like a piston, trying to maintain the pressure constant in the tank and pushing out the propellant from the bottom. So can with this simplification can be evaluated as:

$$W_t = P \cdot (V_{t=t_f} - V_{t=t_0})$$



(a) Emptying of the tank propellant with the different possible positions of the heat exchange and the variations of the volume.



(b) Simplification of the tank emptying processes.

Figure 3.9: Comparison of different tank emptying scenarios.

Efficiency

But the collapse evaluates only the weight of the pressurant used, versus the predictions. An efficiency parameter relative to the energy was needed. In this case, was took inspiration from [10] and [37] where in Section-2, "Methodology Description" an exergy factor was introduce:

$$\phi_i = \frac{W_t}{Q_{tot,i}} \quad (3.17)$$

Where $Q_{tot,i}$ [J]:

$$Q_{tot} = \dot{m} \cdot i_{gi} \cdot \tau_p \quad (3.18)$$

represents the total energy at the entrance of the tank, and the W_t :

$$W_t = P_{tank} \cdot V_{tank} \cdot \tau_{prop} \quad (3.19)$$

is the work done by the pressurant. As mentioned several times above, the job of the pressuriser is to maintain the desired pressure level in the tank, both during maintenance, i.e. pressurisation on ground, and during emptying. The work performed is therefore comparable to that of a piston, which expels the propellant, considering it to be at a constant pressure given the continuous input of gas as the free volume increases 3.9. This exergy factor wants to represent the quote of the work in function of the total energy introduced by the pressurant flow.

Using a similar but specular principle, the efficiency parameter presented in this work will define the amount of heat dissipated relative to the total energy introduced and the work done.

Taking again in consideration energy balance(3.16) but in a steady state condition , can be written as:

$$\Phi_{eff} = \frac{1}{1 + \frac{\Sigma Q_{dissipated}}{(W_t + E_{in})}} \quad (3.20)$$

Where, here:

$$W_t = \frac{P_{tank} \cdot \Delta V}{\tau_{prop}} \quad [W] \quad E_{in} = m_{press} \cdot h_{in} \quad [W] \quad (3.21)$$

And the $Q_{dissipated}$ [W] is the sum of the contributions from (3.14) and (3.15). This parameter so represents the portion of total energy lost, so systems with Φ_{eff} near 1 are the more efficient, and those with near-zero values are the less. In this way, the efficiency is strongly linked to the heat flows, so the function of the entry dimension and direction, obtaining the efficiency plot for each diffuser dimension.

5. **sec 5-6:** Section to plot the results and graphs from the analysis. In these two sections, different figures about the tendency of the heat flow and the h_{sc} values vs the diffuser dimensions, the dimensionless numbers, and the fraction are plotted. Also, the numerical results are collected and saved to the file for more easy access to the results.

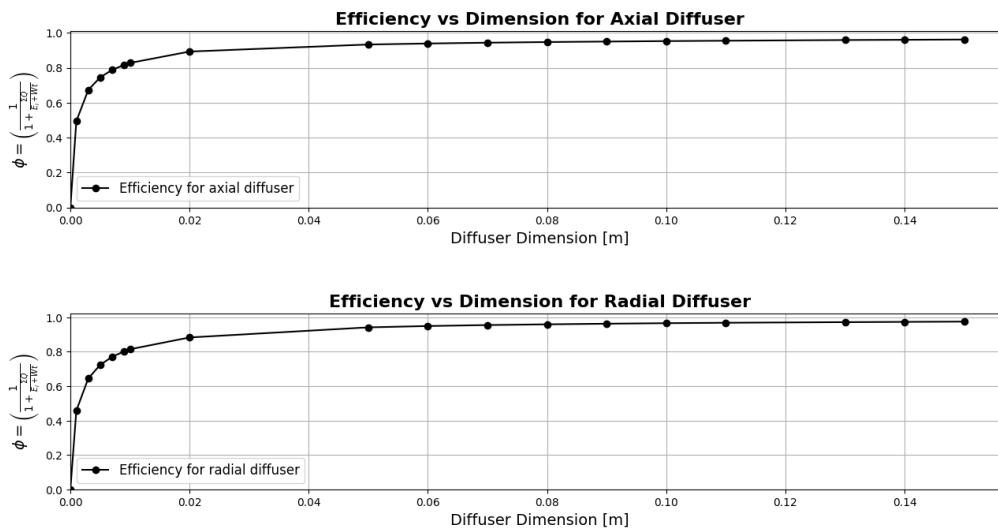


Figure 3.10: Example of efficiency plot vs diffuser dimension for sounding rocket tank filled at 50% of liquid methane

From the efficiency graph is possible to identify the dimension beyond which a change in dimensions does not affect with the same intensity, having the gradient of the curve becoming very small. With this approach, it is reasonable to think of a larger possible entry section to

Inlet size [m]	Inlet area [m ²]	Volume diff [m ³]	Free ullage percentage [%]	Heat lost by AX DIF [J]	AX efficiency
0.001	3,14E-03	3,14E-04	0.9999	3,47E+09	0.4457
0.003	2,83E-02	2,83E-03	0.9998	1,65E+09	0.4941
0.005	7,85E-02	7,85E-03	0.9996	1,16E+09	0.6725
0.007	1,54E-01	1,54E-02	0.9991	9,14E+08	0.7452
0.009	2,55E-01	2,55E-02	0.9986	7,63E+08	0.7876
0.01	3,14E-01	3,14E-02	0.9982	7,06E+08	0.8162
0.02	1,26E+00	1,26E-01	0.9929	4,07E+08	0.8275
0.05	7,85E+00	7,85E-01	0.9555	2,43E+08	0.8927
0.06	1,13E+01	1,13E+00	0.9359	2,21E+08	0.9331
0.07	1,54E+01	1,54E+00	0.9127	2,03E+08	0.9389
0.08	2,01E+01	2,01E+00	0.8860	1,89E+08	0.9436
0.09	2,55E+01	2,55E+00	0.8557	1,78E+08	0.9472
0.1	3,14E+01	3,14E+00	0.8219	1,68E+08	0.9500
0.11	3,80E+01	3,80E+00	0.7845	1,60E+08	0.9528
0.13	5,31E+01	5,31E+00	0.6990	1,46E+08	0.9548
0.14	6,16E+01	6,16E+00	0.6509	1,41E+08	0.9588
0.15	7,07E+01	7,07E+00	0.5993	1,35E+08	0.9602

Figure 3.11: Extract from an iteration of the code with 50% ullage volume and methane propellant from the case study presented in next chapter

minimize the entry velocity so consequently the heat flow⁶ but come into play the geometry restriction, problems with volume size and weight limitations. Users can decide which dimension to select if they earn something in terms of efficiency or something in terms of the volume occupied. In this work, the two configurations are functions of only one dimension, b_0 or r_0 , to allow a more equal comparison. For the Axial configuration, r_0 , as shown in the figure 3.4 extracted from the figure (9.5)[29], represents the radius of the entrance section in the tank. The height of the penetration (h) can be introduced manually in the code and evaluated with the correlations presented in Chapter-1 (1.27).

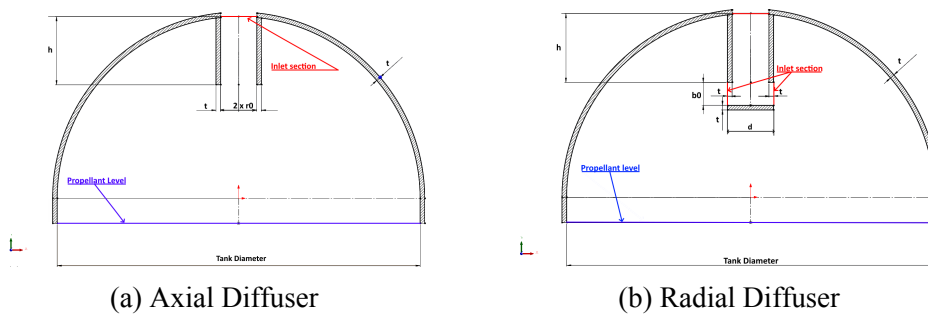


Figure 3.12: Sketch with quote for the Axial and Radial Diffusers

For the radial configurations to allow an equal comparison, the exit section must be at the same dimension, so in this case to also respect dimension b_0 , which represents the height of the dimension of the inlet section, as reported in figure 3.4. To calculate the diameter of the opening d , the code takes the dimension of the inlet Axial section, with the value of $b_0 = r_0$ matching

⁶The natural convection is always present; the objective is to eliminate the forced convection whiuout creating too large diffusers.

the outlet section, and extracts the opening section from this.

$$A_{sectAx} = A_{sectRad} \rightarrow d = \frac{\pi \cdot r0^2}{2 \cdot \pi b0} \quad (3.22)$$

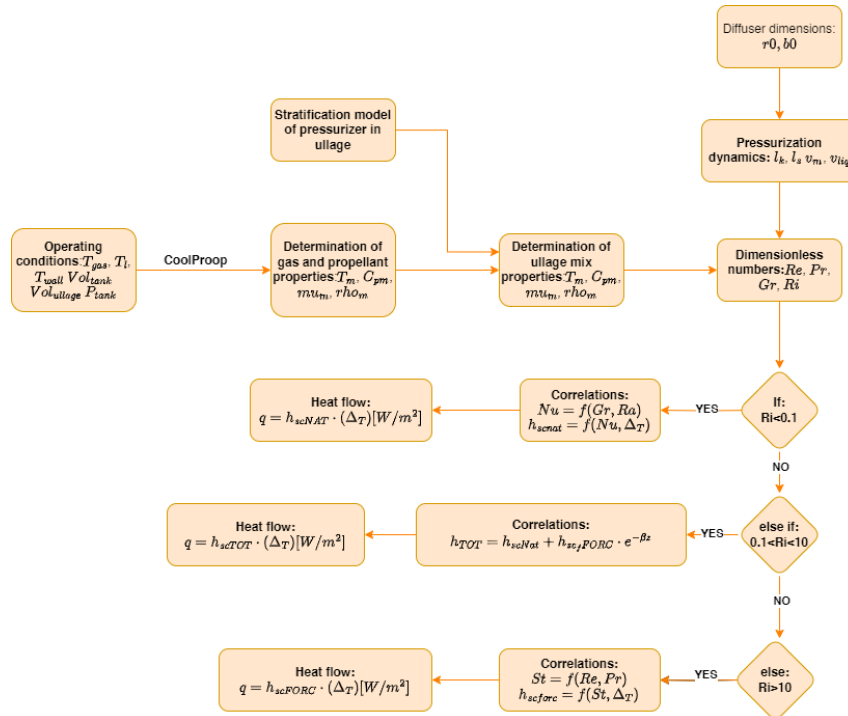


Figure 3.13: Figure 5: Blocks diagram of system operation code

3.1.3 CFD ANALYSIS

As presented above, the code simulation, despite all its limits, can save time before starting the first iteration of fluid dynamics analysis. This second step has multiple objectives. First, it confirms the code simulation in the comparison - geometries. Second, introduce the evolution in the ullage so the steady state is left behind using transient simulations. Last, this is the first implementation of the CAD geometries that permit a visual check of the diffuser's volume encumbrance to the ullage. The analysis has been made using the Ansys Fluent©software, a state-of-the-art computational fluid dynamics (CFD) software tool that enables engineers to simulate fluid flow, heat transfer, and chemical reactions with unprecedented accuracy. It provides a comprehensive suite of modelling capabilities to address the most complex engineering challenges. Ansys Fluent's robust solver algorithms and advanced meshing technologies ensure reliable and precise simulation results, making it an indispensable tool in the field of fluid dynamics and thermal analysis. In the current work, the decision to use Fluent©, besides being one of the most common and best CFD software, was made because this software was introduced

to the author during the internship period. Fluent is one of the multiple specialized modules within the Ansys simulation suite. It belongs to Ansys Workbench, the overarching platform that integrates different simulations made by different Ansys modules. Different steps are necessary before performing a fluent analysis using the module "Ansys Fluent Meshing." The software requests some steps before running the simulation.

Assumption

To be able to carry out several simulations without heavy computational loads and to optimize time (as reported in the 2.2.3 section), these simulations are performed with a series of simplifying assumptions. This is also because at this level it was considered more important to have correct simulations without seeking extreme precision, which would make them unnecessarily heavy. Indeed, together with the company figures who supported the author, it was decided that for this first round of simulations, the following assumptions were justified (some are the same as used in the code section):

- **Only the ullage volume is simulated.** The volume is limited above by the tank dome and below by the propellant level. Linear pressurization from the propellant storage value to the operational value.
- **Maximum pressurizing flow rate as a requirement:** For the first iteration of CFD analysis to better highlight the effect of the heat dissipation is better to use the WCS mass flow.
- **Linear stratification of temperatures in the ullage.**
- **No evaporations:** Like for the code, the evaporations are not considered because the evaporation processes would only have an effect on adding mass on the ullage, helping the pressurization and, at the same time, making the simulation heavier. The downside is the lack of the propellant mass lost in vapour, but that can be verified with a subsequent verification (in particular if configurations will be chosen).
- **Propellant liquid considered as "WALL":** The propellant level is simulated as a "WALL" at constant temperature kept stationary (thus, the discharge is not simulated).
- **Tank dome as WALL:** The tank dome is the boundary condition for the upper geometry, simulated as a WALL with a constant temperature extracted from the case study.
- **No external thermal flows:** No external tank flows are implemented.
- **Ullage filled with CH₄:** Pressurization starts with ullage volume empty of He.
- **Compressible ideal gas:** The chemical species are considered ideal but compressible gases⁷

Geometry

First of all, the geometries must be created using CAD software. To simulate only the fluid volume contained in the tank's ullage, the software *SolidWorks* was used for the construction.

⁷This is because of gas flows in closed volume.

First, the profile was created on the XY plane using the **dimensions obtained in the previous step from the code**. Once the profile was closed and fully defined, the revolution around the z -axis was performed, exploiting the axial symmetry of the code.

Given the full volume, it was necessary to subtract the tank surface and the diffuser from the liquid volume using boolean operations. Thus, obtaining the negative of the initial geometry, this will be the body used in *Ansys*[®].

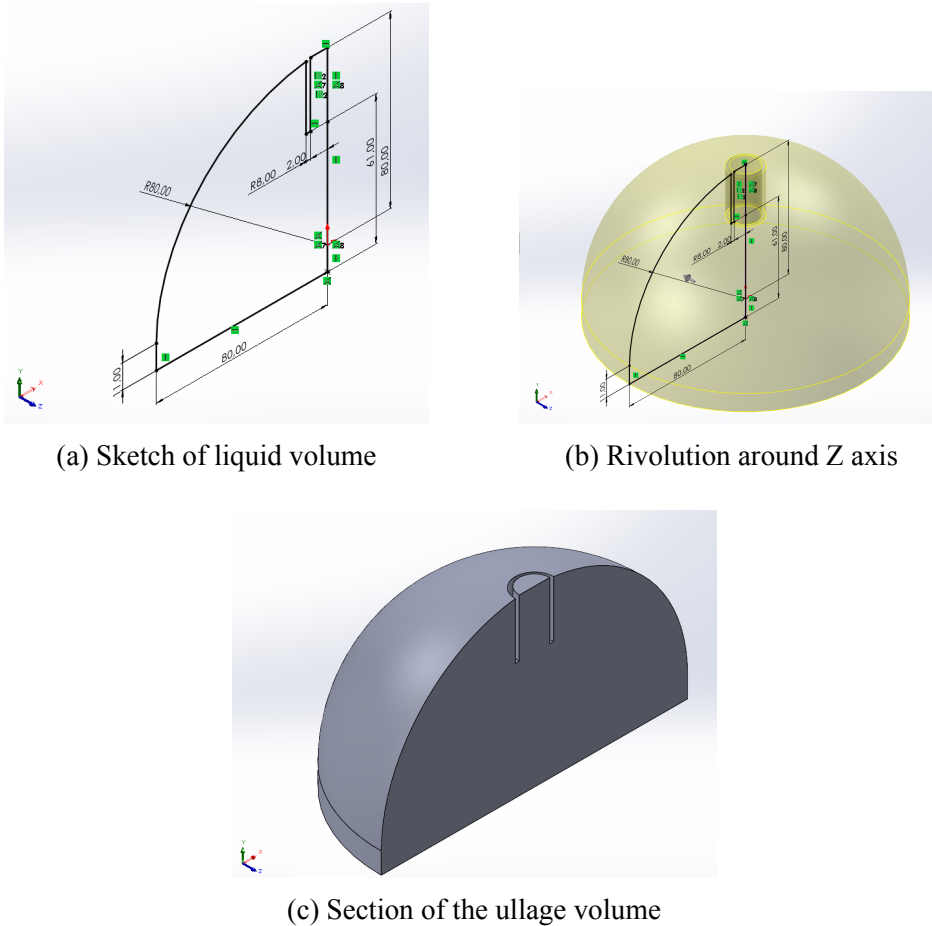


Figure 3.14: Evolution of the ullage volume for the analysis

Once the geometries have been created, they can be imported in the *Geometry* menu, the first step. Using one of the tools presented in the *Fluent* menu (*Space Claim* or *Design Modeler*) the CAD must be checked and set all the name selections for the different regions, like, the inlet zone, the wall zone⁸. In this first round of simulations, the initial useful dimensions for the diffuser were defined, but both configurations (AX and RAD) are possible.

In this initial phase, it is important to define the simulation's input section using the *Name Selection* command as *inlet*, while the tank wall and the propellant are given convenient

⁸Fluent automatically take in consideration as wall every surface which will not be renamed in a different way, but in this work setting the wall name for the dome and the liquid is helpful for next steps

names.

Additionally, it is necessary to check that the ullage volume is a single body and does not contain any foreign elements. If the geometry consists of multiple bodies, it is possible to use the boolean commands provided in *Design Modeler*.

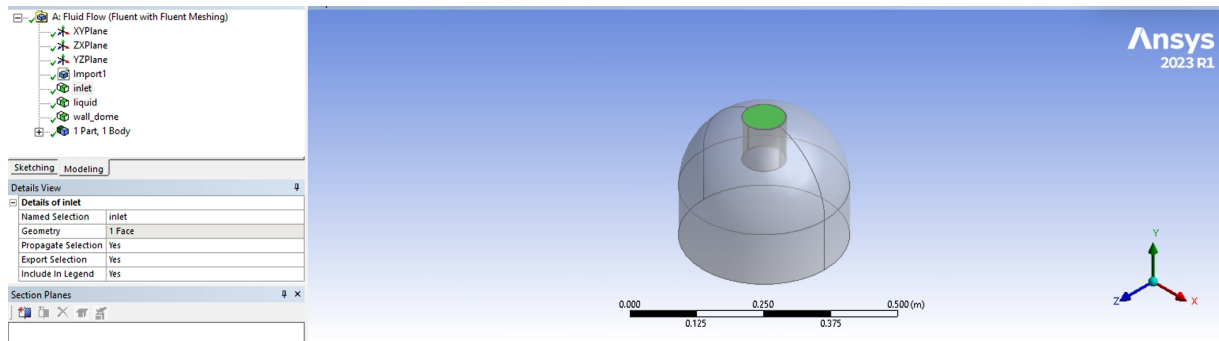


Figure 3.15: Example of design modeler of axial configuration, with the different name selection

Meshing

CFD software like Fluent works by solving the Navier-Stokes equations, which govern fluid flow, through numerical methods. This involves discretizing the volume using the finite volume approach and then solving the equations using matrix inversion techniques. The mesh represents the cells that divide and discretize the entire volume simulated. The solver then uses the mesh nodes to resolve the fluid dynamics equations. As can be imagined, the denser the cells are, the heavier the simulation will be. The first step to execute the mesh is to import the CAD defined in the previous phase.

The meshing process in Fluent first involves creating a surface mesh, necessary to capture all the details accurately.

Only afterwards does the volume discretization follow, where the areas within the surface mesh are considered as "interior", thus constituting the complete mesh. This sequential process ensures a high-quality mesh suitable for accurate simulations.

To obtain a precise mesh, it is important to define a local sizing mesh in certain areas. In this work, the mesh refinement occurs in the area where the fluid exits from the pressurizing outlet section in the ullage and, for the radial configuration, also around the surface where the exiting flow hits to be directed. Both regions have been defined as "Face Size" for the control type, setting case by case the dimension of the *Target Mesh Size [m]* and selecting the zone by labeling.

Successively the surface mesh must be defined, introducing min and max size of the surface cells dimensions, the *Growth Rate Size Function* and so on all the other options. Here is reported a brief explanation for each one.

- **Minimum Size [m] and Maximum Size [m]:** The minimum and maximum cell size of the mesh. Defines the smallest and the largest size of the cells, useful for capturing the finest details of the geometry. \Rightarrow user define
- **Growth Rate:** The rate at which cell sizes increase controls how cell sizes progressively grow from the minimum to the maximum, affecting the transition of mesh density. \Rightarrow Default Value: 1.20 \div 1.15
- **Size Functions:** Method used to determine cell sizes based on geometric features. Selects the sizing function based on curvature and proximity, enhancing mesh accuracy in curved and narrow areas. \Rightarrow Curvature & Proximity
- **Curvature Normal Angle [deg]:** The normal curvature angle in degrees. Determines the mesh's sensitivity to curvature changes. Smaller angles increase mesh density in curved areas. \Rightarrow Default Value
- **Cells Per Gap:** Number of cells per gap. Specifies how many cells should be inserted into narrow gaps, improving mesh resolution in these areas. \Rightarrow Default Value
- **Scope Proximity To:** Scope of proximity for cell sizing. Specifies whether cell sizing should be based on proximity to edges, improving definition along the geometry's edges. \Rightarrow faces-and-edges

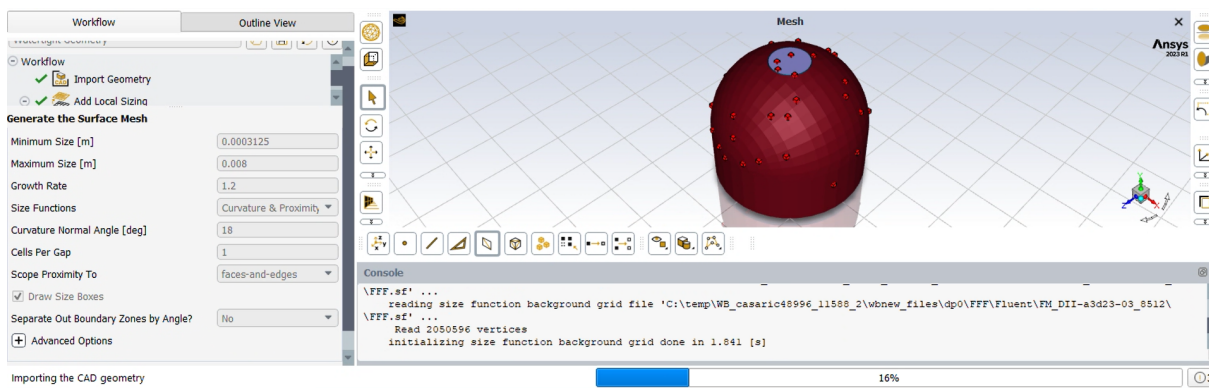


Figure 3.16: Example of surface mesh creation

Then, it is necessary to describe the geometry, so define whether the volume consists of solid or fluid with no voids or both with voids. If there are multiple bodies, use a share topology mesh, and at the end, if there is multizone meshing. In this work section, the volume is only fluid, with no voids, and neither share topology nor multizone is needed.

The next step is to update the boundaries where the zone name selected in Design Modeler can select the type of the boundary. For the current thesis, generally the boundary types can be summarized as :

inlet → mass flow inlet

liquid → wall

wall_dome → wall

As second to last is the definition of the Regions, here is important to set different volume type, like, fluid volume or solid volume. In this stage, if everything has been make in the correctly there will be only one body to set as fluid.

In this second step of the process, to avoid too heavy analysis the application of the boundary layer is omitted.

The generation of the volume mesh represents the last and most important step, with all the options set correctly above the generation of volume mesh can be done using different cell geometries, each with specific characteristics suitable for various types of analyses:

- **Tetrahedral (Tetra) Mesh:** Uses tetrahedral cells, which are polyhedra with four triangular faces. Ideal for complex and irregular geometries where applying more regular cells is difficult. Often used for simulations that do not require extremely fine resolution.
- **Hexahedral (Hex) Mesh:** Uses hexahedral cells, which are polyhedra with six square faces. Preferred for simple and regular geometries. Offers high mesh quality and greater computational efficiency, making it suitable for simulations that require precision.
- **Prismatic (Wedge) Mesh:** Uses prismatic cells with triangular bases and rectangular faces. Primarily used for boundary layers where it is important to capture gradients near solid surfaces.
- **Polyhedral Mesh:** Uses polyhedral cells with a variable number of faces. Combines the advantages of tetrahedral and hexahedral cells, offering good mesh quality and a reduction in the number of required cells. Effective for complex geometries and improving simulation efficiency.

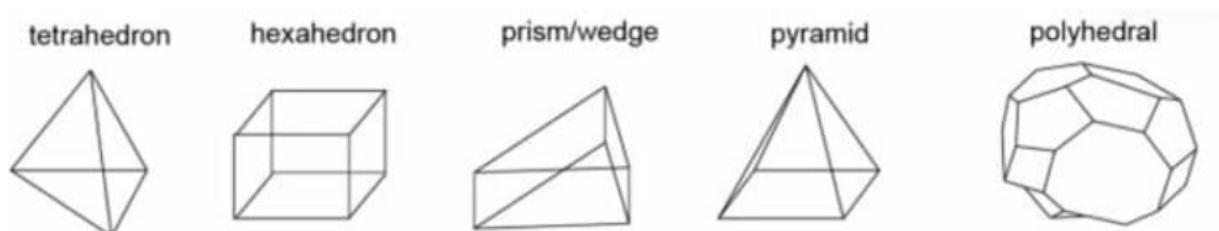


Figure 3.17: Different Possible Mesh Geometries

The applications here needed a correct mesh but were not pushed towards maximum precision, so polyhedra were chosen. As presented in the first section of this chapter, the limited tools and the phenomena to simulate request $4E + 05$ and $1E + 06$ cells to not lose accuracy during the simulation and to take a too long time to process.

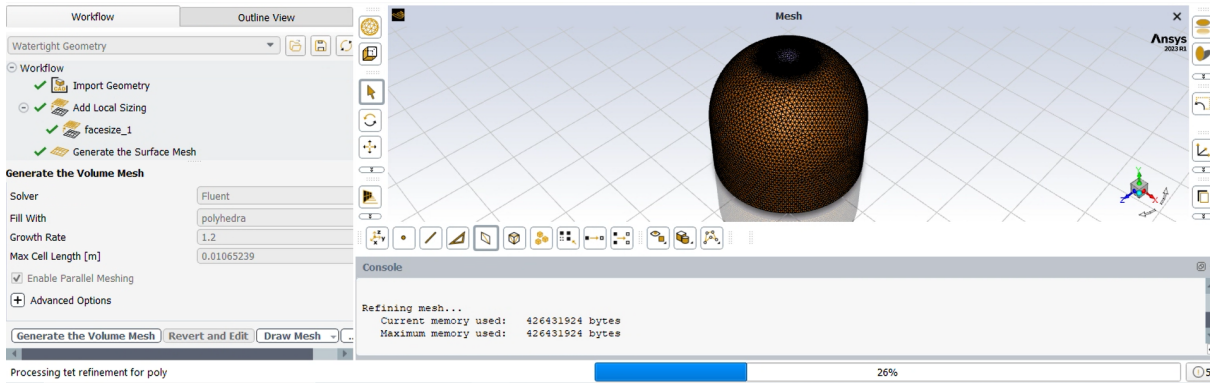


Figure 3.18: Generating the volume mesh

Set Up

Ansys Fluent solves the Navier-Stokes equations of mass, momentum, and energy conservation discretizing over each cell in the mesh. In this step, the user will define which equations will be solved, the species, and the residual levels. In a transient analysis, the domain is analyzed over time by dividing the total interval into small time increments called time steps. For each time steps Fluent©will perform a check or the numerical residual obtained from the previous iteration and to define the convergence and pass to the next time steps the the residual has to be smaller than a threshold previously set by the user. Here will be reported a brief explanation of the element use to prepare the simulation needed in this work.

- **Energy Equation** → **ON**: Enable this option if the analysis involves heat transfer.
- **Viscous** → **SST k-omega Model**: Select the SST k-omega turbulence model, which combines the benefits of k-epsilon and k-omega models to improve prediction in both near-wall and free-stream regions.
- **Cell Zone Conditions**: Define the operating conditions for the system, including pressure and temperature. These conditions serve as the baseline from which the analysis begins and are critical for ensuring accurate simulation results.
- **Boundary Types** → **Inlets, Walls**: Define boundary conditions for each type of boundary in the domain. This includes inlet the mass flow and walls conditions (e.g., adiabatic or with heat transfer or temperatures), etc.

- **Named Expressions:** Where expression can be implemented, useful for the simulation, particularly for the temperature stratification in the ullage, temperature function of z dimensions. Or the inlet flow control, where to use a condition to control the flow activation and deactivation in the function of the pressure level.
- **Report Definitions:** The section introduces the reports file about meaningful dimensions during the analysis in this work.
 - **Absolute Pressure** `repo_abs_press`:: Define a report to monitor the absolute pressure throughout the entire volume. This helps in tracking pressure variations, and the achievement of the threshold level corresponds to the activation or not of the pressurization system.
 - **Static Temperature** `repo_stati_temp`: Define a report to monitor the temperature distribution across the entire volume. It is crucial to determine the impact of one diffuser with respect to another.
 - **Mass Flow Rate through Inlet:** Set up a report to measure the mass flow rate through the inlet. This helps verify that the inlet conditions are met and the flow rate is as expected.
 - **Heat Transfer through Walls:** Define reports to measure the heat transfer through the “Liquid” and “Wall Dome” surfaces. This is important for evaluating the efficiency of one configuration in respect of the other.
- **Residuals:** For every equation is possible to set the threshold for convergence. Typically, residuals should decrease by three to four orders of magnitude to ensure a reliable solution. But is particularly of interest the `Continuity Residuals`. Monitor the residuals related to continuity. Continuity residuals represent the error in the mass conservation equation at each iteration. Fluent aims to minimize these residuals, indicating that the mass is conserved across the domain.
 - **Surfaces:** For the evaluation of the flow rates and velocities around the outlet sections, special surfaces have been created to capture the mass flow. Each surface is created in a way to envelop the speaker; there are 3 surfaces for both configurations. The first is at the entrance to the outlet section, the second is at a distance equal to 2 times the fundamental input dimension (r_0 or b_0), and the third follows the same principle but at three times the fundamental dimension. All surfaces have been positioned so that the flows are collected comprehensively. The surfaces were created by “Iso-surface” in the surface menu, setting the radial or axial dimension as the Iso-value for or configurations. Then, modify them by making a clip of the surface. In this way, it will be possible to

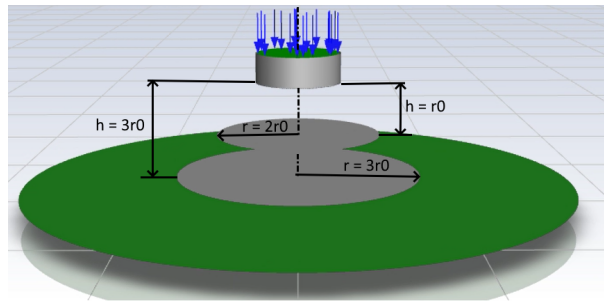


Figure 3.19: Surfaces for configuration

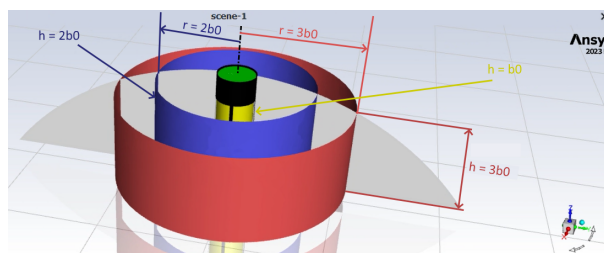


Figure 3.20: Surfaces for RAD configuration

evaluate the mass flow rates through a post-processing analysis of the mean and standard deviation values. As Chapter 2 mentions, a good diffuser can distribute the mod's output flow rate as evenly as possible. It will, therefore, be assessed how these will be distributed around the average value.

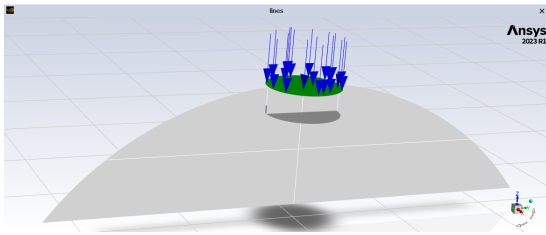
- **Lines** Taking inspiration from other studies, it is helpful to build lines that cut the ullage in a radial and axial direction in order to be able to evaluate the evolution of temperatures on the latter. For both configurations, two lines have been built: the radial one that cuts the ullage in half-height and the axial one that coincides with the z-axis of the geometry.

* Line_rad_ullage

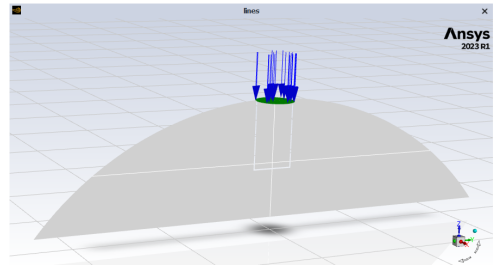
- $x_0 = 0, x_1 = 0$
- $y_0 = -0.7297, y_1 = 0.7297$
- $z_0 = 0.2127, z_1 = 0.2127$

* Line_ax_ullage

- $x_0 = 0, x_1 = 0$
- $y_0 = 0, y_1 = 0$
- $z_0 = 0.4518, z_1 = 0.0014$



(a) Lines on the ullage in AXIAL configuration



(b) Lines on the ullage in the RADIAL configuration

Figure 3.21: Comparison of lines on the ullage in different configurations.

– Reports

As reported above, Fluent uses reports to determine the physical quantities to be evaluated. In ANSYS Fluent, Reports are tools used to extract, visualize and analyze data from Computational Fluid Dynamics (CFD) simulations. They allow obtaining specific information on various parameters of interest, such as speed, pressure, temperature, flows, etc. Reports can help perform fundamental tasks during a fluid dynamic analysis, such as monitoring the analysis or verifying the results. In fact, in this work, they are used to monitor the evolution of the key quantities and evaluate their consistency.

The residues that can be chosen can be many, here are used:

* Mass Flow Rate	* Area-Weighted Average	* Mass-Weighted Average
<ul style="list-style-type: none"> · <i>inlet_mass_flow_rate</i>: To evaluate the mass flow through the inlet surface · <i>outlet_mass_flow_rate</i>: Evaluating the mass flow through the surface at the exit diffuser section 	<ul style="list-style-type: none"> · <i>repo_heat_liquid_flow</i>: Evaluating the flux through the liquid surface per area unit. · <i>repo_heat_wall_flow</i>: To report the heat flux through the tank wall per area unit. 	<ul style="list-style-type: none"> · <i>repo_stati_temp</i>: Evaluate the static ullage temperature over the mass of the fluid · <i>repo_abs_press</i>: Absolute pressure over the fluid volume.

The three types of reports used in this work are the three described above; the first, the

Mass Flow Rate, calculates the net mass flow across a surface, then calculated as:

$$\dot{m} = \int \rho \mathbf{v} \cdot \mathbf{n} dA$$

The second is the Area-Weighted Average, which calculates the weighted average of a variable over an area; in this case, the weighted average takes place on the surface of each cell in the mesh. Finally, the Mass-Weighted Average, i.e., the mass-weighted average of a variable in a volume, which coincides with the mass of fluid in each volume cell divided into meshes. The results of these reports will be taken up again in Chapter 4, where the results will be discussed in detail.

3.1.4 Post Processing

Once the CFD analyses of the two geometries have been made, it is necessary to compare the performance of each configuration. This will allow us to determine which configuration is the best one. For this first comparison, the following quantities are then evaluated:

- **Temperature trends over time:** At defined temperature intervals, radial and axial temperature trends in the ullage are compared.

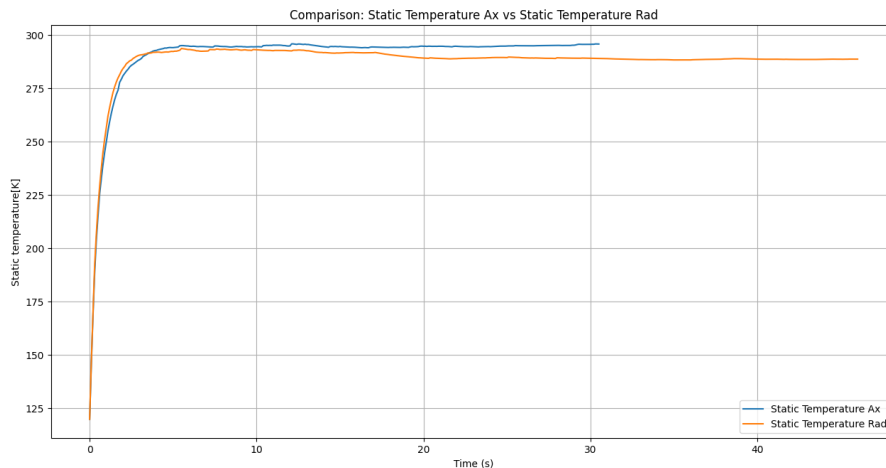


Figure 3.22: Example of the radial temperature in the ullage in different times

- **Pressurization efficiency:** Tests the time it takes to reach the rated pressure. Here, it is necessary to remember that the flow rate for which the pressurization operation is carried out is that of WCS, as dictated by the requirements. The achievement of nominal

pressure is, therefore, much faster than would be realized by a nominal fi operation profile.

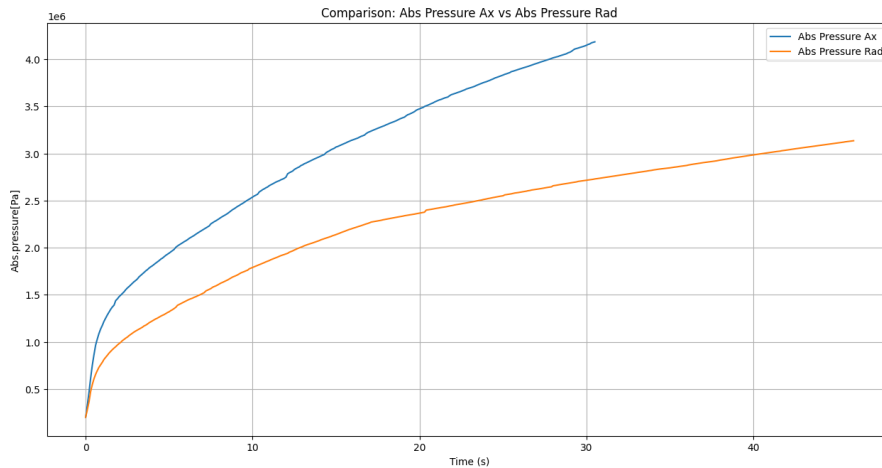


Figure 3.23: Absolute pressure vs time for the axial and radial configurations

- **Equalize the flow rate at the outlet with that at the inlet from the diffuser:** Control surfaces can be made in the respective sections exiting the diffusers to estimate the flow rates passing through them. Subsequent comparisons precisely between the inlet flow rate through the inlet and the outlet flow rate through these surfaces placed in the outlet sections allow one to determine the time interval required for the flow rate to enter a steady state.
- **Standard deviation of velocities:** One of the main functions of a diffuser is to diffuse gases as uniformly as possible. Therefore, in this case, the statistical distribution and standard deviation of the velocities at the nodes of the surfaces enveloping the injector are evaluated. The optimal configuration will have the best distribution around the mean value.

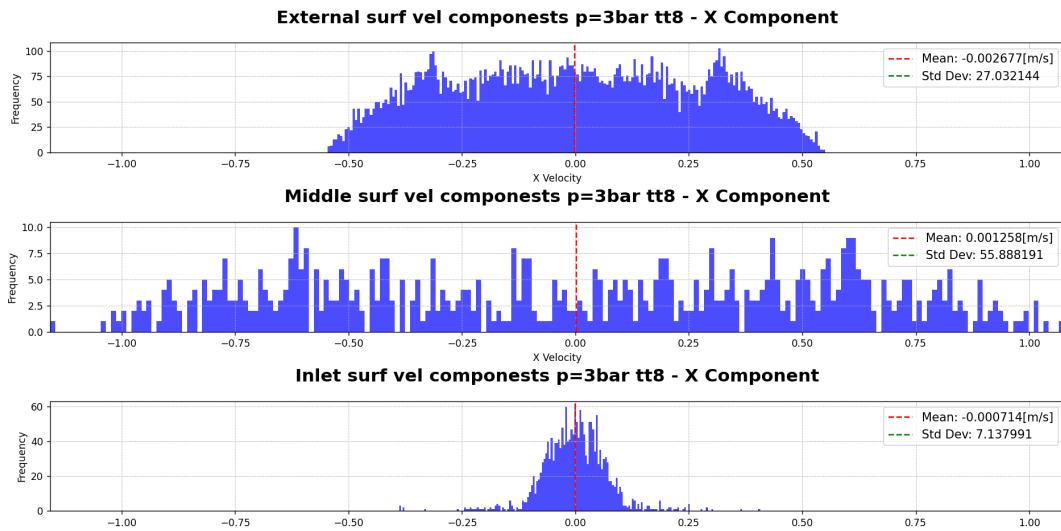


Figure 3.24: Example of velocity distributions through a series of surfaces

- **Thermal efficiency:** A parameter of fundamental importance, in this case we quantitatively evaluate dissipated fluxes, trying to figure out which of the two configurations is the one that achieves better maintenance of the pressurizer temperature level. As presented earlier, it is essential to find the optimal configuration for the highest possible maintenance of the pressurizing gas energy content.

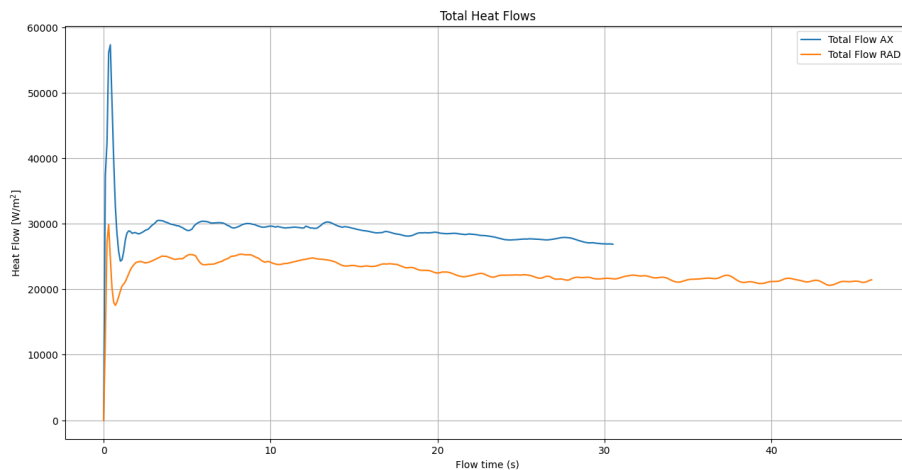


Figure 3.25: Total heat flows for the two configurations

All these parameters are then compared and evaluated, thus allowing us to understand in terms of comparison what the optimal configuration for pressurization could be. However, to obtain the values and make this comparison, it is necessary to extract from the Fluent[®] software the dimensions from the previously compiled reports and, through Python[®], carry out adequate

post-processing. Post-processing is an essential part of the design process; it must be able to transpose the quantities evaluated in the CFD software into plots in a consistent way. For this phase, it was chosen to use Python[®] as a post-processing program rather than the related menu offered by Workbench[®], for greater flexibility and speed of execution.

Chapter 4

Sizing Example

We now move on to a practical demonstration of this methodology. In fact, in this chapter, we will show the entire sizing procedure described in depth in the previous chapter but applied to a real case. All the steps presented at the theoretical level in Chapter 3 will be performed, and how to configure the relative cases and the results will be plotted. These will be discussed, always following the principles of reasoning presented in the previous chapters, and choices will be made to proceed with the sizing.

The cases shown here are generic, obtained through a mixture of research presented in Chapter 2 and elements of the author's personal choice; however, the latter will always be justified.

It is important to specify that the material presented here has the sole purpose of illustrating an application of the methodology previously presented, has no industrial value and is not linked to any present or future project. Geometries and operating conditions refer to material collected from previous studies that have been published or from material in the public domain.

Furthermore, due to lack of time, some points will be accelerated because the purpose of the chapter is not to show precisely this specific case but the applicability of the method. For completeness, the procedure starts with defining the mission objective, which is reported below with its formulation.

Mission objectives: Design and optimize a diffuser for a pressurization system of a liquid technology.

Formulation: Develop a sizing methodology to obtain a technological configuration for the diffusion of pressurant in the propellant tanks for a launch vehicle, aimed at minimizing the amount of pressurant required during all operational phases.

Hence, there is a need to be able to size a diffuser for a generic LPRE technology, thus trying to find the best configuration and optimize it. So, defining which case is referred to and the operating conditions is necessary.

4.1 Analyzed Cases

Pressurant The conditions of the pressurant, as reported in Chapter 1, are the first and key parameters; the temperature and type of the pressurant are crucial. As presented previously, here will be presented the case study of the pressurization with inert gas at ambient temperature, the most common configuration for LPRE engines. So the pressurant will be the Helium, with an inlet temperature of 293 K ($\approx 20^\circ\text{C}$). The pressurant will be stored in a spherical high-pressure tank, typically around 300 bar (30 MPa).

Tank Dimensions, temperature and material For this case, a tank containing liquid methane at an average temperature of 120K will be analyzed. The tank has the common dimensions for launch technology, consisting of a cylindrical body and two spherical caps. Typically, a medium-sized casting technology has tank volumes of 30 000 to 50 000 L. Here, in order to simplify the simulations and make them less computationally demanding, this value is reduced to 10 000 L, a medium-small tank that could be adapted to the advanced stages of medium-small launchers. The tank is simply considered as a cylindrical body with spherical caps:

$$V_{\text{total}} = V_{\text{cyl}} + V_{\text{sphere}},$$

where:

$$V_{\text{cyl}} = \pi r^2 h_{\text{cyl}}$$

$$V_{\text{sphere}} = \frac{4}{3}\pi r^3$$

Substituting the known data:

$$V_{\text{total}} = \pi r^2 h_{\text{cyl}} + \frac{4}{3}\pi r^3$$

For a tank of about $10000\text{L}(\approx 10\text{m}^3)$ assuming a form factor between the height and the radius of the tank of about one, a typical value for small to medium-sized fuel tanks that can maintain a balance between the capacity of the tank and the structural stability of the pressure vessel:

$$h_{\text{cyl}} \approx r$$

Therefore:

$$V_{\text{total}} = \pi r^2 r + \frac{4}{3} \pi r^3$$

$$V_{\text{total}} = \pi r^3 \left(1 + \frac{4}{3} \right)$$

$$V_{\text{total}} = \pi r^3 \times \frac{7}{3}$$

Solving for the radius r :

$$r^3 = \frac{3}{7} \cdot \frac{V_{\text{total}}}{\pi}$$

$$r = \left(\frac{V_{\text{total}} \times 3}{7\pi} \right)^{\frac{1}{3}}$$

Substituting $V_{\text{total}} = 10 \text{ m}^3$:

$$r = \left(\frac{10 \times 3}{7 \times 3.14159} \right)^{\frac{1}{3}} \approx 1.10 \text{ m} = h_{\text{cyl}}$$

By iterating the process and considering practical approximations, we choose a radius of $r = 1.2 \text{ m}$, which leads to a cylinder height of $h_{\text{cyl}} = 1.0 \text{ m}$.

Let's calculate the total volume for these dimensions:

$$V_{\text{cyl}} = \pi \times (1.2)^2 \times 1.0 \approx 4.52 \text{ m}^3$$

$$V_{\text{sphere}} = \frac{4}{3} \pi \times (1.2)^3 \approx 7.24 \text{ m}^3$$

$$V_{\text{total}} = 4.52 + 7.24 \approx 11.76 \text{ m}^3$$

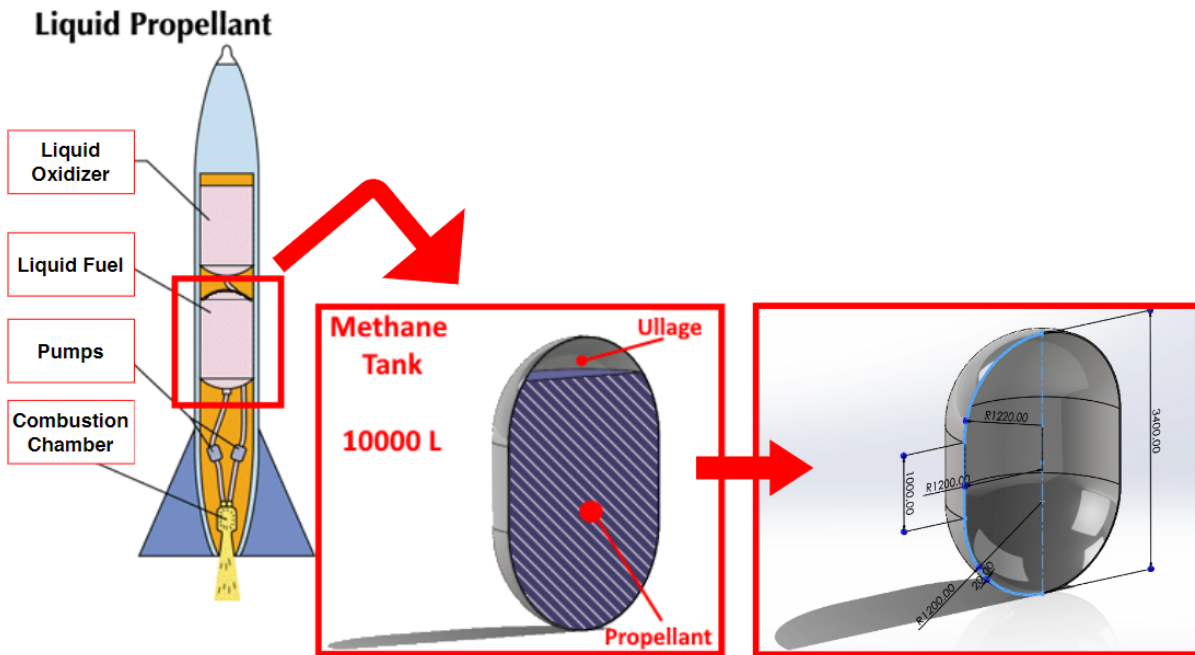


Figure 4.1: Caption

Cryogenic propellant tanks are made of metallic materials such as stainless steel or aluminium alloys, which offer mechanical strength and the ability to withstand low temperatures. Recently, carbon fibre-reinforced composite materials (CFRPs) are also being explored to reduce weight and improve strength. In contact with such low temperatures, some precautions are necessary to prevent excessive thermal stress of the tank material and avoid heating and evaporation of the propellant. For this reason, tank insulation methodologies are often used:

- **Vacuum insulation:** Used to reduce heat transfer by convection.
- **Multi-layer insulation:** Composed of layers of reflective and insulating materials designed to minimize heat loss.
- **Insulation materials:** Perlite or glass foam are used to improve thermal insulation further.

The latter is the methodology used mainly on the shells; in the study [12], it is reported that the flows are limited by the presence of foamy insulators on the two half-spheres placed above and below the tank. In this study, these elements will not be taken into account; an aluminium alloy will be chosen as the material. This does not detract from the possibility of implementing insulation and heat flows in the future.

That said, the value of the temperature of the walls is an essential point in the definition of the case; as mentioned above, external heat flows are not considered, so perfect insulation from

the outside to the inside is simulated; the only sources are therefore the propellant and the pressurizer. As reported in [49], where the methane tank is in conditions similar to the case defined here, the wall temperature fluctuates around 140 K. So, the chosen average temperature of the inner wall is 140 K.

The geometries of the diffuser to which reference will be made are those proposed in figure 3.12; the dimensions that will be taken into consideration will be the radius r_0 for the axial configuration, while for the radial geometry, the input height. For positioning, only the injection configuration from above, coinciding with the tank axis, will be evaluated, and the positioning height from the highest point of the tank dome is set to 10 cm.

Propellant As presented in Chapter 1, methane would be the propellant chosen for the study. Cryogenic propellants must be stored under subcooling conditions, i.e., at temperatures lower than their boiling point at a given pressure. The subcooled liquid region is located to the left of the Andrews curve, where pressure variations are negligible. In this zone, by compressing the gas, the pressure does not increase until all the gas has transitioned to the liquid phase. Referring to the graph for methane in Chapter 1: Additionally, the pressure in the tanks during propellant loading is slightly higher than ambient pressure (1.1 to 1.5 bar) to avoid the ingress of humid air that could condense and freeze inside the tank. In this case, for simplicity, atmospheric pressure has been chosen as 1 bar. For *Pump Feed System* or *Turbo Pump Feed System*, the level of pressurization to be maintained inside the tank can vary from 0.17 MPa (1.7 bar) to 0.34 MPa (3.4 bar). These values allow, as mentioned above, a constant and regular supply of propellant to the engines, while turbopump feed systems have a relatively low inert tank mass. For simplicity, 0.30 MPa (3 bar) is taken as the operating pressure value.

The mass flow rate of the pressurizer has also been taken here for simplicity at 100 g/s, which is a very common value in pressurization systems. However, if we want to achieve a sizing in the WCS condition, the value represents the maximum pressurizer flow rate reported in the study [49]. In this case, 100 g/s is presented as the maximum permissible value of GHe at room temperature in a methane tank at 50 psia (≈ 3.45 bar).

For the expulsion times of both the pressurizer and the propellant, which are necessary, the second is for the calculation of the work done by the propellant, while the first is for the calculation of the energy contribution introduced into the tank; usually, these values are given by the mission requirements. The pressurization time can be estimated by evaluating the expected pressurizing mass divided by the nominal flow rate while maintaining a safety margin, given the discrepancy between the calculated mass and the actual used. For that of the propellant, the time of use of a stage can be taken as a reference. In this case, to follow the same

simplification that “the work is given by the product of constant pressure of the tank and the Δ volume”, a single engine shot with constant thrust is assumed.

Thus, as extracted from the rejection flow rates of other studies, such as [49], reasonable values can be between 1 kg/s and 3 kg/s. Flow rates of this kind for a tank of 10 m³ of methane at 120 K (density of 1.6776 kg/m³) mean about 13.42 kg and, therefore, an expulsion time of about 13 to 5 seconds. We assume the lowest flow rate to have more exposure time of the pressurizer with the walls (therefore, greater heat exchange and worst-case scenario).

For the pressurant flow, as reported in the study [37], the best condition of efficiency is obtained when the ratio between the expulsion time of the propellant and the pressurizer is about one. So, we can assume that the pressurizer will also have an ejection time of around 10 seconds during the entire mission.

These are all the minimum inputs needed to have a first evaluation of diffuser’s dimensions, of course to have a better simulation or precise code results other parameters can be implemented.

Variable	Value	Variable	Value
<i>Pressurant-Propellant</i>	<i>He – CH₄</i>	<i>Ullage %</i>	20%
<i>m_gas_dot [kg/s]</i>	0.1	<i>t_discharge_prop [s]</i>	13
<i>h_tank [m]</i>	3.4	<i>Tank_diameter [m]</i>	2.40
<i>Pressurant_tank_volume [L]</i>	≈ 10000	<i>Pressurant_T [K]</i>	293
<i>P_tank_0 [bar]</i>	1	<i>T_prop [K]</i>	120 ¹
<i>Final_P_tank [bar]</i>	3	<i>T_wall[k]</i>	140 ²

Table 4.1: Case study selected

For this case study, it is now necessary to define a series of possible input dimensions, taking into consideration the two main geometries, i.e., the axial and the radial, for which the reference dimensions r_0 are the radius of the inlet section and b_0 are the exit height. As presented in depth in Chapter 3 (figure 3.4), the code will calculate the efficiencies for each dimension, evaluating their heat exchanges.

The dimensions chosen for this case are:

$$\text{list_diff_dim} = \left\{ \begin{array}{l} 0.001, 0.01, 0.02, 0.05, 0.06, 0.07, \\ 0.08, 0.09, 0.10, 0.11, 0.12, 0.131, \\ 0.14, 0.15, 0.16, 0.17, 0.18, 0.20, \\ 0.25, 0.30, 0.35, 0.40, 0.45, 0.50 \end{array} \right\} \text{ [m]}$$

4.2 Calculations and Simulations

4.2.1 Python Code Interpretation

In this section will be reported the variables values from the Python[®] code presented in the following paragraphs; the relative plots with a brief explanations for each of them.

Geometries and positions Once all these inputs have been entered, you can run the code a first time to get the results.

```
Total tank volume: 11.7621 m^3
Ullage volume: 2.3524 m^3
Ullage height: 0.4680 m
Total tank surface: 25.6354 m^2
Ullage surface: 3.5286 m^2
Liquid height: 2.9320 m
Total tank volume: 11.7621 m^3
Ullage volume: 2.3524 m^3
Ullage height: 0.4680 m
Total tank surface: 25.6354 m^2
Ullage surface: 3.5286 m^2
The N1 position relation to the diffuser (x = 0): 0.2340 m
Free propellant surface in relation to the diffuser (x = 0):
X_POS_vap: 0.4633 m
Position of conversion from free to constricted flow:
X_costr_AX: 0.2330 m
X_costr_RAD: 0.1923 m

charact_flow_length
{'l_k_AX': 0.2350 m, 'l_k_RAD': 0.2350 m, 'l_s_AX': 0.2757 m, '
  l_s_RAD': 0.2757 m}
```

Chemical species' properties For the different chemical species used in this case

```
dati_LCH4_prop_AX
{'rho_1': 409.9023 kg/m^3, 'cp_1': 3549.2961 J/(kg*K), 'Beta_1
  ': 0.0038 1/K, 'mu_1': 9.8138e-05 Pa*s, 'Tm_1': 120.0000 K,
  'Lambda_1': 0.1720 W/(m*K), 'Molar Mass_1': 16 g/mol, '
  n_MOL_LCH4': 241066.0848 mol}

dati_\acrshort{GCH4}_prop_AX
{'rho_1': 3.2619 kg/m^3, 'cp_1': 2293.0000 J/(kg*K), 'Beta_1':
  0.0099 1/K, 'mu_1': 4.5837e-06 Pa*s, 'Tm_1': 120.0000 K, '}
```

```
Lambda_l': 0.0127 W/(m*K), 'nMOL_\acrshort{GCH4}': 0.1384  
mol, 'mole fraction': 0.5000}
```

```
gas_prop_data_AX
```

```
{'rho_g': 0.1659 kg/m^3, 'cp_g': 5193.2045 J/(kg*K), 'beta_g':  
0.0034 1/K, 'mu_g': 1.9611e-05 Pa*s, 'T_g': 293.0000 K, '  
Lambda_g': 0.1535 W/(m*K), 'Molar Mass_g': 4 g/mol, '  
n_MOL_gas': 1500.0000 mol, 'evap mole fraction': 0.5000}
```

```
HE-LCH4_AX_mix_data
```

```
{'rho_m': 2.5515 kg/m^3, 'cp_m': 3743.1016 J/(kg*K), 'beta_m':  
0.0067 1/K, 'mu_m': 9.5927e-06 Pa*s, 'T_m': 206.5000 K, '  
lambda_m': 0.0831 W/(m*K)}
```

Adimensional Velocity They represent the dimensionless values for calculating local velocities at certain points within the tank.

```
local velocity
```

```
{'um_1': 0.0400 m/s,  
'um_2': 0.2023 m/s,  
'um_11': 0.0204 m/s,  
'um_12': 0.1445 m/s,  
'um_costr_AX': 0.0402 m/s,  
'um_costr_RAD': 0.2221 m/s,}
```

Plots

- Dimensionless numbers Here, the different graphs are reported and discussed. In this first graph, the nature of the phenomena inside the tank can be guessed immediately. The dimensionless numbers allow us to understand the ranges in which the pressurizer flow is located at specific points and how the pressurizing propellant interactions evolve.

The Reynolds number (red quarters) upstream of the diffuser, and therefore only a function of the adduction section, shows how, for all dimensions, a mixture between turbulent and laminar characterizes the flow. The values for very small sections are around 10^5 , indicating quite accentuated degrees of turbulence, mainly due to the high input speed. These values then tend to decrease exponentially, as is logical given the increase in section and decrease in speed. For both geometries, the input flux tends to become laminar for medium-large sizes, while remaining around the values of 10^4 .

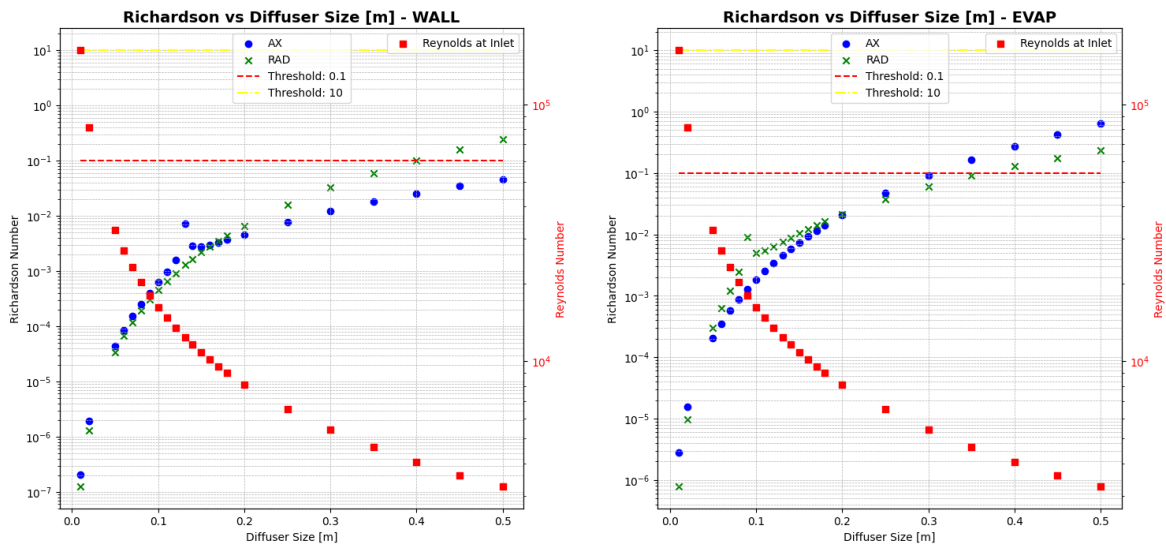


Figure 4.2: Dimensionless Numbers

The graphs then show the local Richardson values; remember that the Richardson number allows us to have an estimate of the type of convection with which the heat exchange takes place. Convection that can be forced or free, or mixed. The thresholds representing the zones are also represented, to allow the reader to immediately notice where the phenomena for the different configurations are positioned. As is logical here too, smaller sections and therefore higher inlet speeds mean that for both configurations and phenomena, exchange with the propellant (EVAP) or with the wall (WALL), the main form of convection is the forced one. While for sections that gradually grow the free component grows up to the area of convection mixed for the dimensions at the bottom of the scale. This immediately makes it clear that in this case study, we will have to work on finding a compromise between limiting forced convection as much as possible and not exceeding the size of the diffuser.

- Heat flux As mentioned above, heat fluxes must be limited during pressurization because they decrease the energy content introduced by the pressurizer. Therefore, understanding their magnitude and intensity remains one of the main factors of this work.

It is also relevant to understand the intensity ratio between the two primary sources of dissipation: wall exchange and that lost through the liquid. The figure allows us to understand that the phenomenon of wall leakage remains dominant for both configurations, with the flow towards the liquid representing only 30% on average for the axial configuration while counterintuitively greater for the radial one. In fact, if the latter has a share of 20% lost to the propellant for small outlet sections, with the increase of the

section, it tends to increase until it even exceeds the wall for full-scale values. This result is probably due to two factors: the first is the lack of an adequate evaporation model that would have enhanced the contribution to the propellant of the axial diffuser. The second, on the other hand, is linked more than anything else by the physics of impingement; on the one hand, the flow arrives perpendicular to the propellant and therefore, tends to bounce towards the walls (and not lap it as per the diagrams and drawings of the sources); the pressurizer will return upwards, limiting the exchange to a very short phenomenon. For the radial configuration, the exit towards the walls of the gas that then slows down and moves downwards can justify this phenomenon. Even more so when the input reaches significant dimensions and, therefore, the output takes place at much more limited speeds.

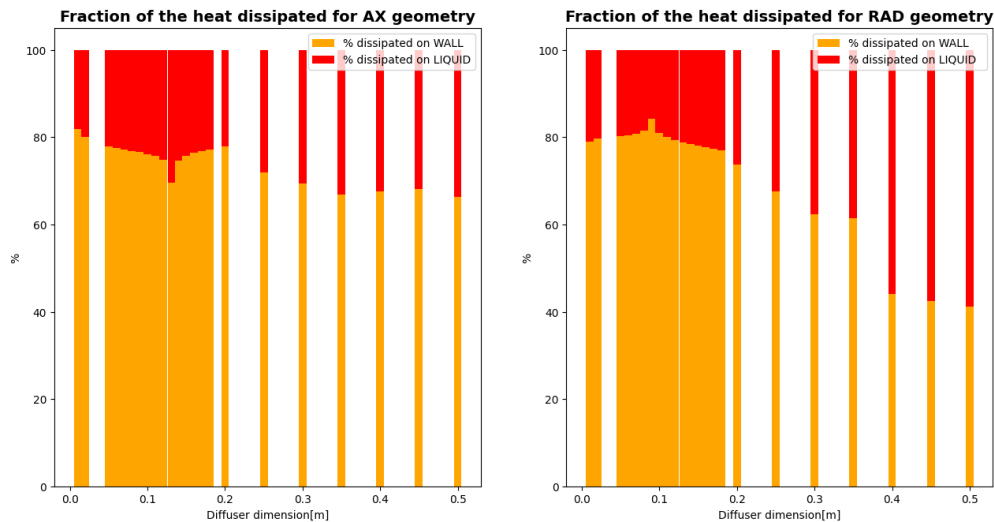


Figure 4.3: Heat Fluxes vs Diffuser dimensions

- Penetration limit: The pressurizer impingement must be included to address the problems presented in the previous chapters. This requirement is then implemented in the code in order to be able to define a speaker placement height. The limit presented is that of the study [37], which defines the threshold below which to stand. The ordinates show the ratio between the value of the deflection of the liquid created by the jet and the equivalent diameter of the inlet. Also, in this case, the decrease is almost related to the speed and, therefore, to the inlet section; smaller sections translate into higher speeds and, therefore, higher deflection levels above the limit. In this case, the inlet height of the pressurizer ($H_{g,0}$) of which H_{fr} is a function is placed at 10 cm from the highest point of the dome. It should also be remembered that in this study, we analyze an input

from above in a direction perfectly perpendicular to the liquid. In this case, the position concerning the incoming liquid seems to be adequate since the threshold intersects the ratio curve between the dimensions 0.14–0.15 for the axial configuration and 0.16–0.17 for the radial configuration. If there was no intersection point, the positioning distance in the code should have been increased.

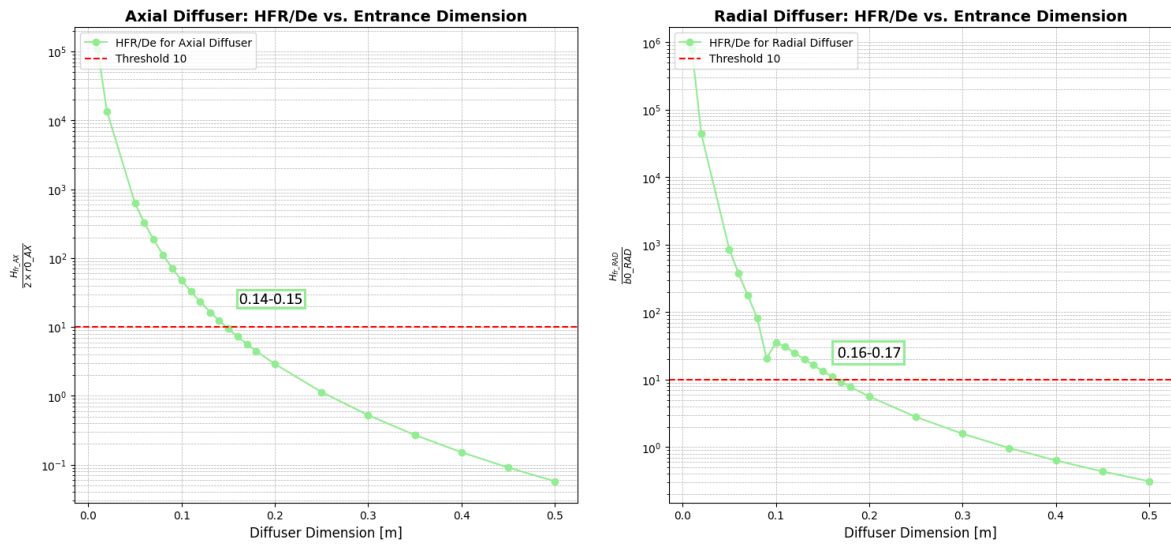


Figure 4.4: Penetration of diffuser

- Efficiency The efficiency curve then represents the last graph presented by the code. The efficiency, as presented in Chapter 3, is a helpful parameter to understand, as a function of the input sections, the contributions of the energy balance (3.16) as they change as a function of the input size. The trend is that of an asymptotic curve approaching 1 for the largest dimensions.

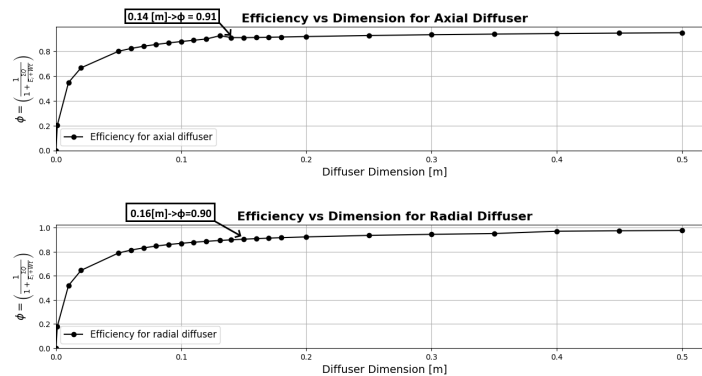


Figure 4.5: Efficiency for different dimensions

The asymptotic behavior occurs because the only elements to change are the dissipative phenomena which, as seen above, decrease as the input speed decreases (larger sections) because the forced convection phenomena are increasingly limited. Once the flow rate, pressure, and volume values have been fixed, the work and the input energy cannot be varied. In addition, these graphs are useful to understand the value of the size of the diffuser, such that the efficiency changes little despite further size increases; therefore, increases are not very useful.

Post Processing and models

The graphs shown in the previous paragraphs allow us to understand several significant conditions. The importance of the forced convective flow was immediately emphasized, as well as the almost always greater extent of the heat lost on the wall compared to the evaporative one. These are two excellent ideas for a reflection presented in this section, at the end of which the dimensions of the gas injectors used in the subsequent CFD checks will be defined. Therefore, the distribution of temperatures inside the ullage becomes important in terms of diffuser performance and, at the same time, the minimization of dissipative flows, especially those on the wall.

As was logical, the larger the size of the diffuser, the better the efficiency; a concept similar to that of the section of a divergent, where the greater the outlet area (with fixed inlet area), the greater the slowdown of the gas. It is, therefore, tempting to take the configuration with the largest size of all, but a choice of this type would not even have needed a pre-analysis code. To get the best possible diffuser, you just need to make it as large as possible, but at this point, some constraints related to mass and dimensions come into play. The diffuser is an element that most of the time is detached and independent from the tank; inserting a diffuser with a radius of 30-50 cm would mean having an element that, in this case, is almost half the width of the tank itself, affecting the integrity of the structure as well as all the problems related to assembly. A more appropriate size is then selected. It could be a good choice to select the size straddling the propellant deflection requirement. The values respectively are:

$$r_0 \rightarrow 0.14 \text{ [m]}, r_0 \rightarrow 0.16 \text{ [m]}$$

Also, both have an efficiency above the threshold value of 90%. As previously presented, the configurations chosen are axial and radial; the studio desires to study both behaviours according to the dimensions presented several times, r_0 and b_0 . However, we have always tried to link both exit sections to make an equal comparison despite the different geometries. The axial configuration, characterized by a duct of radius r_0 and the height simply h , instead of the radial one, to have the same output area, therefore presents that the bottom of the diffuser

of dimension d , which is obtained by (3.22) thus obtaining all the dimensions necessary for the construction of a geometric model using geometric modelling software. The model that is created will only include what is present in the ullage, so a negative of the profile of the upper part of the tank is created, and consequently, the volume of fluid that is contained in the ullage itself, the will will be studied the ullage environment and its dynamics.

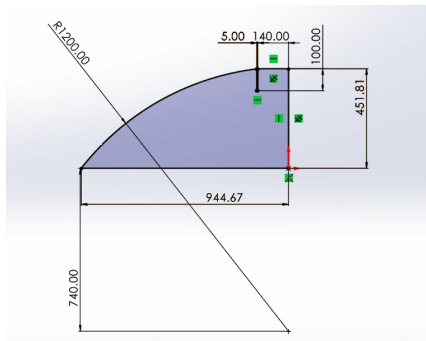


Figure 4.6: Ullage profile

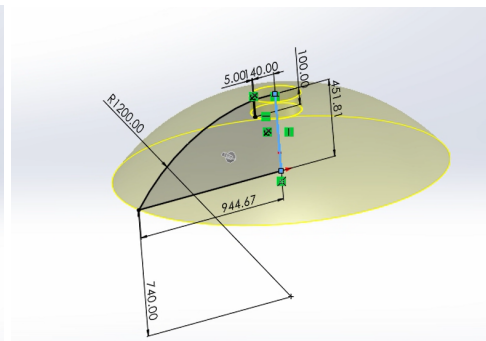


Figure 4.7: Revolution technique

Figure 4.8: Axial ullage using Solidworks©

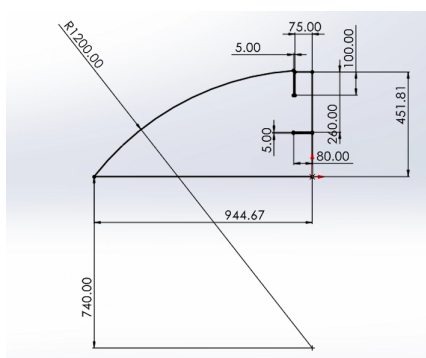


Figure 4.9: Ullage profile

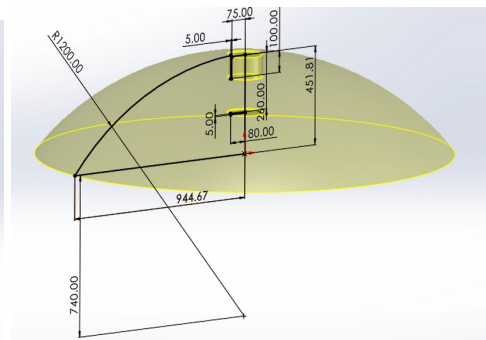


Figure 4.10: ullage construction by revolution

Figure 4.11: Radial ullage using Solidworks©

4.2.2 CFD Cases Used for Verification

Once the dimensions of the two configurations chosen to be simulated have been defined, the next step is to set up the fluid dynamics simulations using the Fluent© software. The steps are defined in Chapter 3; the procedure, however, consists of defining some areas necessary for the analysis, such as INLET and WALL. We then move on to the meshing phase where, given the connection between the mesh's goodness and the simulation's correct success, it is necessary to define both in the most similar way possible with a good degree of precision.

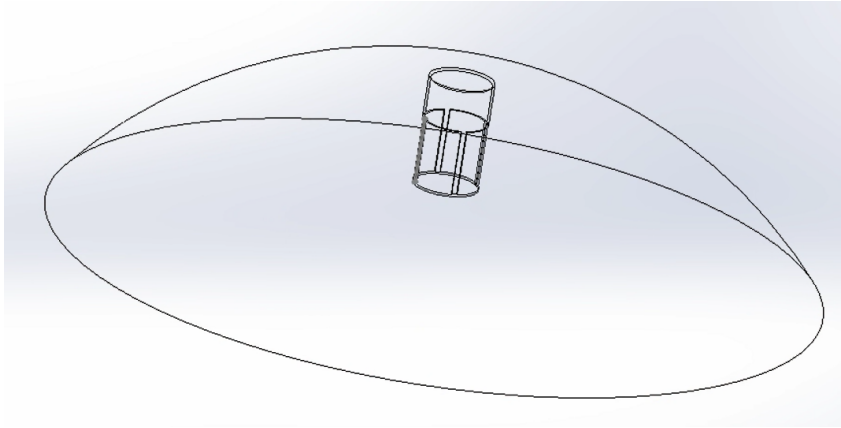


Figure 4.12: design- Geometry completed

Then follows the case set-up phase, then the definition of the operating and boundary conditions, the equations solved in the process, the physical quantities to be evaluated and the convergence conditions. Meshing and analysis set-up are two of the most complicated steps in the entire process. The parameters set for the analyses are shown below:

Meshing For meshing processes, special attention is paid to the liquid where the pressurant hits, especially for the axial configurations and the respective outlet section of the diffuser, which are the more difficult zones to simulate. For both configurations, we have chosen to use 3 boundary layers in the wall section and add a mesh refinement with a growth rate of 1.15. That is because the past simulations highlighted a convergence problem where propellant hits the liquid, which is considered a wall, so particular attention is needed. For the configuration, as with the bottom of the diffuser, a 3-layer-thickness boundary layer has been implemented for the zone's importance.

The parameters have been kept as similar as possible for both configurations. The number of cells, both around 700000, is the compromise between obtaining a good degree of precision of the solutions and, at the same time, simulations that are not too demanding in terms of calculation time. As reported in Chapter 3, it has been shown that this is not the place to carry out advanced analyses in terms of simulations. The need to create local sizing of meshes in certain zones and boundary layers generated this final number of cells. A polyhedral mesh was then chosen as reported in the previous chapter of the description of the methodology, thus obtaining a slightly larger mesh for the geometry, which is reasonable given the local sizing area also at the output section of the speaker. Despite this, the second mesh has a minimal, lower orthogonal quality, which suggests that the first is probably less distorted. At the same time, the "Maximum Aspect Ratio" of the former is higher than the latter, indicating that the latter has a character of greater stability than the simulations. Neither of them has isolated

cells, also because they are made only of a single piece, the volume of ullage.

Set Up Once the mesh has been defined for both configurations, the simulations must be set up. In this step, the fluid dynamics simulation will represent the entire ONG pressurization phase, from 1 to 3 bar, with a constant flow rate corresponding to the WCS conditions. When the value is reached, the inlet flow rate is cancelled in order to analyze the evolution of the ullage and thus be able to determine which of the two configurations best maintains the pressure level. The goal is to examine the behaviour in the worst possible operating condition, evaluating the thermal flows, but not only; the aim is also to determine which configuration has the best speed distribution through a series of surfaces built ad hoc to “collect” the components and the velocity module. The simulations were carried out under the same conditions and are also presented in the 4.1 section, with the tank wall and the liquid considered as walls at constant temperatures, while ullage presents a linear distribution of temperatures from the free surface of the propellant to the tank wall. All tank surfaces comply with the principles of adiabatic and “No slip” conditions. For the distribution of chemical species, on the other hand, unlike the section of code where an instant of the entire pressurization process was represented, in this case, the pressurization is simulated in full; therefore, at the initial instant, the ullage will only present methane. The starting gauge pressure will be $-200,000[Pa]$.

To capture all the phenomena correctly, a time step of 0.01 was necessary, and 70 iterations were needed for each time step to achieve convergence.

Simulations Multiple simulations were carried out to set up correctly, although fundamental support was that of the company figures who followed the author during the internship period, allowing him to acquire the fundamental skills for the realization and compression of this step. Several attempts were made due to the low stability of the first configuration, demonstrated by residues that did not reach the convergence condition despite the high number of iterations per time step. Then, subsequent mesh models were created, simultaneously modifying the simulation parameters until the results presented here were achieved. Approximately five models have been defined for each configuration and no less than the changes to the test settings.

As mentioned above, the simulations required much effort, given the number of cells and the means available. Several analyses have been carried out with subsequent improvements; the results and contours obtained are reported below. To have a complete view, 4-time instants of the process have been selected, respectively, $t = 0s$, in order to show the conditions at initialization, then $t = 1s$, in the middle of the pressurizer adduction phase, $t = 2s$ a few

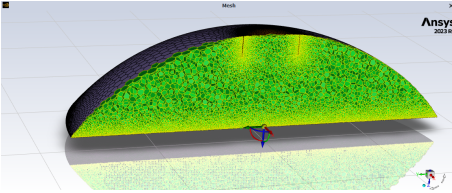
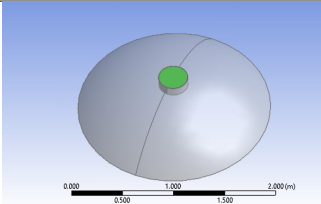
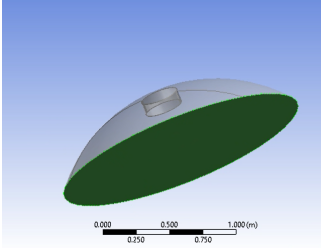
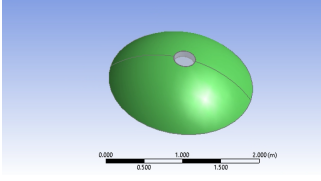
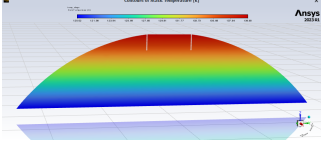
Element	Hypo/Model	Notes/Images
Reference File	Diffuser: Diff with dimensions from code TEST_TANK_9 CAD: Cupola_diff_RAD.STEP Mesh: FFF.2.msh.h5	Diffuser dimensions from Python code. $r_0 = 160$ [mm] $h = 100$ [mm], $d = 0.160$ [mm]
Iterations	Time Step Size: 0.01 [s] No. Of Time Steps: 1000000	
Mesh	Boundary: inlet -> Mass-flow-inlet liquid -> wall wall_dome -> wall Regions cupola_radlprt -> fluid Add local sizing: liquid_sizing-> Growth Rate 1.15 Target_mesh size[m]-> 0.005845 Liquid layer: Number of Layers:3 Transition Ratio:0.272 Growth Rate: 1.15 Volume Mesh: Polyedra Max Cell Length [m]: 0.047434 Volume Diagnostics: Total Number of Cells = 772668 Minimum Orthogonal Quality = 0.2323 Maximum Aspect Ratio = 14.84 Number of Isolated Cells = 0	
Inlet (Fluent)	-Type: mass-flow inlet (100 g/s) Till reaching the Nominal pressure level when mass-flow inlet = 0 g/s -Normal to Boundary	
Species	ch4->0	In the inlet section is assumed no CH4
Temperature	293 K	Temperature from the case
Wall: liquid	Stationary Wall Species: Mass Fraction: ch4 = 1 No slip condition, temperature 120 K ch4 -> 1	
Wall: cupola_diff_ax:1	-Stationary Wall -Species: Mass Fraction: ch4 -> 0 -Heat flux = 0	
Wall: wall_dome	-Temperature: 1400 K -ch4 -> 0 -Stationary Wall -No slip	
Operational conditions	-Operative Pressure: 300000 [Pa] -Temperature: 293 [K]	
Initialize	-Gauge Pressure: -200000 [Pa] -ch4: 1 -Temperature Patch: 43.4783 [K/m]*z + 120 [K]	
Mixture Template	Density: Ideal Gas	

Table 4.2: Summary Table for the Simulation with Large Dome and Tank

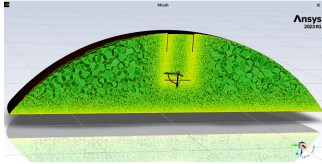
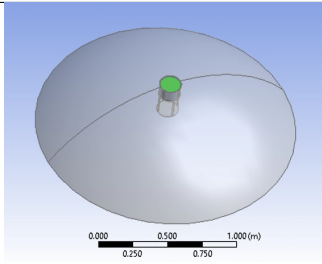
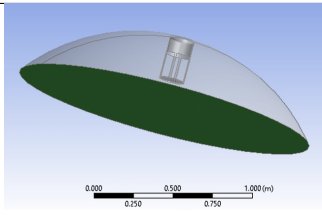
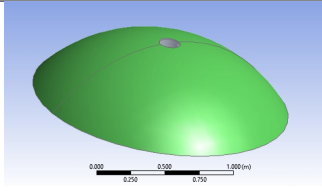
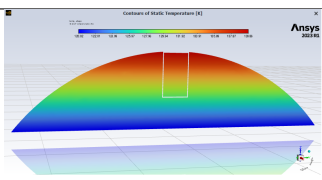
Element	Hypo/Model	Notes/Images
Test for AXIAL ullage configuration		
Reference File	Diffuser: Diff AX with dimensions from code TEST_TANK_8 CAD: Cupola_AXLDPRT.STEP Mesh: FFF.msh.h5	Diffuser dimensions from Python code. $r_0 = 140$ [mm] $h = 100$ [mm]
Iterations	Time Step Size: 0.01 [s] No. Of Time Steps: 1000000	
Mesh	Boundary: inlet -> Mass-flow-inlet liquid -> wall wall_dome -> wall piastra->wall Regions cupola_diff_ax -> fluid piastra->dead Add local sizing: liquid_sizing -> Growth Rate 1.15 Target_mesh size [m] -> 0.005845 fondo_sizing-> Growth Rate:1.15 Target_mesh size [m] -> 0.03 [m] Volume Diagnostics: Total Number of Cells = 796081 Minimum Orthogonal Quality = 0.262 Maximum Aspect Ratio = 9.61 Number of Isolated Cells = 0	
Inlet (Fluent)	-Type: mass-flow inlet (100 g/s) Till reaching the Nominal pressure level when mass-flow inlet = 0 g/s -Normal to Boundary	
Species	ch4->0	In the inlet section is assumed no CH4
Temperature	293 K	Temperature from the case
Wall: liquid	Stationary Wall Species: Mass Fraction: ch4 = 1 No slip condition, temperature 120 K ch4 -> 1	
Wall: cupola_diff_rad:1	-Stationary Wall -Species: Mass Fraction: ch4 -> 0 -Heat flux = 0	
Wall: wall_dome	-Temperature: 1400 K -ch4 -> 0 -Stationary Wall -No slip	
Operational conditions	-Operative Pressure: 300000 [Pa] -Temperature: 293 [K]	
Initialize	-Gauge Pressure: -200000 [Pa] -ch4: 1 -Temperature Patch: 43.4783 [K/m]*z + 120 [K]	
Mixture Template	Density: Ideal Gas	

Table 4.3: Summary Table for the Simulation with Large Dome and Tank

moments after reaching 3 bar, part of both configurations. Finally, $t = 6s$, to analyze the evolution of ullage after pressurization.

CFD Results

Residuals In both analyses, the convergence parameters were left with the default ones of the program 0.001, except for continuity and energy, where the values of 1×10^{-6} were set. The lowering of the threshold was necessary due to the various convergence problems obtained in previous simulations. For both simulations, a maximum of 70 iterations was set for time steps and 0.01s as the time interval of iterations; with these parameters during the pressurizer supply phase, both configurations presented a stable behavior for each time step, often reaching pre-established thresholds even before iterations were finished.

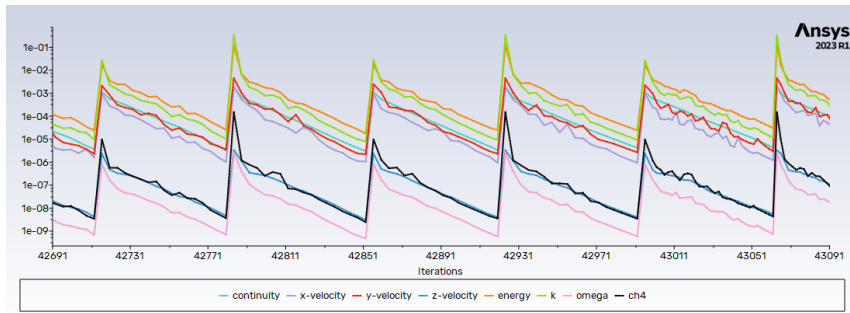


Figure 4.13: Residuals for TT8 analysis

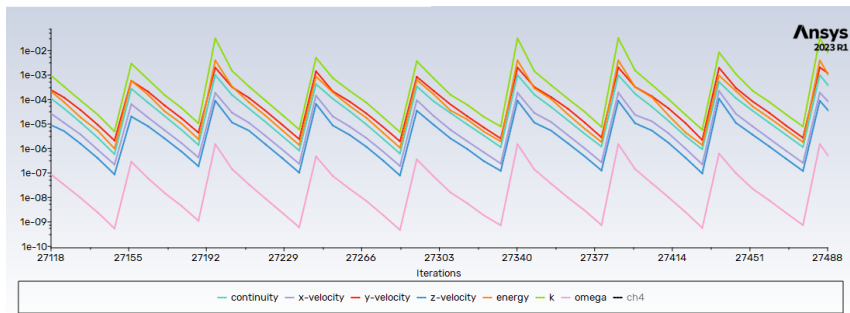


Figure 4.14: Zoom of the residuals after the analysis

On the other hand, when the nominal pressure value was reached, and the subsequent shut-down of the flow rate ($\dot{m}_{gas} \rightarrow 0 \text{ Kg/s}$) led to minor problems in terms of residue stability, especially in the seconds just after. In this case, the simulations required all 70 iterations imposed to achieve convergence. For the rest of the simulation, there were no problems related to the numerical stability of the simulations. In performance terms, the two configurations reached the value of the nominal pressure at instants:

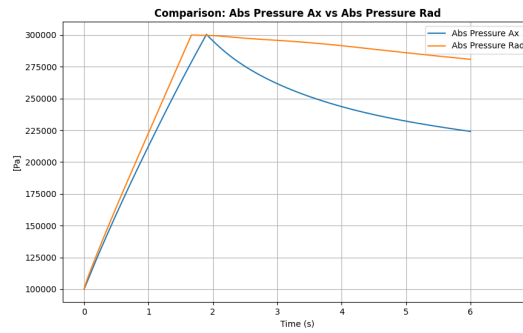


Figure 4.15: Absolute pressure vs time obtained during CFD simulations

- $P = 3 \text{ bar} \rightarrow t = 1.67 \text{ s}$
- $P = 3 \text{ bar} \rightarrow t = 1.90 \text{ s}$

Compared to the axial analogue, the radial configuration reaches the operating condition a few moments earlier. The latter could, in fact, suffer from the lack of the evaporative contribution of the liquid, which could have helped it. For both configurations, a constant increase in pressure is noticeable, consistent with the constant flow supply for pressurization.

Contours The contours of the main physics dimension evaluated using the contours will be reported here. Taking different contours at different times instants it possible to build the time evolution.

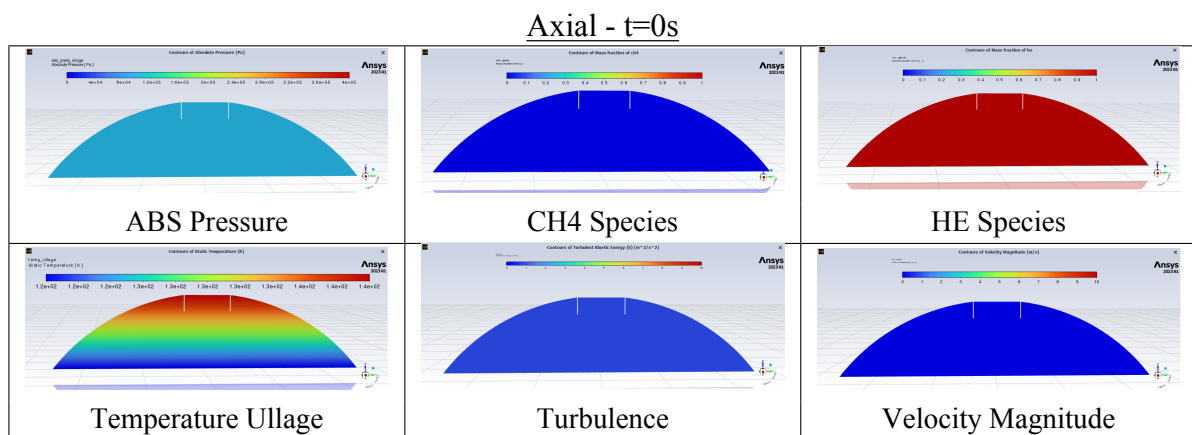


Table 4.4: Contours of dimensions after 0s of flow time.

Axial - $t=1s$

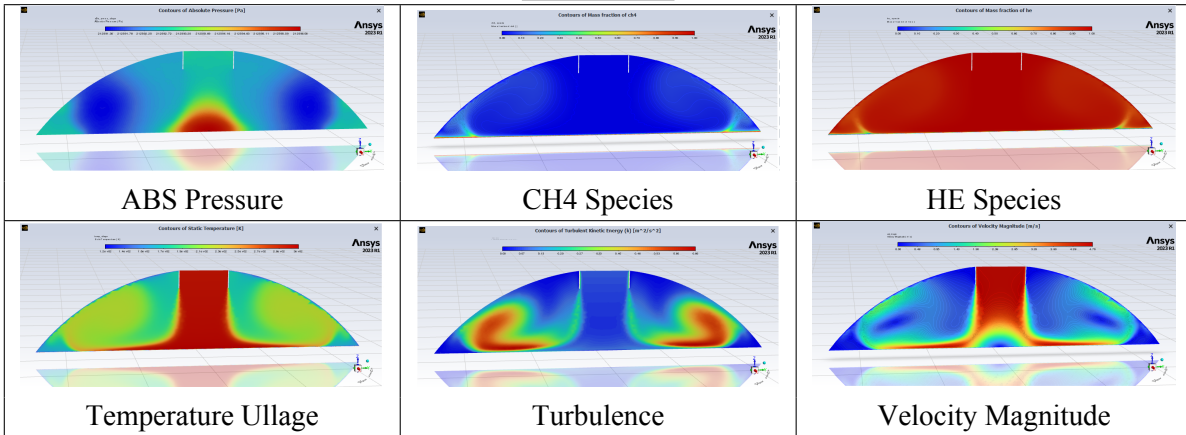


Table 4.5: Contours of dimensions after 1s of flow time.

Axial - $t=2s$

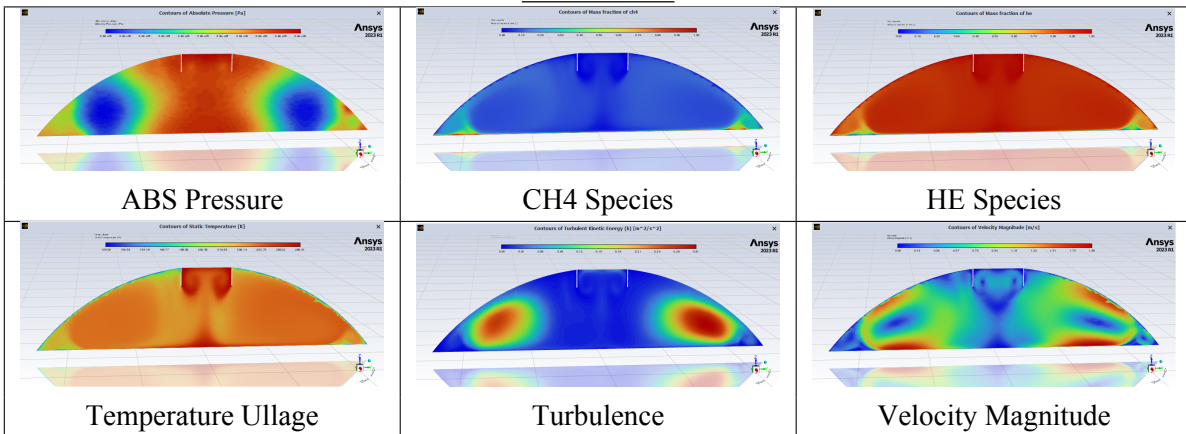


Table 4.6: Contours of dimensions after 2s of flow time.

Axial - $t=6s$

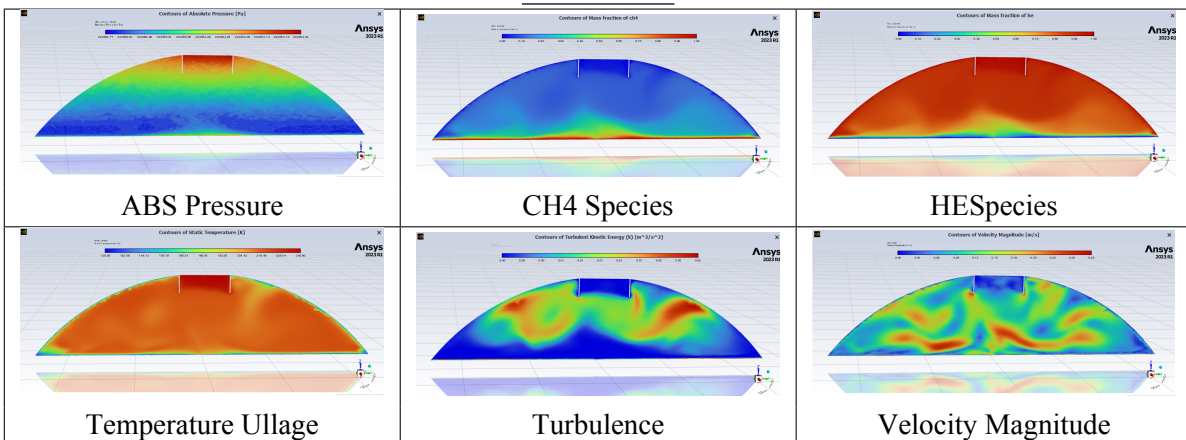


Table 4.7: Contours of dimensions after 6s of flow time.

Radial - t=0s

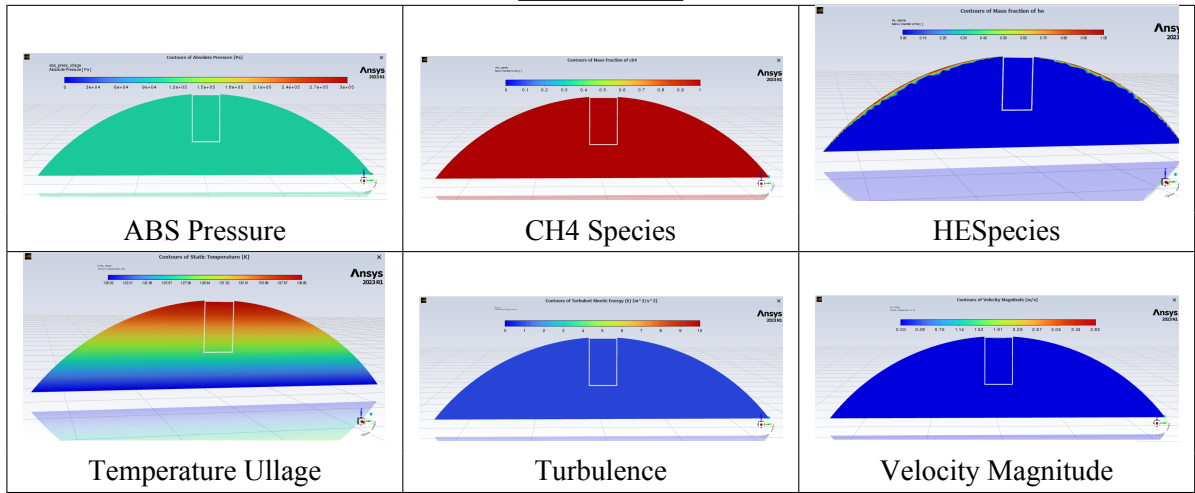


Table 4.8: Contours of dimensions after 0s of flow time.

Radial - t=1s

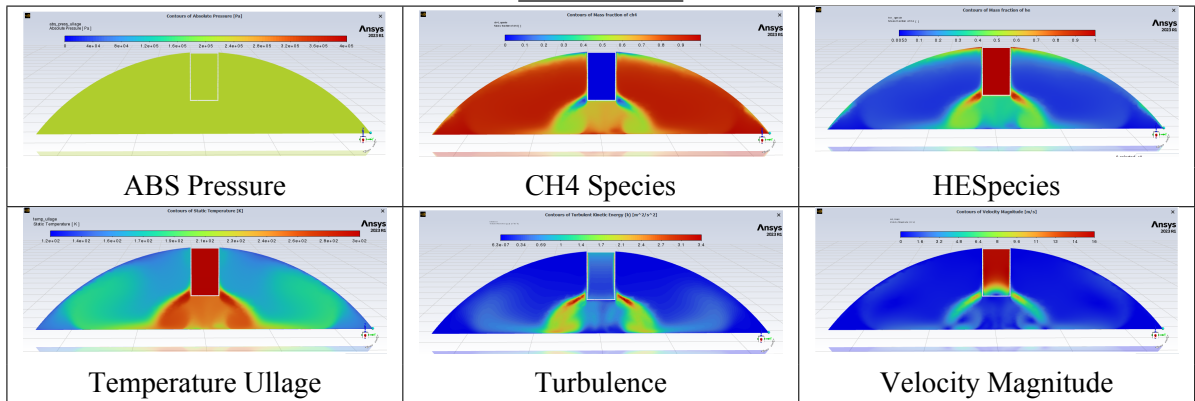


Table 4.9: Contours of dimensions after 1s of flow time.

Radial - t=2s

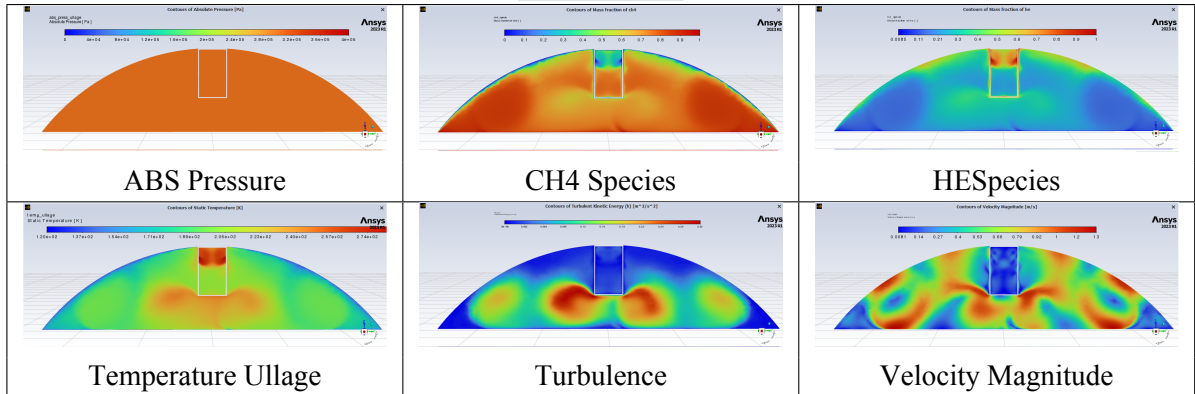


Table 4.10: Contours of dimensions after 2s of flow time.

Radial - t=6s

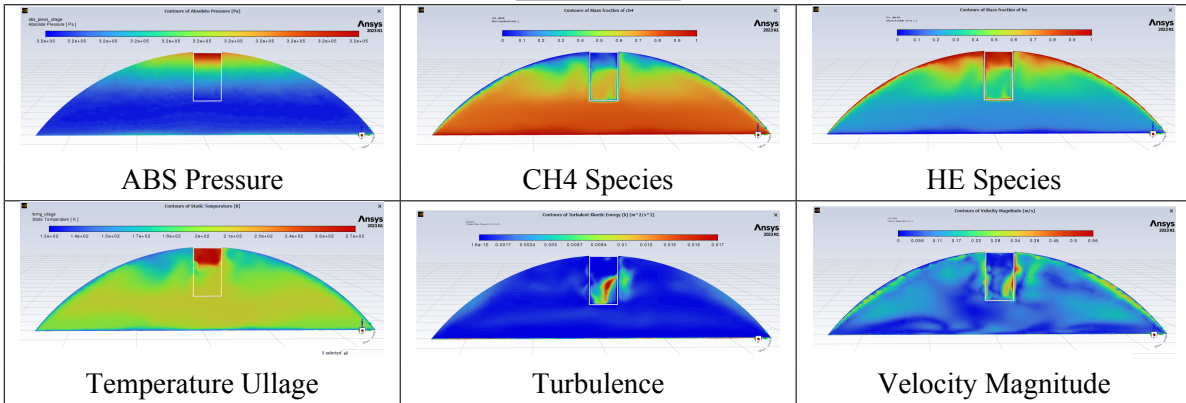


Table 4.11: Contours of dimensions after 6s of flow time.

Post Processing

When the operating pressure is reached, the pressurizing flow rate, previously constant for both configurations at 0.1 kg/s, is cancelled. As can be seen from Figure 5.5, where the flow rate that crosses the inlet surface and that which surrounds the two sections of the outlet from the diffuser (outlet surface) are compared, after an initial instant of peak flow through the outlet due to the mass of methane that had invaded the interior of the diffuser, the geometry approaches the value of the inlet of about one-tenth of a gram for both configurations. It should be noted in the radial configuration that at the instant of closure of the flow, the flow through the outlet surface of the diffuser becomes even negative, probably due to the onset of instability at the moment of transition between the open and closed flow condition.

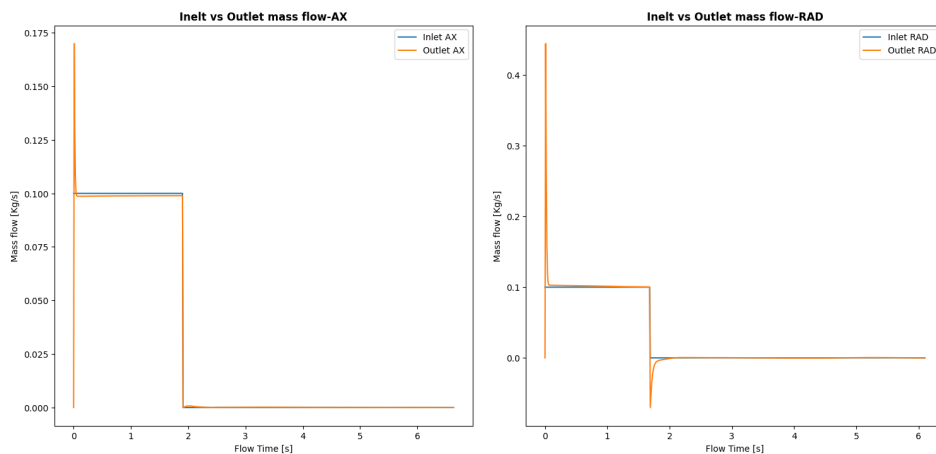


Figure 4.16: Mass flow inlet and outlet through the control surfaces for both configurations

The temperatures in the ullage, obtained as a "Mass Average" report through the entire volume of the fluid analyzed, show how the temperatures for both tend to decrease exponentially. The

axial configuration has a much more marked trend than the radial one, which instead has a much less steep slope. The slope indicates, in line with the pressure trend, how the axial configuration loses its pressurization capacity more quickly, thus indicating a greater degree of dispersion that will be discussed later.

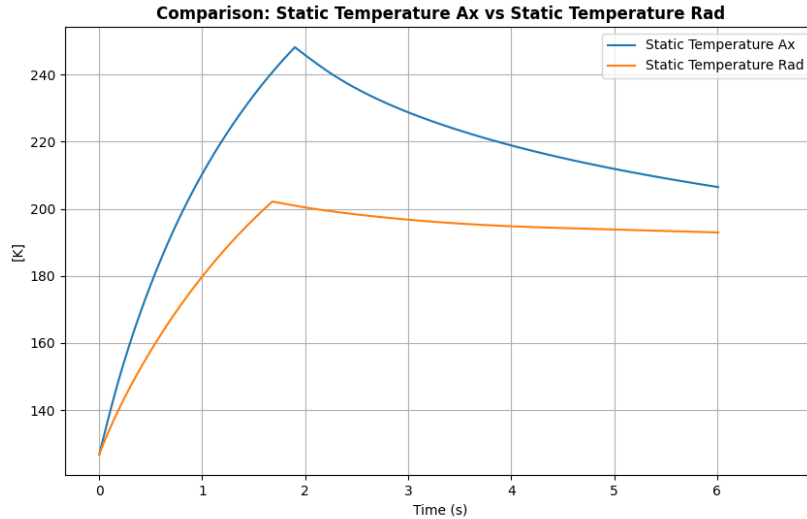


Figure 4.17: Static ullage temperature vs. time

Still on the subject of temperatures, once the control lines that cut the ullage in both radial and axial directions have been defined, the distributions are reported with the evolution of pressurization from the initial instant $t = 0$ to the final instant of the process $t = 6$ seconds. Analyzing first the radial distribution through the ullage, it is interesting to note that contrary to what was imagined, it is the axial configuration that, over time, sees an accumulation of higher temperatures in the direction of the walls. In fact, there is an evident plateau right at the ends of the lines with temperature values that are always higher than the relative axial configuration. In addition, at different times, the average temperature of the axial configuration is always greater than that of the radial one.

Time (s)	Average Temperature (AX) [K]	Average Temperature (RAD) [K]
0	129.2421	129.2434
1	223.4349	222.3991
2	239.1505	208.6489
6	211.0634	203.6954

Table 4.12: Average Temperature Comparison- (Radial Trend)

This, therefore, partially contrasts with previous studies. It would seem that in these conditions, the radial configuration affects the walls less than the axial counterpart.

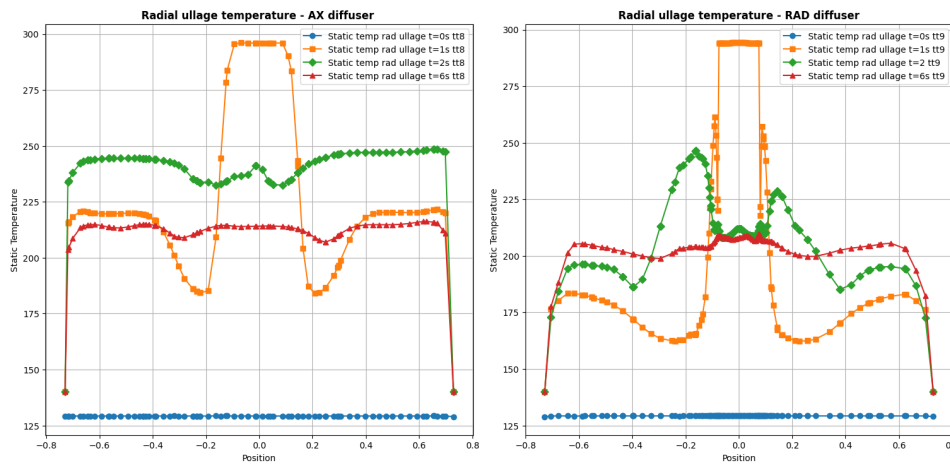


Figure 4.18: Arrangement of temperatures on radial lines at ullage at different time points

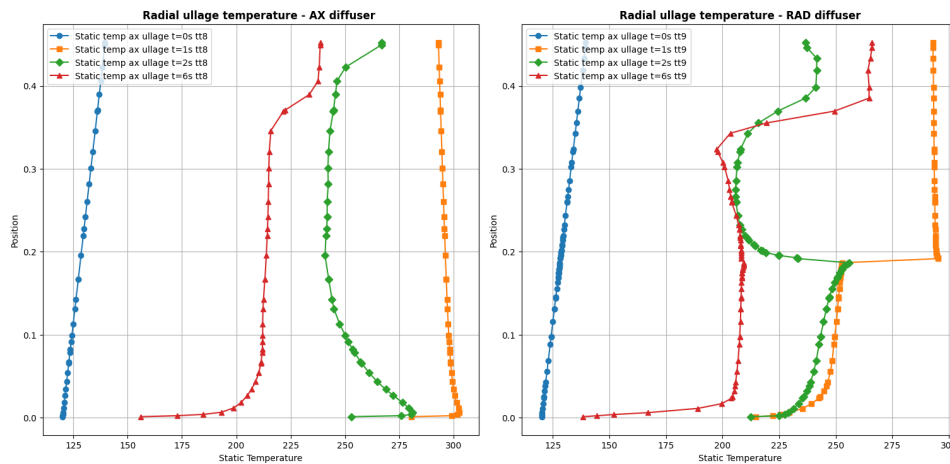


Figure 4.19: Arrangement of temperatures on axial lines at ullage at different time points

If, on the other hand, we look at the trend of axial temperatures in reference from the axis of the tank, we can see the very high gradient near the liquid ($y = 0$) for both configurations, but this is the only degree of similarity. Moving towards the dome of the tank (about $y = 0.450$ m), you can see how the temperature is almost constant with zero slopes in this case. For the radial geometry, on the other hand, there is a point of discontinuity, which is the passage through the bottom of the diffuser; after passing the physical element in the moments of pressurization, the value moves upwards with a constant value equal to that of the inlet flow rate. For both configurations, it can be seen that starting from the linear temperature distribution, there is a leap forward in temperatures as long as pressurization continues and then retreats with the stop of the inlet flow. In this case, the average temperatures are much more similar, presenting only an important difference during pressurization due to the presence of the diffuser body.

Other strategic parameters of importance are thermal flows, which are necessary to under-

Time (s)	Average Temperature (AX) [K]	Average Temperature (RAD) [K]
0	127.8220	128.3849
1	296.5843	269.8965
2	254.1081	230.4771
6	211.7913	208.9639

Table 4.13: Average Temperature Comparison (Axial Trend)

stand which geometry has greater dissipation through the liquid or the wall. As mentioned in the previous chapter, among the standard reports introduced in the simulations, there are the thermal fluxes per unit area, therefore the $[W/m^2]$, one for the terms lost on the wall and the second for the terms lost on the liquid:

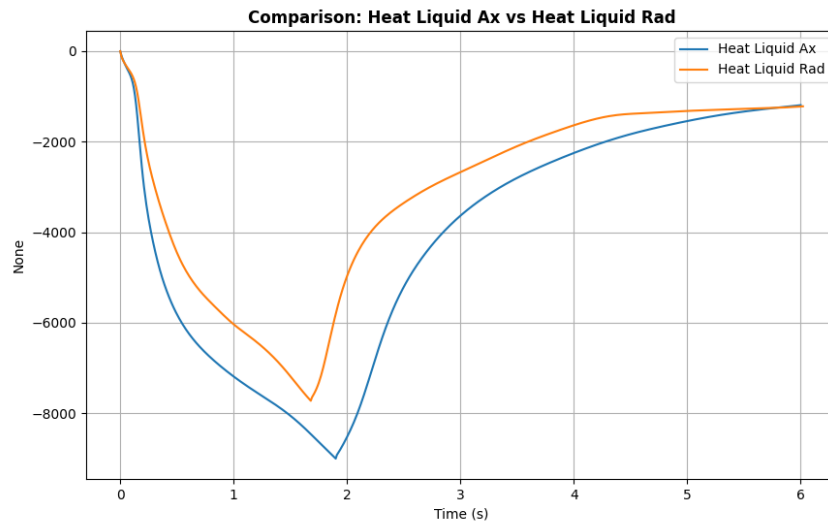


Figure 4.20: Heat fluxes per unit area on propellant for both configurations as a function of time

In both configurations, shown in Figures 4.20 and 4.21, it is possible to see that the geometry with the greatest dissipation fractions is the axial one, both in the propellant (reasonable given by the impingement) and in the wall one. These graphs also agree with those relating to the temperature distribution commented above; the axial has, in fact, higher temperatures, both in coincidence with the walls and the propellant. The fluxes to both sources of dissipation increase with increasing pressurization; this is due to the increase in the average temperature of the ullage in contrast to the temperatures of the WALL liquid and tank_wall. When the pressure value is reached, and the flow rate closes, the flows gradually decrease.

Therefore, taking the absolute values of the flows into consideration and summing them together, the axial configuration is more dissipative.

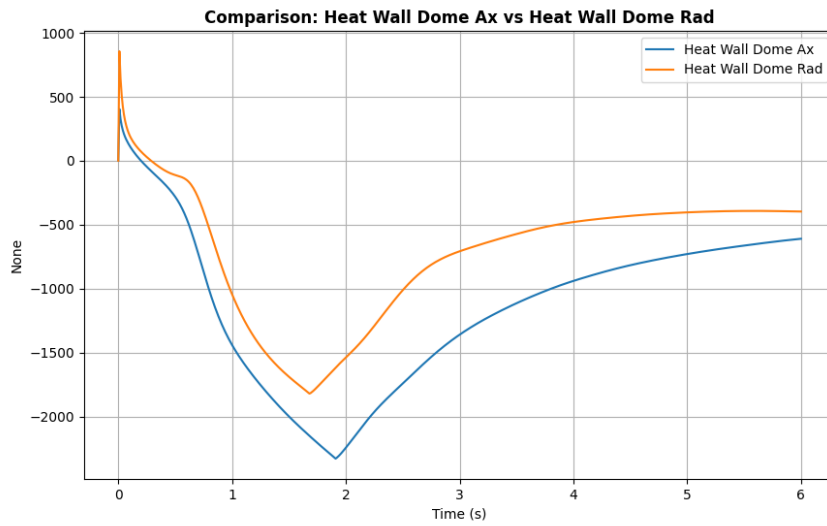


Figure 4.21: Heat flux on the tank walls as a function of time

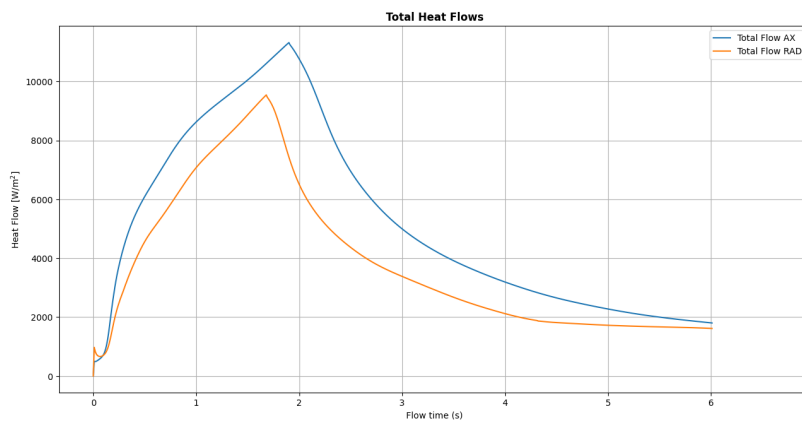


Figure 4.22: Sum of heat flux modules in both configurations as a function of time

Let's look at the velocity distribution across the surfaces created during the simulation in Fluent[®]. As reported in Chapter 3, studying the output flow rates is necessary to evaluate whether the diffuser does its job more rigorously. This step is carried out in the post-processing phase, thanks to a Python[®] program that reads the values exported at different times from the Fluent[®] analyses of the velocity components that pass through the surfaces defined above.

In order to evaluate the diffuser, we use the definition given in Chapter 2, that of a device that slows down and tries to standardize the output speed profiles. In the post-processing, the velocities in modulus and the most relevant components will be examined by graphing the frequency histograms to see their distribution. The chosen components that will be compared will be, respectively, for the axial configuration, the z component of the speed, the one coinciding with the axis of the tank, while for the radial geometry, it will be the radial speed. The other components have small values on which to carry out an analysis.

The distributions of the velocities will be reported at the time in which the nominal pressure is reached.

The standard deviation will be used as a means of post-processing, i.e. the degree of dispersion of a certain series of values around the mean value.

The formula for the standard deviation is given by:

$$\sigma = \sqrt{\frac{1}{N} \sum_{i=1}^N (x_i - \mu)^2}$$

where:

- N is the total number of observations in the dataset,
- x_i is each value in the dataset,
- μ is the mean of the dataset.

A low standard deviation value is a symptom of low variability, i.e., the data are well grouped around the average; on the contrary, high means that the variability rate is high. According to the reasoning carried out in the previous chapters, the evaluation method will be to obtain the lowest possible values own for the terms of standard deviation.

Axial Configuration (AX) - Modulus Surface 1 - At diffuser exit surface:

Average speed: 2.71 m/s

Standard Deviation: 0.96

The flow just outside the duct in the axial configuration is characterized by a relatively high

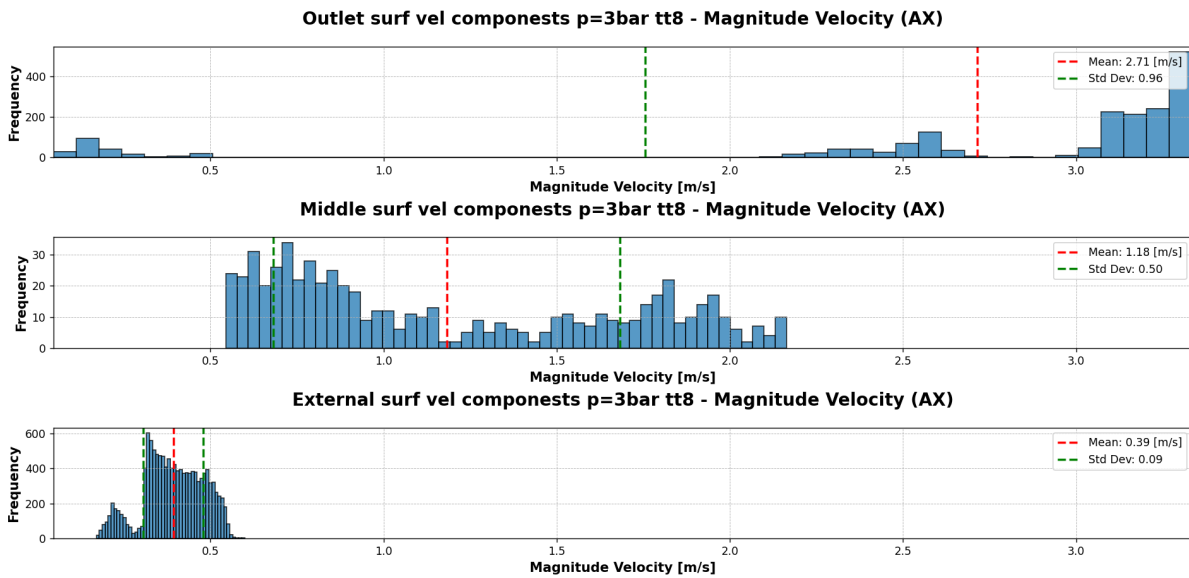


Figure 4.23: Magnitude velocity distribution around AXIAL diffuser at the instant of reaching P = 3 bar

velocity, with a moderate standard deviation. This indicates that the flow has a fair velocity with variations around the mean but is not excessively turbulent.

Surface 2 - Two r_0 radius surface:

Average speed: 1.18 m/s

Standard Deviation: 0.5

The average velocity decreases concerning Surface 1, so the flow slows down as it moves away from the conduit. The standard deviation is lower, suggesting that the flow is more uniform than in Surface 1, as was intended to be demonstrated by moving away, the flow reaches a certain degree of uniformity.

Surface 3 - Three r_0 radius surface:

Average speed: 0.39 m/s

Standard Deviation: 0.09

The average velocity is reduced further, close to zero, indicating that the flow has lost much of its energy; the standard deviation has also decreased, suggesting that the flow is extremely uniform at this distance.

Radial Configuration (RAD) - Velocity Modulus

Surface 1 - At diffuser exit:

Average Speed: 5.64 m/s

Standard Deviation: 3.82

Remark: The flux just outside the diffuser has a high average velocity and standard deviation.

This indicates that the flux has a fair degree of variability and can, therefore, be characterized by significant turbulence.

Surface 2 - Two b_0 radius surface:

Average speed: 0.71 m/s

Standard Deviation: 0.23

Remark: The average velocity decreases dramatically from Surface 1, indicating that the flow is slowing down. It also reduces the standard deviation, thus suggesting that the flow has less variability than of Surface 1, but is still far from uniformity.

Surface 3 - Three b_0 radius surface:

Average speed: 1.98 m/s

Standard Deviation: 0.73

The mean velocity and also the standard deviation increase; such an increase is unusual and could indicate a complex interaction of the flow with turbulence. However, the standard deviation remains lower than that of Surface 1, suggesting that the flow is more even despite the increase in velocity.

General Observations

Axial (AX): The velocity modulus decreases progressively as you move away from the duct, with a significant decrease in standard deviation. This suggests that the flow becomes more uniform and less energetic with distance before it interacts with the liquid.

Radial (RAD): The velocity modulus starts with a very high value and great variability just outside the duct, then slows down before increasing again. The standard deviation follows a similar trend, with high variability near the duct, decreasing at an intermediate distance and then increasing slightly at a greater distance. This complex behavior could be indicative of more turbulence, and it is, therefore, a bit unexpected.

In summary, both datasets show a loss of velocity with distance but with different behaviours: axial flow becomes calmer and more uniform, while radial flow shows more complex variations, probably due to its nature or radial duct conditions.

To perform a more complete analysis, the two most important components for both configurations were also analyzed.

Z COMPONENT VS RADIAL COMPONENT

Axial Configuration (AX) - Axial Component (Z-Axis)

Surface 1 - At diffuser exit:

Average speed: -2.70 m/s

Standard Deviation: 0.99 m/s

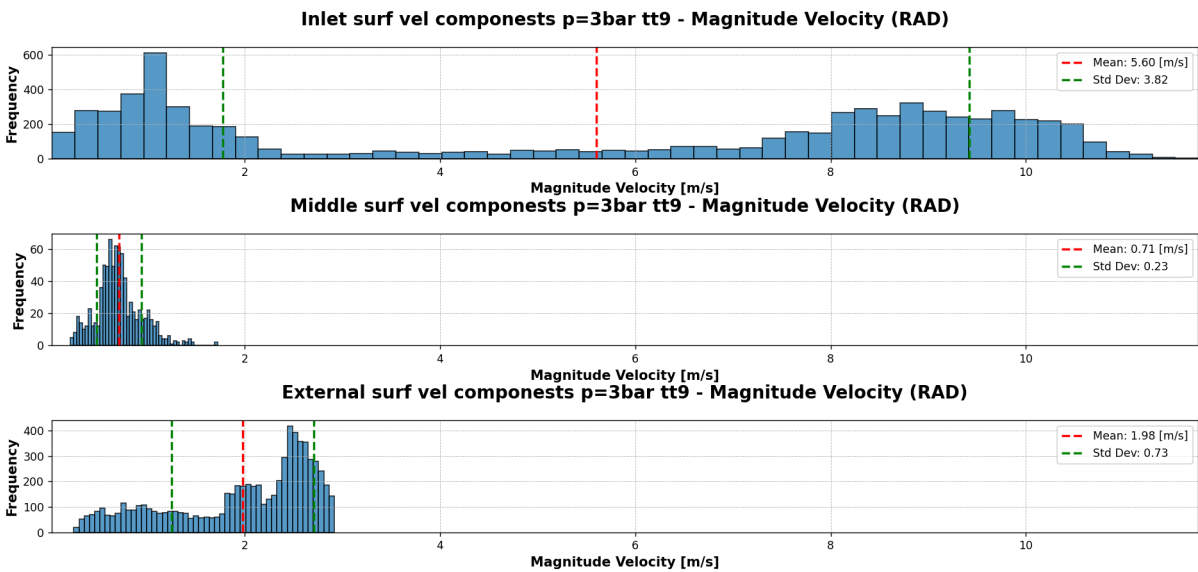


Figure 4.24: Magnitude velocity distribution around RADIAL diffuser at the instant of reaching P = 3 bar

The average velocity has a high value while the standard deviation is moderate, suggesting that there is some variation around this average velocity, but not too much. The high speed is a symptom of the marked speed for exiting the section.

Surface 2 - Two r_0 radius surface:

Average Speed: -0.61 m/s

Standard Deviation: 0.8 m/s

Remark: The average velocity approaches zero, indicating that the flow has slowed down sharply with respect to Surface 1. The standard deviation decreased slightly, suggesting that there are still variations in the flow, albeit less intense than at Surface 1.

Surface 3 - Three r_0 radius surface:

Average speed: 0.03 m/s

Standard Deviation: 0.12 m/s

The average velocity is practically zero, indicating that the flow is almost at a standstill or has reached equilibrium. The standard deviation is very low, suggesting that variations around the average velocity are minimal. The velocity component is, therefore, almost zero, in agreement with the value from the velocity modulus.

Radial Configuration (RAD) - Radial Component

Surface 1 - At diffuser exit:

Average speed: 2.34 m/s

Standard Deviation: 3.01 m/s

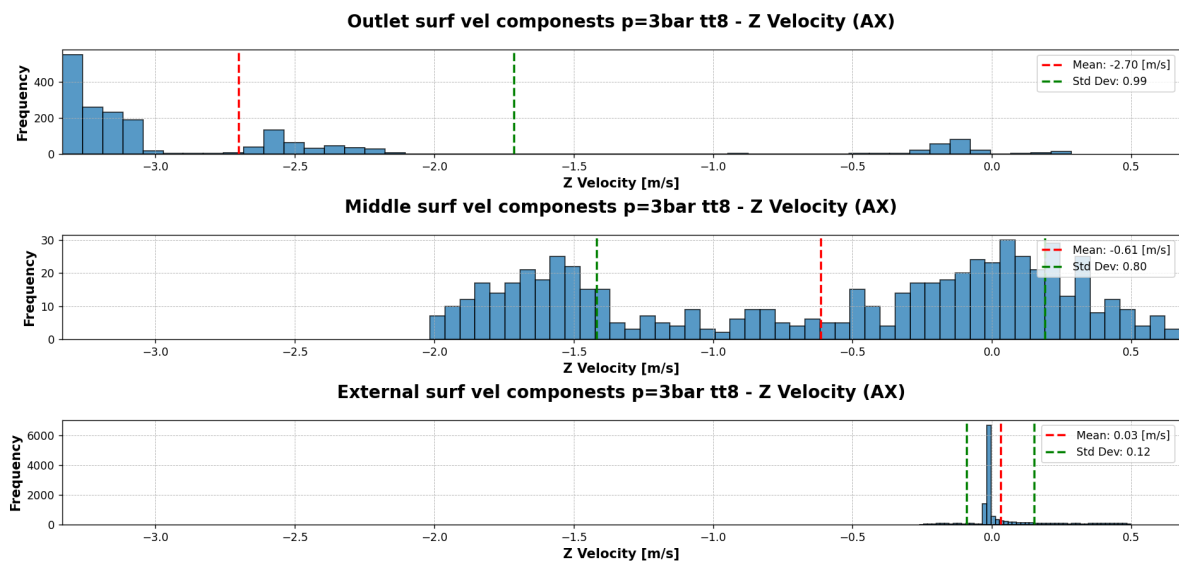


Figure 4.25: Axial velocity distribution around AXIAL diffuser at the instant of reaching P = 3 bar.

The average velocity is positive and quite high, indicating that the flow is actively directed radially outwards. Compared to the configuration, it is higher. The standard deviation is also high, suggesting that there is a large variation in flow, with many fluctuations around the average velocity.

Surface 2 - Two b_0 radius surface:

Average speed: -0.05 m/s

Standard Deviation: 0.51 m/s

The average velocity is very close to zero and slightly negative; the negative sign indicates that the flow may have local reversals. The standard deviation is lower than Surface 1, suggesting that variations in flow are less intense. In general, the flow is slowing down.

Surface 3 - Three b_0 radius surface:

Average speed: 1.84 m/s

Standard Deviation: 1.01 m/s

Remark: The average velocity is again positive and relatively high, a behavior very similar to that seen in the velocity modules. This indicates a strengthening of the radial flow, but less intense than at Surface 2. This means that turbulent flows are present. The standard deviation is moderate, suggesting that there are still variations in flow, but not as extreme as in Surface 1.

General Observations

Axial (AX): The velocity behaviour is linear as you move away from the duct, significantly

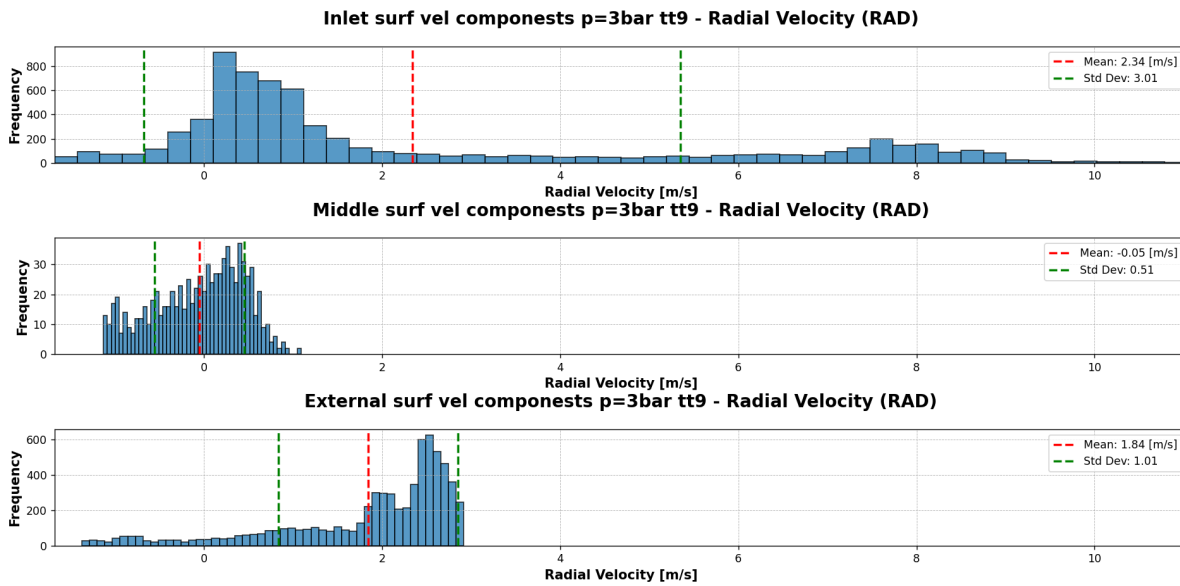


Figure 4.26: Radial velocity distribution around diffuser at the instant of reaching $P = 3$ bar.

reducing variations around the average velocity. This suggests that the flow is losing its kinetic energy and becoming more uniform.

Radial (RAD): The radial flow resumes similarly to the trend seen for the radial velocity, an initial increase followed by slowing down and then resuming. This behaviour could further prove that radial flow is experiencing complex phenomena such as turbulence or interactions with other flow structures.

These data generally show how the flow evolves as it moves away from the duct, with clear trends in axial and radial behavior.

Conclusions

From what has been seen above, two considerations can be made. The one that evaluates the heat exchange condition, the best configuration, is the radial one, both in the direction of the wall exchanges and in those in the direction of the propellant. This behaviour, as described above, seems to be very strange compared to expectations, given that in the studies reported, the radial one was the main suspect to be the most dispersive version in the direction of the wall, due to the dynamics, than in the direction of the tank walls. On the other hand, studying the results obtained in terms of surface distribution, it can be seen that the situation is reversed. In this case, the axial configuration represents the most ordinary solution, presenting both for the velocity modulus and for the axial component a decreasing slowdown trend moving from the internal to the external surface.

On the other hand, the configuration has more unusual behaviour, first a fast exit and a subsequent and abrupt slowdown. Finally, it returns to accelerate. In both configurations, it is noticeable that the speed tends to stabilize before arriving directly on the external surface. It is synonymous with kinetic energy consumption by the flow from the outlet and through the subsequent surfaces. For the radial configuration, it is most likely important to be confined by leading it to interact with the walls through turbulence, thus generating possible velocity recoveries. In conclusion, a decision must therefore be made on this example chapter regarding which configuration is the best to use.

By making an overall radial seem to have the best behaviour towards almost all the drivers chosen. The dissipative sources are lower than the AX one. The pressure reached faster (with the limit of the evaporation model missing) and it maintains the pressure level for more extended periods. Speaking about the temperature arrangement, the configuration presents lower temperatures for both Axial and Radial trends at different times. The only partial downside is the somewhat unusual physics in speed and velocity distribution, which we want to better understand in the next chapter; for this reason, after all the processes the radial configuration could be the best.

In this case, the author chose a series of drivers and the minimums necessary for a sufficient evaluation. This does not preclude the possibility of adding other parameters/reports for particular reasons; this is at the reader's description.

Table 4.14: Comparison table of AX and RAD configurations

Driver	Description	RAD	AX
Heat Dissipation	“Presents an average dissipative trend of 17% less during pressurization and 30% less during depressurization.”	x	
Temperature	Radial Trend: “For the AX configuration, near the wall, it shows an average temperature 16% higher than the radial one at t=1 s.”	x	
Distribution	Axial Trend: “For the AX configuration, near the liquid, the temperature is 20% higher at t=1s.”	x	
Achieving Nominal Pressure	“The RAD configuration reaches nominal pressure 0.27 s earlier.”	x	
Maintaining Nominal Pressure Condition	“At t=6s, the AX configuration has lost 20% more of the absolute pressure.”	x	
Velocity Distribution	“The radial geometry presents a higher degree of instability and turbulence, with a recovery of velocity at a distance from the outlet.”		x

Chapter 5

Optimization

This section discusses about the possibility to improve the geometry diffuser chose in Chapter 4. The process will first consist of a brief discussion of the findings of the previous chapters and highlighting the main shortcomings. Then, it will be followed by a brief review of some of the configurations presented in Chapter 2, which may give some ideas for reasoning. Once this has been identified, we will move on to the implementation in the chosen configuration using CAD software. Subsequent analysis using fluid dynamics simulations, on the other hand, will allow us to understand if there have been any possible improvements in operation. This part of the work is the least standardized compared to the previous process because it strongly depends on upstream choices. In this case, the radial configuration has been chosen; in fact, we will mainly reason about the latter, but this does not mean that what has been said can be applied to the other configuration in different operating conditions.

In this Chapter, we will use the same ones seen above, then modelling using SolidWorks and simulations using Fluent. The setting, especially for the analysis condition, will also occur similarly to those shown in Chapter 3. So, some of the passages will be omitted for simplicity, and the reader is invited to return to the previous chapters in case of doubt.

5.1 Objectives of optimization

As can be seen, especially in speed distribution, neither of the two configurations presented above shows a uniform trend around the average value. This is a symptom of a low intrinsic ability on the part of the two configurations to perform the task of a diffuser, i.e., to distribute the flow rate in a balanced way. In this chapter, therefore, we will find a way to optimize the diffusion, an optimization that will result, in the first place, in redistributing the speeds to

limit the turbulent phenomena seen above. In order to find an optimization methodology, one of the configurations seen in Chapter 2 could be helpful.

5.1.1 Possible solutions

Taking up the Table 2.2 where all the configurations have been presented, we find how the radial configuration is presented using a perforated structure.

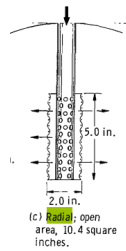


Figure 5.1: Focus on the radial diffuser from [10]

In the study, it is reported that the chosen configuration has a height of 12.7 cm (5.0 in) while the diameter D is 5 cm (2.0 in), meaning that the lateral surface area of expulsion of the pressurizer is;

$$A = \pi \cdot d_{cylin} \cdot h = \pi \cdot 5 \cdot 12.7 \approx 200 \text{ cm}^2$$

While the document states that the open area is about 61.19 cm^2 (10.4 in^2), this means that the perforated area of the total area represents 30%. The presence of a perforated surface in the outlet section of the pressurizer could be considered an optimization option, given the many examples that present this trick. Similar configurations, such as the multiple-screens and the hemispherical, can be seen in [10]. In contrast, in other examples, it is possible to see the one used in the Centaur in the study [44] where the dissipator is presented, a diffuser that consists of a conical element with a series of successive perforated plates. However, this series of perforated elements has a declared purpose: to slow down the flow in adduction. It is reported that in that configuration, the plates can slow down the flow of helium (0.15 kilograms per second) in adduction into the tank from a maximum velocity of about Mach 0.37 at the inlet of the diffuser to an exit Mach number of about 0.05. It means a reduction of over 86% of the initial value. Unlike the geometry, in [10], the reason for the drilling of the different configurations is not represented; only the multi-screen reports that the series of holes and structures are used to slow down the flow on purpose, making it a dissipator.

Perforated Surface

The idea of using a perforated surface may not be explained in the document. Several hypotheses have been put forward, such as:

- **Reduction of turbulence:** The presence of holes allows you to "break the flow" by decreasing its turbulence.
- **Uniformity of flow rates:** Passing through the holes would allow an improvement in the arrangement of the outlet flow rates rather than from a single surface.
- **Improving mixing:** The gas could enter much lower flow rates, allowing for better mixing in the ullage.
- **New speed gain:** The presence of a shrinkage section may allow the pressurizer to increase its speed locally.

In summary, the perforated surface of the diffuser is likely designed to improve the distribution and control of pressurizing gas within the tank, reducing turbulence and stabilizing pressure. In this section, we will therefore try to verify whether the introduction of a perforated cavity could actually increase its diffusion capacity.

Geometry

Having decided to introduce a perforated surface as an optimization element, it is necessary to create a model to conduct the necessary analyses. The geometry taken up is that of the radial configuration where the exit section was the lateral surface of 160 mm height and the radius of 150 mm, therefore a lateral section of $\approx 754 \text{ cm}^2$. Taking as an example the dimensions presented in [10], i.e., where 30% of the lateral surface was drilled, we take a cue from the value, in order to be able to transpose it into our geometry. By choosing holes with a diameter of 1 cm at the discretion of the author, an excellent compromise between a size that is not too large and, at the same time, a reasonable size for the creation of the correct mesh, the total number of holes to be made is obtained. The % of the perforated surface, for construction reasons, is decided to halve it, thus bringing it to the value of $\approx 14\%$, thus obtaining:

$$n_{\text{holes}} = \frac{(753.9822369 \cdot 0.14)}{\pi \cdot (0.5)^2} \approx 140$$

Arranged in 20 rows of 7 over the entire external surface:

For CAD realization, just take the radial file, remove the spars connecting the bottom to the rest of the diffuser, and extrude the holes on the outer surface. Remember that in this case, the

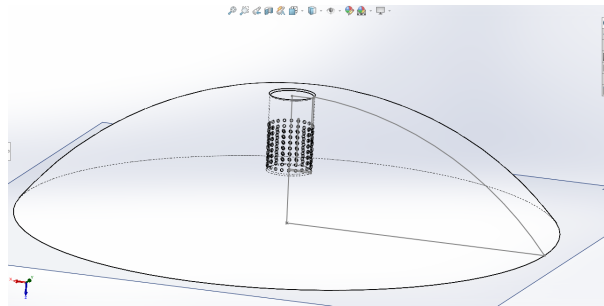


Figure 5.2: CAD completed with perforated holes

volume of fluid is also being realized, therefore the negative of a real diffuser, which instead represents the vacuum areas in the CAD.

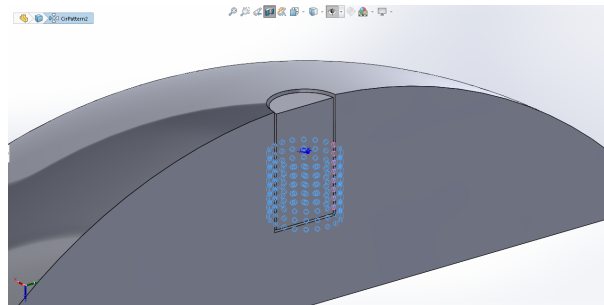


Figure 5.3: SolidWork sections with the extruded holes highlighted

This results in the geometry that will be, then, introduced for fluid dynamic analysis and referred to, from now on, with the acronym GRID.

5.1.2 CFD Analysis

The fluid dynamic analyses carried out in this section will have the main purpose of verifying whether or not the presence of the perforated surface helps the pressurization trend, comparing them with those obtained through the simple configuration presented in the previous Chapter. The comparison will be performed on the same parameters of choice, therefore in terms of dissipation and maintenance of pressurization, but above all verifying the trend of the velocities in the surfaces outside the geometry. In fact, in this case all the structures presented in Chapter 3, necessary for post-processing, are reported too. Also, in this case, pressurization from 1 bar to the nominal value at 3 bar will be simulated using a transient simulation with a maximum pressurizing flow rate of $100g/s$. When the MEOP is reached, a few seconds of hold will be waited to check how the system responds to cooling.

SetUp

The setup will be practically the same, followed by the same steps. For brevity, all the assumptions reported in Chapter 3 are resumed. In this case, the evaporation condition will not be present. The mesh required a greater degree of attention, with a particular refinement in the area of the holes, where a careful meshing operation was necessary to avoid numerical instability phenomena near these areas. It has a local sizing of $0.0008[m]$ on the holes and has decreased the surface cells' maximum angle to 10° . This aims to improve the surface cells that would have been created. In addition, the boundary layer, represented by five layers with a growth rate of 1.15 and a transition factor of 0.25, was created to better capture all the phenomena in the perforated areas. All this is done to obtain a 2.368.616-cell mesh, i.e., a value almost three times higher than that used in previous simulations, greatly increasing the computational load of the simulation. This took a long time to make. Below is the table showing all the factors that characterize the setup of the simulations.

In the simulations the same reports set for the previous analysis have been used (3.1.3).

5.1.3 CFD Results

Residuals The simulation was completed with good results; there were no stability problems, and the residuals went to cover with a decreasing exponential trend without any oscillation or disturbance, as shown in Figure 5.4. As with the previous analyses, once the pressure value of 3 bar was reached, the flow rate was brought to zero, which caused a slight change in the trend of the residues. The analysis took almost four days, so it was necessary to set everything up correctly right away to avoid wasting time. Fortunately, there were no problems.

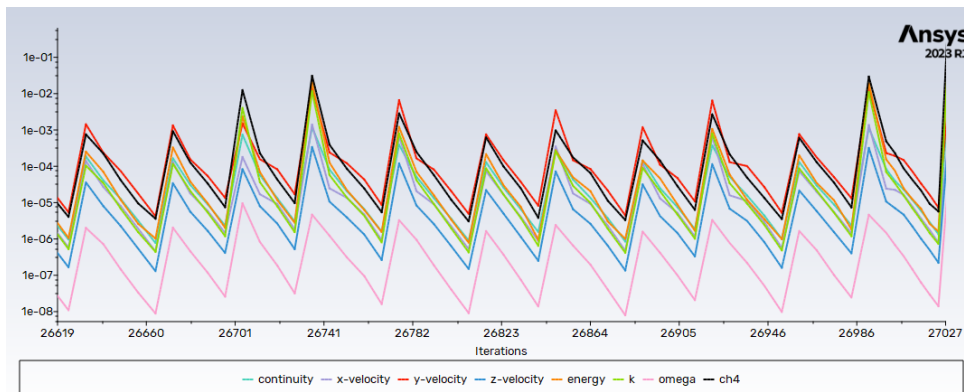


Figure 5.4: Residuals for the simulation.

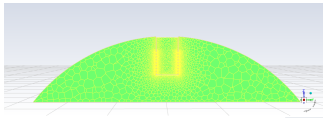
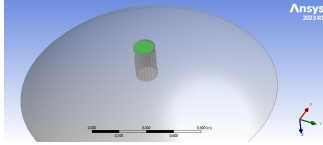
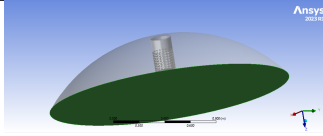
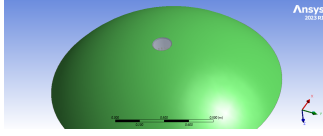
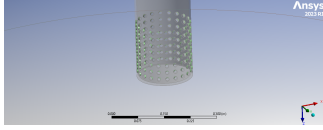
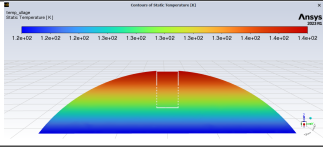
Element	Hypo/Model	Notes/Images
Test for AXIAL ullage configuration		
Reference File	Diffuser: Diff AX with dimensions from code TEST_TANK_8 CAD: Cupola_AXLDPRT.STEP Mesh: FFF.msh.h5	Diffuser dimensions from Python code. $r_0 = 140$ [mm], $h = 100$ [mm]
Iterations	Time Step Size: 0.01 [s] No. Of Time Steps: 1000000	
Mesh	Boundary: inlet -> Mass-flow-inlet liquid -> wall wall_dome -> wall grind_surf->wall Regions cupola_radlprt_grind_surf -> fluid Add local sizing: grind_sizing -> Growth Rate 1.15 Target_mesh size [m] -> 0.0008845 Volume Diagnostics: Total Number of Cells = 2368616 Minimum Orthogonal Quality = 0.2 Maximum Aspect Ratio = 16.15 Number of Isolated Cells = 0	
Inlet (Fluent)	-Type: mass-flow inlet (100 g/s) Till reaching the Nominal pressure level when mass-flow inlet = 0 g/s -Normal to Boundary	
Species	ch4 -> 0	In the inlet section is assumed no CH4
Temperature	293 K	Temperature from the case
Wall: liquid	Stationary Wall Species: Mass Fraction: ch4 = 1 No slip condition, temperature 120 K ch4 -> 1	
Wall: cupola_diff_rad:1	-Stationary Wall -Species: Mass Fraction: ch4 -> 0 -Heat flux = 0	
Wall: wall_dome	-Temperature: 1400 K -ch4 -> 0 -Stationary Wall -No slip	
Wall: grind_surf	-Adiabatic K -ch4 -> 0 -Stationary Wall -No slip	
Operational conditions	-Operative Pressure: 300000 [Pa] -Temperature: 293 [K]	
Initialize	-Gauge Pressure: -200000 [Pa] -ch4: 1 -Temperature Patch: 43.4783 [K/m]*z + 120 [K]	
Mixture Template	Density: Ideal Gas	

Table 5.1: Summary Table for the Simulation with Large Dome and Tank

The continuity and the energy residual, the most significant interest for these simulations, reached the convergence set at 1×10^{-6} at each time step. Speaking in terms of the physics of analysis, introducing the perforated surface would have brought a slight improvement in pressurization, which reaches the value of 3 bar in 1.60 s, 0.07 less than the configuration without holes. This may be an indication that something has indeed changed in the fluid's dynamics, but in terms of mere performance, it matters little.

Contours Here reported the evolutions contours to better understand the evolution of the system, six important quantities were chosen, such as:

- Ullage temperature,
- Absolute pressure,
- Modulus velocity,
- Chemical species,
- Turbulence.

As in the previous analyses, four different instants are shown, which attempt to compress the entire course of the simulation:

- $T = 0$ to represent the starting conditions,
- $T = 1$ s to demonstrate full operation,
- $T = 2$ s to show the trend just after the flow rate closure,
- $T = 6$ s showing the trend a few seconds after closing the flow rate.

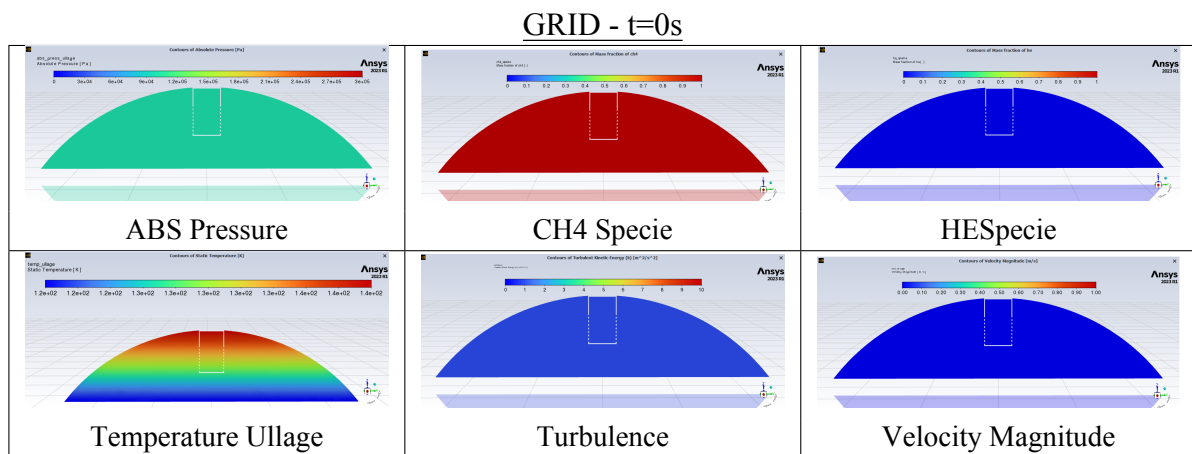


Table 5.2: Contours of dimensions after 0s of flow time.

GRID - t=1s

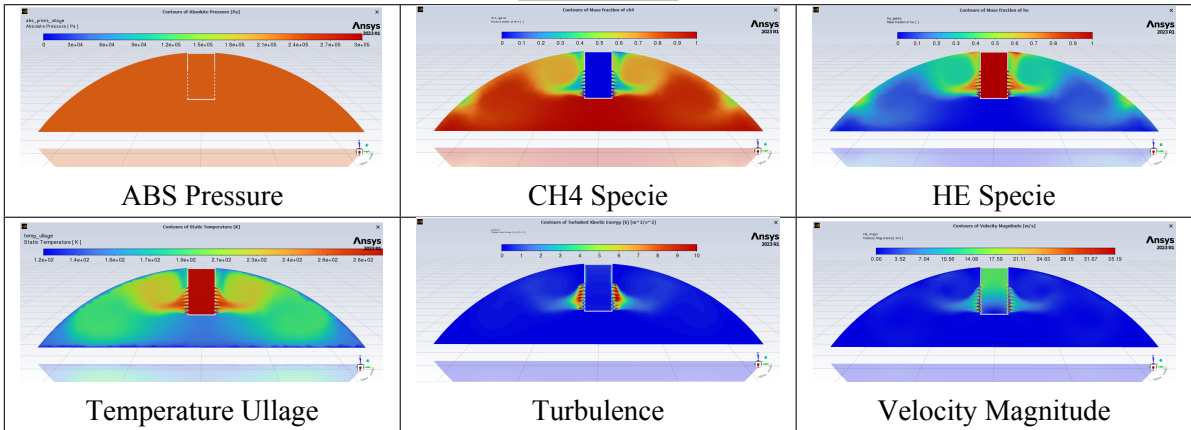


Table 5.3: Contours of dimensions after 1s of flow time.

GRID - t=2s

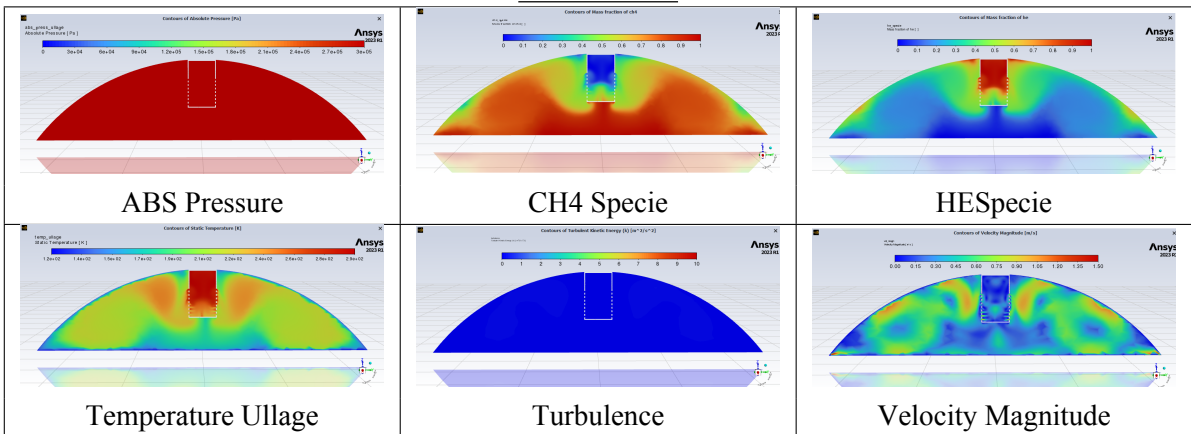


Table 5.4: Contours of dimensions after 2s of flow time.

GRID - t=6s

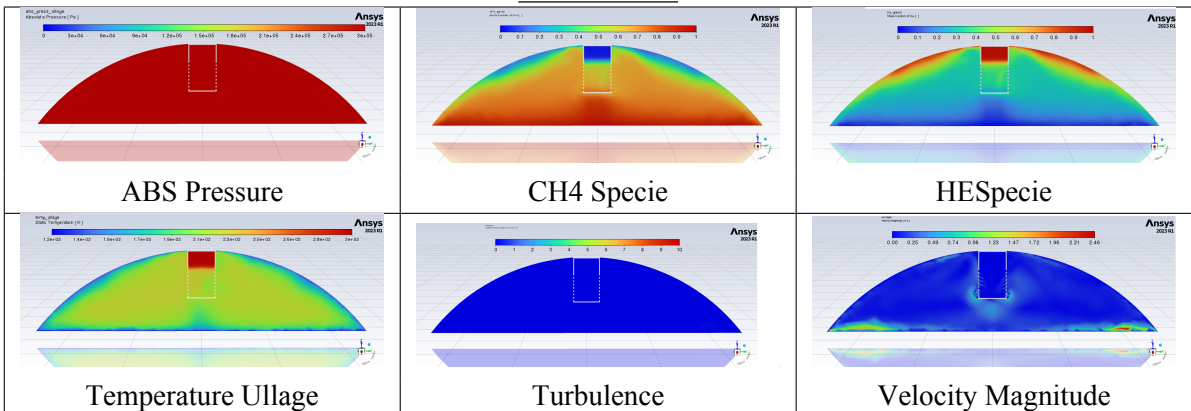


Table 5.5: Contours of dimensions after 6s of flow time.

5.1.4 Post Processing

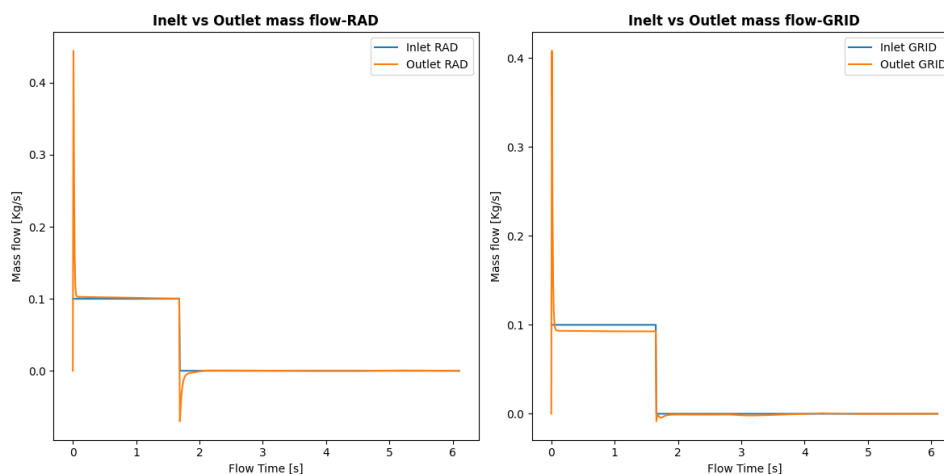


Figure 5.5: Mass Flow inlet and outlet for both configurations vs time.

First of all, we analyze the mass flow rate through the surfaces shown in Figure 5.5. In this case, we notice that through the outlet section (orange line), there is a shift concerning the inlet mass, a shift that is also important since it is about 2% of the inlet flow. This could be sobering because it could cause mass stagnation of the pressurizer inside the diffuser. In terms of reactivity, despite a more "complicated" outlet section to find, the pressurizer reaches a stationary flow rate value through the outlet section of about a tenth of a second more than the simply radial condition (remember that the report does not distinguish between methane vapor or pressurizing outlet). Speaking instead in terms of temperature, the trend between the RAD and GRID versions is very similar, with faster heating in the pressurization phase, then a slightly steeper curve, with a peak value, at the reach of 3 bar of about 205 K, more or less similar to the 201 K of the RAD configuration, as shown in Figure 5.6. The higher temperature maintains a higher value than the analogue without holes, even during depressurization. It can be seen that the entry through holes allows for better heat transfer into the ullage.

On the other hand, discussing one of the main factors, the presence of dissipative phenomena through the graphs obtained by post-processing, some significant variations are immediately noticeable. The most important is the further decrease in the flows on the propellant; in this situation, in fact, compared to the configuration without holes, there is a robust decrease; this is because, as can be seen in the Tables ??, the dynamics move all to the upper area of the diffuser because the gas loses almost all its axial velocity component, leaving the one due to the buoyancy forces as predominant. Therefore, there is a solid decrease, to have a peak in modulus of about 1660 W/m^2 while the configuration of the perforated surface is 7760 W/m^2 , as shown in Figure 5.7.

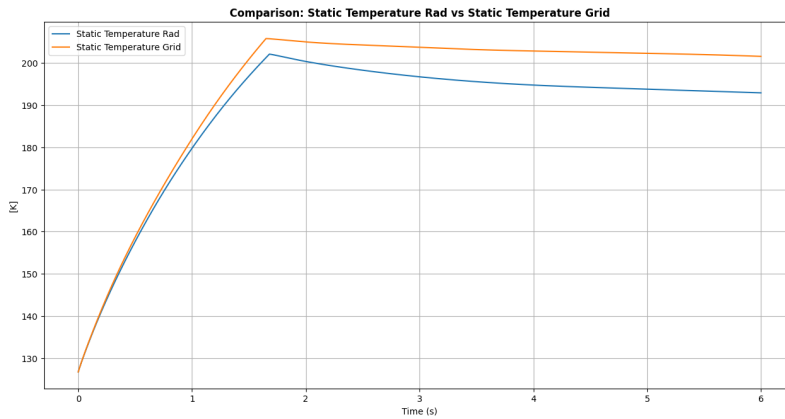


Figure 5.6: Temperature in ullage for both configurations vs time.

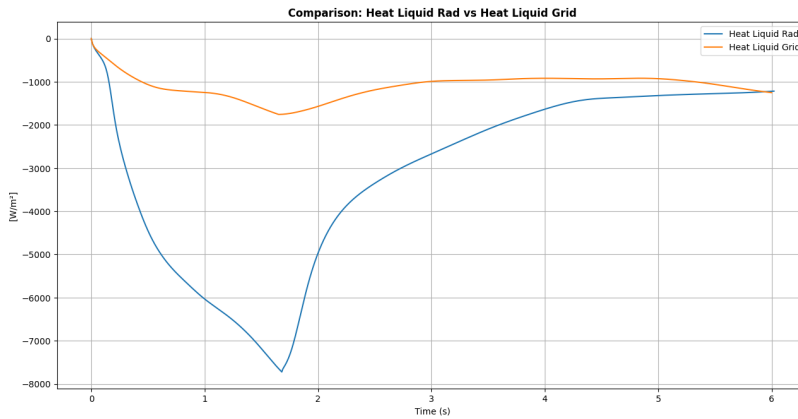


Figure 5.7: Heat flow on the propellant.

On the other hand, as far as the dissipated component on the wall is concerned (Figure 5.8), we are dealing in this case with two flows with a very similar trend over time, with the perforated configuration which, as expected, has a more intense interaction with the tank; this is always due to the stagnation of the pressurizer near the upper cap. However, the gap between the two tends to get closer during depressurization, until it overlaps between two and three seconds and then returns to divide definitively. This behaviour could be given by the fact that the flow in the supply of pressurizer goes off, thus ending all the forced phenomena; the subsequently limited permanence in the upper part of the tank in the GRID condition causes the free type phenomena to return to move the two curves away again. In the peak area, the two realize a difference of 1000 W/m^2 , respectively for the condition a minimum value in modulus of $\approx 1800 \text{ W/m}^2$ while for the perforated version of $\approx 2800 \text{ W/m}^2$.

Adding the contributions for both configurations, despite the greater exchange with the wall,

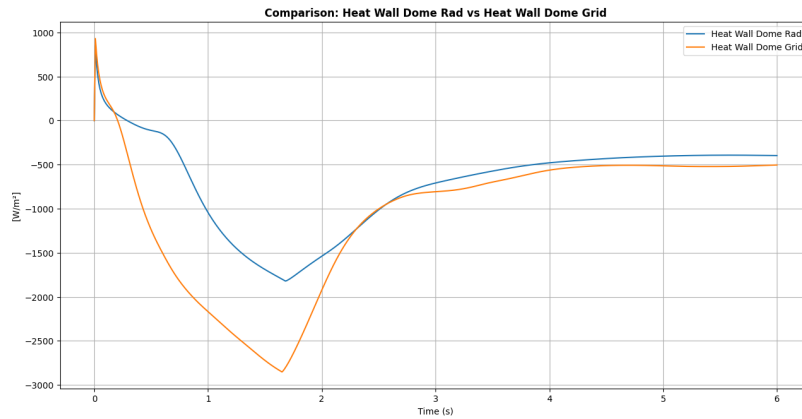


Figure 5.8: Heat wall flow for both configurations versus time.

the most efficient configuration in terms of dissipative parameters is the perforated one, as shown in Figure 5.9. It's, therefore, further evidence that in this condition, the wall represents one of the dissipative components but is far from the condition of “heat sinks” as described in previous studies.

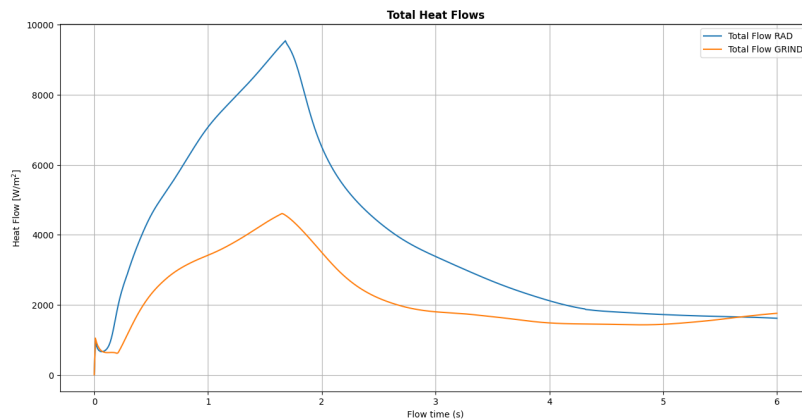


Figure 5.9: Sum of the modulus contribution of the dissipative sources for both configurations, versus time.

Post-Processing Speed The velocities are always post-processed through the built surfaces, as in the previous tests, through the extraction of the components obtained with fluid dynamics analyses.

Magnitude Velocity Surface at the exit of the holes from the diffuser:

Average speed: 5.60 m/s

Std deviation: 3.82 m/s

The velocity modulus is analyzed first, and it can be immediately seen at a glance as having a more orderly distribution around the average value but with a wide distribution. The speed value is very high; this is mainly due to the condition of the section narrowing section that acts as a “throat” to the flow. The standard deviation has a high value even though, by eye, an orderly and specular trend around a value close to the average one. Making a comparison with the result seen in the previous post-processing, we see an increase in speed in the area just outside the holes where the average value of the module has more than tripled, going from 5.60 m/s for the configuration to 17.36 m/s for the GRID configuration. The increase, as mentioned, is due to the narrowing of the exit section. The greater amplitude of the scale values, which previously ranged from 0 to 10 m/s, now stretch up to 25 m/s, partly deforming the standard deviation information, which is greater for the GRID configuration.

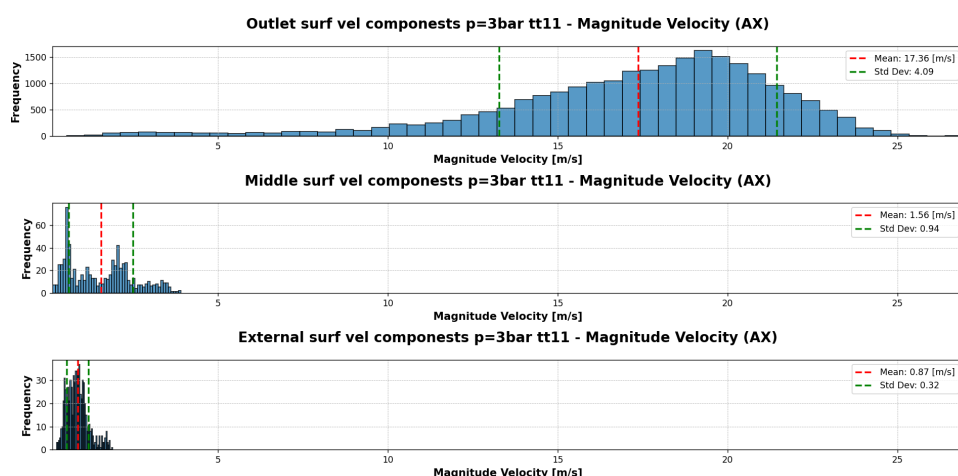


Figure 5.10: Magnitude velocity for the GRID configuration at the three different surfaces and at the reach of the pressure level.

Surface 2 - Two b_0 radius surface:

Average speed: 0.87 m/s

Std deviation: 0.32 m/s

On the middle surface, the average speed is very low, which means that it has slowed down sharply after entering a small space. The standard deviation value is also close to zero; this can be seen immediately from the concentration around the mean value, which has a very small amplitude.

Surface 3 - Three b_0 radius surface:

Average speed: 1.56 m/s

Std deviation: 0.94 m/s

The value of the average velocities in modulus has increased again, and the standard deviation slightly, the same behaviour seen for the configuration without holes. The values are, how-

ever, low and attributable to turbulent motions within the ullage itself. A general observation of the trend, therefore, shows that it is only the first surface that presents the most significant differences. At the same time, the other two have behaviours similar to the configuration expected in the condition without any perforated surface; therefore, this is a clear indication that the perforated surface makes its effect felt only in the close vicinity of the diffuser. Let us see if this trend is repeated for conditions with radial velocities.

Radial Velocity:

The surface at the exit of the holes from the diffuser:

Average speed: 13.67 m/s

Std deviation: 4.06 m/s

Also in this case, the radial velocity component was considered to understand the fluid dynamics better. At the exit of the diffuser holes, the speed represents a very high value; as for the speed in modulus, this is always due to the narrowing of the section. The standard deviation also has a very high value, but even in this case, the distribution is ordered in a range from just below zero to almost 25 m/s.

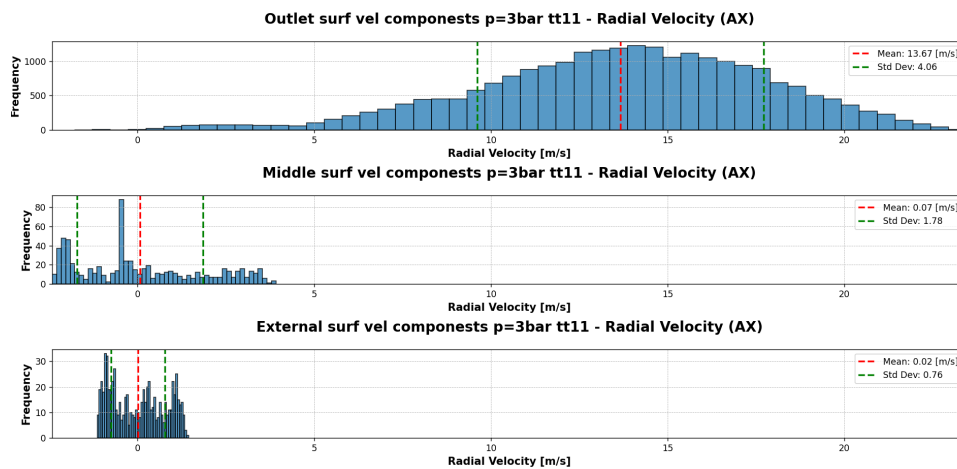


Figure 5.11: Radial component velocity for the GRID configuration at the three different surfaces and at the reach of the pressure level.

Surface 2 - Two b_0 radius surface:

Average Speed: 0.02 m/s

Std deviation: 0.78 m/s

The value of the velocity in this case is very close to zero. Therefore, it represents that the flow in the direction has undergone a sudden slowdown, having almost half of the negative values, so the flow would tend to reverse its motion. A much smaller, limited range around zero guarantees a better, contained standard deviation.

Surface 3 - Three b_0 radius surface:

Average speed: 0.07 m/s

Std deviation: 1.78 m/s

On the outermost surface, the average velocity remains around zero. Hence, a good half of the reference surface records negative velocities, which could be due to the return of the flow after an iteration with the tank wall, given the proximity to the latter. The velocity spectrum increases again, thus further proof of the high randomness of the velocity components that cross the reference surface. A general observation of the three surfaces shows how the radial velocity is accentuated as a component of the velocity modulus, especially on the output surface, where in addition to the value (13 m/s of the radial component alone, against 17 m/s of the modulus), the values of the standard deviation and the amplitude of the distributions are also similar. While the other two surfaces show some detachment between the radial component and the modulus, the inertia due to the input is probably lost and instead becomes a much more chaotic motion. On the other hand, if we want to compare the relative velocities on the other two surfaces, we note that the radial velocity component in the intermediate surface has similar values, both close to zero, with a fair standard deviation. This also represents that the effect of the perforated surface on this velocity component is minimal at a certain distance. Slightly different is the surface at a greater distance; the latter had the characteristic speed recovery in the configuration without the presence of perforated surfaces. In this case, however, the average speed value remains close to zero but with a wide distribution that achieves a fairly high standard deviation. In general, the presence of the perforated surface influences the motion near the outlet from the diffuser, but its effect is lost as moving away from the inlet.

5.2 Conclusions

In this brief section will be made a reasoning about the utility of the holes presented in the surface to conclude if this particular case can be helpful or not. The starting point was the conviction that the presence of the perforated plate could improve the flow dynamically, reducing the turbulence and make uniform. The analysis highlighted a change in the flow dynamic, not only in its velocity but also in speaking about dissipative heat flows, pressurization performances and pressure levels. In all these aspects, the GRID configuration has little but important improvements. The most important result can be the reduction of the total heat lost, with the fraction towards the propellant subjected to a very strong decrease. For this result alone, the grind configurations can be justified. Speaking about velocity and particularly velocity distribution, the influence of the surface can be helpful near the diffuser's outlet

surface, accelerating the flow and improving the distribution around the mean velocity. However, no clear evidence has been found on the influence of the new geometry increasing the distance from the diffuser inlet. A resume table to better envision on all evaluation aspects implementing the perforated surface will follow.

Table 5.6: Comparison table of GRID and RAD configurations

Driver	Data	GRID	RAD
Dissipated Heat	The GRID configuration shows a heat flux almost 50% lower than the radial one.	x	
Ullage Temperature	The ullage temperature for the GRID configuration is slightly higher than the radial one throughout the pressurization phase.	x	
Reaching Nominal Pressure	The GRID configuration reaches the nominal pressure 0.07 s earlier.	x	
Velocity Distribution	The GRID geometry shows a better distribution at the hole exits and a velocity magnitude three times higher. Effects reduced at greater distances from the diffuser.		x

This analysis confirms that implementation of the perforated surface can be considered to optimize the dynamic of the flow but is not strictly necessary. Other analysis, possibly more detailed, could be performed in the future with different numbers and dimensions of the holes to verify if different dimensions could generate a more intense effect on the diffuser's dynamic.

Chapter 6

Conclusions

In this last chapter will be a resume of the entire work, starting from the beginning to the conclusion made in the previous two Chapters. Here, the objectives are to allow the reader to introduce a clearer and more general view of the subject. The difficulties encountered during the acquisition of knowledge, the critical issues, and the strengths of the methodology presented here will then be addressed. In addition, some of the most important concepts obtained from the passages dealt with throughout the pages will be repeated. We will then come to conclusions, enriched in this case by some particular considerations of the author.

It is better to remember that this work is experimental and conducted with all the possible effort to create a valuable and helpful methodology. Still, certainly, there are some errors or mistaken reasoning because the subject is very large and the work crosses over between different fields and demands different skills. If some of these errors are found, it is encouraged to bring them to the author's attention.

6.1 Resume of the activities

Difficulties

From the beginning of the work, the difficulties that will be encountered were clear, with the presentation of the problems in Chapter 1 and all variables linked. None debut about the challenging of the task: find a way to better understand the diffuser functionalities and physics while at the same time translating this knowledge to practical sizing processes. Then, collect all the information and find a way to evaluate the diffuser's efficiency. Check the possibility of combining different correlations and relationships and, from all of these information, obtain

the dimensions needed to realize the necessary geometries. Another difficult task was to setting up the analysis in Fluent[®], understanding the behaviour of the fluid, the right parameters and the meshing process. A very helpful contribution came from the figure who supported the author during the internship.

6.2 Results from the processes

6.2.1 CODE

The implementation of the code section took a long time. The objectives were clear from the beginning: to determine which was the principal source of the dissipative phenomena and their intensity. Then, the section about efficiency was introduced, giving an idea of the magnitude of these phenomena. The code was a 0D stationary Python code, with some similarities with the other works, but here, the dynamic of the flow from the diffuser was implemented. In fact, that is the distinguishing feature of the code. All previous work often neglected the dynamic of the pressurant. The same studies sometimes concluded with the possibility that a better modulation of the outlet diffuser flow could lead to a more efficient diffuser. Another peculiarity is the link between the different contributors to the energy balance and the dimensions of the diffusers. No other example in the SOA have been found. Managing all the variables and the possible conditions explained above has been challenging; one of the operational requirements for the work was the possibility of using a wide range of propellants and pressurants. For brevity, no examples with different conditions were introduced, but implementing different technologies can only be done by introducing the new species in the relative section. Despite the large number of variables and the assumptions made, the code discreetly simulated the behaviour of the pressurant mixed with the methane, capturing the different behaviour of the forces and the free convictions obtaining results with physical meaning and constructively possible. At first reading, this might not be a great achievement, but the time required to achieve it and all the versions can guarantee its significance. In the end, the code part plotted the different possible dimensions, having an idea of the possible dimensions which was its work.

The author is conscious that the phenomena occurring inside the tank are probably more complex and different; describing it with a simple code has some limitations. The turbulent flow generated by the pressurant entrance plays a key role in the physics of the heat dissipated, as can be seen in the contours sections. The lack of an evaporation model is another big limitation of the code, but speaking again about the flexibility, the code can be implemented.

6.2.2 CFD simulations-Axial vs Radial

Obtained the first possible values of diffuser dimensions. The next step was the fluid dynamics campaign. The objective were to simulate as accurately as possible the presence of on-ground pressurization of the tank chosen as the case. Only the fluid part of the ullage was modelled in order to obtain a limited number of cells and having initialised both the inner surfaces of the tank and the liquid as 'WALL'. This choice certainly somewhat limited the link between analysis and reality, but it was necessary in order to maintain the principle of simplicity and relative lightness of the method. Despite the simplification, the analysis took a long time to complete, so a short flow time is reported. After all the simulations converged, thanks in part to the precise work of setting up the simulations and meshing the geometry itself. The values found were in agreement for both simulations, an indication that the tests were carried out precisely and methodically. The analyses did, however, reveal a few surprises compared to the work the author had seen. Speaking first of nominal comportances, pressurization, which we recall is by means of a constant flow rate (assumed to be the maximum flow rate provided by requirement), proceeds linearly until the operating condition is reached. Which however does not happen during the hold phase, in fact reached threshold the inlet flow rate is reset to zero and the ullage is left to evolve over time. In this second phase the pressure drops but not following a straight line, but through two curves. These trends resume that of the average ullage temperature evaluated over the entire volume; this value rises linearly up to the setpoint and then falls following a slight curve. This nonlinear cooling, and the consequent depressurization, are caused precisely by the cessation of the flow rate which kept the heat exchange phenomemni strong. Once the inflow ceases, the velocity decreases, which takes on a chaotic character, but even the latter goes off toward free convection phenomemni only. Here is the a speiged the exponential decreasing trend. Speaking instead of thermal flux terms, one has the main surprises. Despite multiple sources reporting that the component to be more dissipative during ground pressurization is the wall component; for both configurations, in this case , the highest flux intensity is that of the component in the liquid direction with values about $7000 - 8000[W/m^2]$, instead the component towards the wall has values of about $1500 - 2000[W/m^2]$. Moreover, it is even more surprising that the axial configuration undergoes greater interaction with both sources, making it less efficient than the radial one. It was expected that there would be more loss in the direction of the liquid, but this behavior is also observed in the fraction lost to the wall. This unusual behavior could be caused by the modeling of the liquid as a wall; indeed, it is possible that the presence of the propellant might slow down the pressurizing agent, causing it to reach the wall to a lesser extent. This remains a matter of speculation that would require further analysis.

Regarding velocity, rather variable distributions with low symmetry are observed around the

surfaces of the diffuser, so the flows exit in a somewhat disordered manner. However, the more interesting surfaces are those at a greater distance than capture the behaviour within the ullage. Here, the radial configuration is of greater interest, specifically the velocity recovery observed on the third surface around the diffuser. This recovery suggests that the radial configuration likely generates a higher degree of turbulence, although this is not reflected in the contours and thermal exchanges.

Therefore, the final choice between radial and axial configurations was made based solely on the energetic considerations of the thermal fluxes, which show greater efficiency for the radial geometry.

This testing campaign has limitations, such as the lack of modeling the propellant as a liquid, a choice made in agreement with the company tutor and the individuals who supported the author during this work. It was known that this choice might partially influence the results, but it certainly allowed the simulations to be simplified and completed in a timeframe consistent with the drafting of this work.

6.2.3 CDF Analysis GRID vs RAD

The optimization chapter allowed for a deeper understanding of the physics of the problem and explored whether it was possible to improve the aspect that previously showed the greatest deficiency: the dynamics of the flow exiting the diffuser. The solution presented was directly inspired by some studies conducted earlier, specifically the implementation of a perforated surface for the “diffuser-injectors”.

This surface was not well understood, as it was described in the referenced studies as an element for slowing down the flow, but this was in configurations specifically defined as “dissipators”. During the author’s internship, this type of surface was discussed with the supervisors, leading to various conclusions about its use in the geometries presented in the cited studies. Among the many possibilities, it was believed that it could help to equalize the pressurization flows, increasing their fluid dynamic resistance and thereby, by analogy with electrical resistance, allowing for more uniform distribution of the flow rates. Chosen as a possible optimization configuration, with the aim of verifying the actual effectiveness of this geometry, a series of additional fluid dynamic analyses was carried out. The choice of the perforation degree in the configuration presented in this work followed a reasoning based on modeling practicality, choosing a series of holes with a diameter of 1 cm.

Once the model was created, the mesh was set up, which in this case grew by a factor of three compared to previous ones, increasing from 7×10^5 cells in the first iterations to 2.3×10^6 .

This increase was due to the large number of holes, which necessarily required a higher degree of modeling detail. As the number of cells increased, so did the computational time required to complete the simulation, causing several issues. The series of simulations conducted in this phase was almost identical to the one previously presented: a transient pressurization from 1 bar to 3 bar, with a constant maximum pressurizing flow rate in this case as well.

This simulation, benefiting from the experience of the previous ones, was successfully completed in one attempt, with the residuals showing an exemplary convergence pattern. There were no stability problems, even when the flow rate was reduced to zero, which had previously caused various issues.

The post-processing behaviour revealed that the presence of the perforated surface allowed for slight performance improvements. However, what was more interesting was the alteration of the flow direction, which affected the dissipative aspect of the latter. The main dissipation source in the study presented here was with the propellant, but the presence of the perforated surface limited the flow in that direction, consequently minimizing that part of the dissipation. This is because the gas, having to rise and exit the diffuser, slows down in the axial direction, where buoyancy forces tend to carry it upwards towards the dome. This is a very interesting result that would justify the implementation of the holes, although in this case, the size and type of holes might not significantly influence the performance.

All the hypotheses regarding the influence on the fluid dynamics derived from the post-processing of the velocities are partly disproved; the presence of the holes does indeed help to equalize and break the flow of the pressurizing gas, but this effect only occurs in the immediate vicinity of the diffuser itself and diminishes with distance, as no related effects are observed on the two subsequent surfaces.

This section concludes by choosing to use the perforated configuration (GRID) as the diffuser, effectively completing the sizing process presented here. However, it must be acknowledged that the choice made does optimize the diffuser, but not in the expected way—rather than improving the distribution of the incoming flow rates, it minimizes the energetic flow lost to the liquid. Furthermore, it is likely that the actual influence this “improvement” has on the lost component depends on the size, number, and arrangement of the holes, which could be further investigated in future works.

6.3 insights for the reader

The work concludes by offering some brief insights for the reader and suggestions for future improvements.

As has been observed, the subject of diffusers is very broad, so much so that one might, in some cases, fall into excessive simplifications that could undermine the purpose of the work itself. It is, therefore, necessary to identify and manage the conditions and the many variables that affect the system.

As a component, the diffuser is extremely complex to manage, making it very difficult to standardize, as seen in this work. Consequently, it is necessary to define an initial geometry among those presented in Chapter 2 and proceed with the work from there.

Trying to optimize such a component, which is involved in many phenomena, without fully understanding its operation could be equally misleading and almost pointless. It is, therefore, advisable to complement preliminary work like this with a physical testing campaign that would certainly improve the understanding of the configuration in question.

Appendix A

Detailed tables and graphs

Appendix B

Code

Appendix C

Studies

Here, a collection of the main studies and documents linked to pressurization and diffuser is briefly reported. In the third column, there is a short resume of the study's challenge. ¹

Study Name	Author	Factors Studied
Predicting fluid thermal stratification in closed tanks	Bailey, Jefferson, Skartvedt and Vandekoppel (1963)	Calculation algorithms, fluid thermal stratification
Normal Gravity Self-pressurization of 9-in. (23 cm) Diameter Spherical Liquid Hydrogen Tankage	J.C. Aydelott (1967) [3]	Self-pressurization of an LH2 spherical tank in normal gravity, with variable fill percentage, wall heat flux, and heating position
Self-pressurization of a spherical liquid hydrogen storage tank in a microgravity environment	C.S. Lin, M.M. Hasan (1992) [4]	Thermal stratification and self-pressurization of an LH2 spherical tank in microgravity

¹These studies has not been directed used in this work for this reason are not inserted in the bibliography

Study Name	Author	Factors Studied
On the validity of purely thermodynamic descriptions of two-phase cryogenic fluid storage	C.H. Panzarella, M. Kassemi (2003) [5]	Pressurization of large cryogenic tanks in normal and microgravity conditions, using a lumped thermodynamic model
Modeling of propellant tank pressurization	Z. Greg, K. Mustafa (2005) [6]	Quasi-equilibrium phase thermodynamic model to predict tank pressurization
Process of submerged helium injection into bulk liquid oxygen	Cho et al. (2006); Jung et al. (2014)	Helium injection into liquid oxygen, cooling effect
CFD modeling of helium pressurant effects on cryogenic tank pressure rise rates in normal gravity	G. Gary, L. Alfredo, C. Frank, H. Leon, H. Ali, B. James (2007) [7]	Use of Flow-3D software to investigate the pressurization performance of LH2 and LN2 cryogenic tanks with helium injection
Cryogenic pressure control modeling for ellipsoidal space tanks	L. Alfredo, G. Gary, C. Frank, H. Leon, H. Ali (2007) [8]	Development of a CFD model to study the pressure control of an ellipsoidal LH2 tank under normal and reduced gravity
Cryogenic pressure control modeling for ellipsoidal space tanks in reduced gravity	L. Alfredo, G. Gary, C. Frank, H. Leon, H. Ali (2008) [9]	Development of a CFD model to study the pressure control of an ellipsoidal LH2 tank under normal and reduced gravity

Study Name	Author	Factors Studied
Pressure variation in a liquid hydrogen tank under low gravity	Lopez et al. (2008)	Pressure variation, liquid hydrogen tank, low gravity
Lumped parameter model	Oliveira, Kirk and Schallhorn (2009); Liu, Wang, Jin and Li (2015)	Lumped parameter model
Thermal diffusion model	Seo and Jeong (2010)	Thermal diffusion model
Two-phase numerical model for tank self-pressurization	Kartuzova (2011)	Tank self-pressurization, liquid-vapor heat transfer
Long term cryogenic storage technologies overview for NASA exploration applications	G. David, S. Jeffrey, M. Christopher, M. Gary (2011) [1]	The role of cryogenic propellants LH2 and LOX in future space exploration
Transient thermal process in a liquid oxygen tank with helium pressurization	Kim et al. (2012)	Transient thermal process, helium pressurization
Effects of liquid filling level and heat load on thermodynamic process	Barsi and Kassemi (2013)	Liquid fill level, heat load, thermodynamic process

Study Name	Author	Factors Studied
Cryogenic thermal system analysis for orbital propellant depot	P.R. Chai, A.W. Wilhite (2014) [2]	Sensitivity of liquid propellants to heat loss from the external environment
Thermodynamic phenomena during active-pressurization in a liquid nitrogen tank	Ludwig and Dreyer (2014)	Thermodynamic phenomena, active pressurization
Influence of wall rib on thermal physical process in a liquid hydrogen tank	Fu et al. (2014)	Influence of wall ribs, thermal and physical processes
Fluid thermal stratification in cryogenic fuel storage tanks	Kassai and Simonson (2016); Kassai (2017); Kassai (2018)	Fluid thermal stratification, pressure rise in the tank, evaporation at the liquid-vapor interface
Tank pressurization and temperature stratification during ground pre-pressurization and ascent	Liu et al. (2016a, 2017a)	Tank pressurization, thermal stratification
Sensitivity to external heat invasions	Liu, Li, Xie and Zhou (2016b); Liu, Li and Zhou (2018d)	External heat invasion, aerodynamic heating, space radiation, tube conduction, convective heat exchange

Study Name	Author	Factors Studied
Pressurization performance in liquid oxygen and liquid methane tanks with cold helium	Morehead et al. (2016)	Pressurization performance, liquid oxygen and liquid methane tanks, cold helium injection
Liquid-vapor mixture model for natural convection	Choi et al. (2017)	Liquid-vapor mixture model, natural convection, thermal stratification
Tank pressure control with thermodynamic vent	Wang et al. (2017); Liu et al. (2017b, 2018b,c)	Tank pressure control, refrigeration capacity of thermodynamic venting
Two-phase CFD model for tank pressurization	Kassem et al. (2018)	Two-phase CFD model, tank pressurization
Effect of slosh baffle on pressurization performance in a liquid hydrogen tank	Liu and Li (2018a)	Effect of slosh baffle on pressurization performance

List of Figures

1.2	Comparison of VEGA launcher and its stages	4
1.3	Comparison of VEGA launcher and its stages	4
1.4	Three VEGA at comparison, credit for the figure [6]	5
1.5	Space rider render from [7]	6
1.6	Aster-30 Sea Viper from [8]	6
1.7	a) Tank Cycle 125s	7
1.8	b) Tank Cycle 493s	7
1.9	Figure 8 pag 20[10]	7
1.10	T-S diagram for methane (T= 90-300 K) -From page 201 Figure 5.23[16] . . .	10
1.11	TQ-12 Engine[19]	11
1.12	Raptor Engine V2[20]	11
1.13	Aeon-R Engine [21]	11
1.14	BE-4 Engine [22]	11
1.15	Prometheus Engine[23]	11
1.16	M60-Engine [18]	11
1.17	Schematic of a tank with aerothermal phenomena[29]	18
1.18	Figure 7 -(a) and 10 (b) from [31]	19
1.19	Scheme of the tank with the injection(left) and injection (right) -from figure 9-5 [29]	21
1.20	Figure 9-21 and 9-23 from Cap.9 [29]	22
1.21	Scheme of the main flow in the entire tank Green: Environmental fluxes Red: Internal tank fluxes Orange: Inlet and outlet flow rates Gray: Mass transfers Aqua green: Work done by the pressurizer Lilac: Outgoing vapor flow rates	24

1.22	Comparison of energy distribution between radial diffuser case and anti-cone diffuser case -Figure 16 [30]	30
1.23	Some tank configurations reported in figure 6-2 [14]	31
1.24	Scheme of ribs in cryogenic tanks	31
1.25	Heat flow to tank walls (a) and ratio between heat flows and the total energy lost-[10] figure 15	33
2.1	Generic Motor scheme from [14]	36
2.2	Four subsequent events during the ATLAS Agena D collapse, May 11, 1963[38]	36
2.3	Illustration of helium pressurization systems: (a)HE pressure tank with no heat exchanger; (b)HE pressure with a heat exchanger in CC; (c) Cascade system; (d)HE exchanger inside the tank. (Adapted from [39].)	38
2.4	A-2 Evaporated propellant system figure 5-8 of [39]	39
2.5	Common pressurization system from [40]	40
2.6	Diffuser schematic	42
2.7	Nozzle schematic	42
2.8	Axial (a) and Circunferential diffuser(c)[39]	43
2.9	Lateral tank diffuser(b)[29]	43
2.10	Submerged diffuser (d)[42]	43
2.12	Instrumentation inside the tank[10] figure 4 page 8	54
2.13	Temperature profile from [10] figure 12 pag 24	57
2.14	Comparison of axial temperature and gas required for different pipe dimensions	58
2.15	Schematic tank numerical investigation (Figure 1 in [11]) (left) and grid used for CFD simulation (figure 2 in [11])	59
2.16	Stratos II+ comparison and mission patch	61
2.17	Scheme of feeding sounding rocket	62
2.18	Axial, radial and vortex scheme	63
3.1	Methodology scheme	66
3.2	Schematic representation of the ullage nodes	71
3.3	Pressurant percentage trend in the ullage zone	72

3.4	Image extracted from figure 9.5 Calculation schemes of pressurizing gas flows in the ullage pag 350 of [29]	74
3.5	Zoom of Initial Emptying for Axial and Radial Injectors: Green circle for the Evaporation, Red for the wall	76
3.6	Forced Correlations	79
3.7	Mixed correlations	79
3.8	Natural Correlations	79
3.9	Comparison of different tank emptying scenarios.	81
3.10	Example of efficiency plot vs diffuser dimension for sounding rocket tank filled at 50% of liquid methane	82
3.11	Extract from an iteration of the code with 50% ullage volume and methane propellant from the case study presented in next chapter	83
3.12	Sketch with quote for the Axial and Radial Diffusers	83
3.13	Figure 5: Blocks diagram of system operation code	84
3.14	Evolution of the ullage volume for the analysis	86
3.15	Example of design modeler of axial configuration, with the different name selection	87
3.16	Example of surface mesh creation	88
3.17	Different Possible Mesh Geometries	89
3.18	Generating the volume mesh	90
3.19	Surfaces for configuration	92
3.20	Surfaces for RAD configuration	92
3.21	Comparison of lines on the ullage in different configurations.	93
3.22	Example of the radial temperature in the ullage in different times	94
3.23	Absolute pressure vs time for the axial and radial configurations	95
3.24	Example of velocity distributions through a series of surfaces	96
3.25	Total heat flows for the two configurations	96
4.1	Caption	102
4.2	Dimensionless Numbers	107
4.3	Heat Fluxes vs Diffuser dimensions	108

4.4	Penetration of diffuser	109
4.5	Efficiency for different dimensions	109
4.6	Ullage profile	111
4.7	Revolution technique	111
4.8	Axial ullage using Solidworks©	111
4.9	Ullage profile	111
4.10	ullage construction by revolution	111
4.11	Radial ullage using Solidworks©	111
4.12	design- Geometry completed	112
4.13	Residuals for TT8 analysis	116
4.14	Zoom of the residuals after the analysis	116
4.15	Absolute pressure vs time obtained during CFD simulations	117
4.16	Mass flow inlet and outlet through the control surfaces for both configurations	120
4.17	Static ullage temperature vs. time	121
4.18	Arrangement of temperatures on radial lines at ullage at different time points	122
4.19	Arrangement of temperatures on axial lines at ullage at different time points .	122
4.20	Heat fluxes per unit area on propellant for both configurations as a function of time	123
4.21	Heat flux on the tank walls as a function of time	124
4.22	Sum of heat flux modules in both configurations as a function of time	124
4.23	Magnitude velocity distribution around AXIAL diffuser at the instant of reaching P = 3 bar	126
4.24	Magnitude velocity distribution around RADIAL diffuser at the instant of reaching P = 3 bar	128
4.25	Axial velocity distribution around AXIAL diffuser at the instant of reaching P = 3 bar.	129
4.26	Radial velocity distribution around diffuser at the instant of reaching P = 3 bar.	130
5.1	Focus on the radial diffuser from [10]	134
5.2	CAD completed with perforated holes	136

5.3	SolidWork sections with the extruded holes highlighted	136
5.4	Residuals for the simulation.	137
5.5	Mass Flow inlet and outlet for both configurations vs time.	141
5.6	Temperature in ullage for both configurations vs time.	142
5.7	Heat flow on the propellant.	142
5.8	Heat wall flow for both configurations versus time.	143
5.9	Sum of the modulus contribution of the dissipative sources for both configurations, versus time.	143
5.10	Magnitude velocity for the GRID configuration at the three different surfaces and at the reach of the pressure level.	144
5.11	Radial component velocity for the GRID configuration at the three different surfaces and at the reach of the pressure level.	145

Nomenclature

$\bar{u}_{ac1C}, \bar{u}_{ac2C}$ Dimensionless constrained velocity for AX and RAD diffuser respectively

β Thermal expansion coefficient [1/K]

\dot{m} Mass flow

η Mass flow ratio

λ Heat conductivity [$W/m \cdot K$]

Nu Nusselt number

Pr Prandtl number

Re Reynolds number

Ri Richardson number

St Stanton number

μ Dynamic viscosity [Pa·s]

ν Cinematic viscosity

ϕ Efficiency of the diffuser

ρ Density

θ Ratio between pressurant and propellant temperature

Fr Froude number

H_{fr} Propellant deflection by the pressurant flow

$H_{g,0}$ Height of pressurant inlet in the tank

L^* Reference length for dimensionless numbers

l'_k Local length for in tank near wall

l_s, l_k Local length for in tank near propellant
 m Ullage mixing
 R_t Tank radius
 u, ω_g Velocity [m/s]
 u_{m1} Ratio between local pressurant velocity and entry pressurant velocity in AX configuration
 u_{m2} Ratio between local pressurant velocity and entry pressurant velocity in RAD configuration
 y_{vl}, y_{rg} Molar fraction for propellant and pressure respectively
 Y_{vl}, Y_{rg} Mass fraction for propellant and pressure respectively
 \bar{x} Local position along tank's axis
forced Forced convection
free Free convection
 h_{sc} Heat convection coefficient
 H Total entalpy [J]
 h Entalpy per mass unit [J/kg]
 P Power [W]
 Q Heat [J]
 W Work [J]
 $c1, c2, c3$ Constants for free convection correlation from [34]
Cyl Cylindrical
 $d1, d2, d3$ Constant for the forced convection correlation from [34]
entr entry
 j j-th node
press Pressurant gas
Propellant Evaporation segment propellant
wall Tank walls

Acronyms

AX Axial Diffuser Geometry.

GOX Oxygen Gas.

GRID Geometric configuration of the Diffuser with perforated surface.

HE Helium.

LCH4 Liquid methane.

LH2 Liquid Hydrogen.

LN2 Liquid Nitrogen.

LOX Liquid Oxygen.

RAD Radial Diffuser Geometry.

Bibliography

- [1] Avio S.p.A. “Avio - space propulsion systems and launchers.” Accessed: 2024-07-26. (2024), [Online]. Available: <https://www.avio.com/>.
- [2] Wikipedia contributors. “Vega (lanciatore).” Accessed: 2024-07-26. (2024), [Online]. Available: [https://it.wikipedia.org/wiki/Vega_\(lanciatore\)](https://it.wikipedia.org/wiki/Vega_(lanciatore)).
- [3] Spaceflight Now. “Vega vv03 vehicle.” Accessed: 2024-07-26. (2024), [Online]. Available: <https://spaceflightnow.com/vega/vv03/vehicle.html>.
- [4] Avio S.p.A. “Completato con successo volo inaugurale del vega-c.” Accessed: 2024-07-26. (2024), [Online]. Available: <https://www.avio.com/it/comunicati-stampa/completato-con-successo-volo-inaugurale-del-vega-c>.
- [5] Universe Magazine. “The first flight of a new rocket with a ukrainian engine is to take place on july 13.” Accessed: 2024-07-26. (2024), [Online]. Available: <https://universemagazine.com/en/the-first-flight-of-a-new-rocket-with-a-ukrainian-engine-is-to-take-place-on-july-13/>.
- [6] L. Daniele, “Architecture trade-off for the vega-e upper stage lox / ch 4 engine,” Engineering, Environmental Science, 2017.
- [7] European Space Agency (ESA). “Space rider overview.” Accessed: 2024-07-26. (2024), [Online]. Available: https://www.esa.int/Enabling_Support/Space_Transportation/Space_Rider_overview.
- [8] The Italian Shiplover. “Effettuato il primo lancio di un missile aster 30 da nave bergamini.” Accessed: 2024-07-26. (2024), [Online]. Available: <https://www.italianshiplover.it/>.
- [9] Y. M. Park, S. In, and S. Jeong, “The size optimization of the liquid helium pressurant tank for liquid propellant rocket,” Dept. of Mechanical Engineering, Korea Advanced Institute of Science and Technology,

- [10] R. L. D. Witt, R. J. Stochl, and W. R. Johnson, “Experimental evaluation of pressurant gas injectors during the pressurized discharge of liquid hydrogen,” National Aeronautics and Space Administration, Tech. Rep., 1966.
- [11] L. Wang, Y. Li, Z. Zhao, and J. Zheng, “Numerical investigation of pressurization performance in a cryogenic tank of new-style launch vehicle,” School of Energy and Power Engineering, Xi’an Jiaotong University, 2013.
- [12] Y. J. Zhan Liu Yanzhong Li, “Pressurization performance and temperature stratification in cryogenic final stage propellant tank,” School of Energy and Power Engineering, 2016.
- [13] L. de Quay and B. K. Hodge, “A history of collapse factor modeling and empirical data for cryogenic propellant tanks,” NASA Stennis Space Center and Mississippi State University, Tech. Rep.
- [14] G. P. Sutton and O. Biblarz, Rocket Propulsion Elements, Ninth. John Wiley Sons, 2016.
- [15] A. Simonini, M. Dreyer, A. Urbano, et al., “Cryogenic propellant management in space: Open challenges and perspectives,” npj Microgravity, 2024, Check for updates. doi: 10.1038/s41526-024-00377-5.
- [16] J. W. Leachman, R. T. Jacobsen, E. W. Lemmon, and S. G. Penoncello, Thermodynamic Properties of Cryogenic Fluids, Latest. Unknown Publisher, 2017.
- [17] Wikipedia contributors, Prometheus (motore a razzo), Accessed: 2023-09-08, Sep. 2023. [Online]. Available: [https://it.wikipedia.org/wiki/Prometheus_\(motore_a_razzo\)](https://it.wikipedia.org/wiki/Prometheus_(motore_a_razzo)).
- [18] SpaceNews. “Avio secures italian government funding for methane engine and small launch vehicle prototype.” (2023), [Online]. Available: <https://spacenews.com/avio-secures-italian-government-funding-for-methane-engine-and-small-launch-vehicle-prototype/>.
- [19] A. Jones. “Landspace closes in on orbital launch with liquid methane rocket.” Accessed: 2023-08-20, Posted in Commercial. (Feb. 2021), [Online]. Available: <https://spacenews.com/landspace-closes-in-on-orbital-launch-with-liquid-methane-rocket/>.
- [20] Wikipedia contributors, SpaceX raptor, Accessed: 2024-08-10, Aug. 2024. [Online]. Available: https://en.wikipedia.org/wiki/SpaceX_Raptor.
- [21] R. Space. “Terran r.” Accessed: 2023-08-20. (2023), [Online]. Available: <https://www.relativityspace.com/terran-r>.

- [22] Blue Origin, Be-4: America's next rocket engine, 2023. [Online]. Available: <https://www.blueorigin.com/engines/be-4/>.
- [23] Prometheus® engine towards the engines for europe's launchers from 2030, <https://www.ariane.group/wp-content/uploads/2023/02/Fiche-Moteur-Prometheus-EN-version2023-pourWEB.pdf>, Accessed: 2023-08-20, ArianeGroup, 2023.
- [24] A. Rudolf and D. Slayton, "Saturn v: Flight manual," George C. Marshall Space Flight Center, Tech. Rep., 1968.
- [25] Spaceflight101. "Falcon 9 – countdown timeline." (Accessed 2024), [Online]. Available: <https://spaceflight101.com/falcon-9-countdown-timeline/> (visited on 07/15/2024).
- [26] T. D. Bostock and R. G. Scurlock, "Low-loss storage and handling of cryogenic liquids," in Switzerland: Springer Nature Switzerland AG, 2019, ch. 2, pp. 25–50, © Springer Nature Switzerland AG 2019.
- [27] R. L. Morehead, M. J. Atwell, J. C. Melcher, and E. A. Hurlbert, "Cold helium pressurization for liquid oxygen / liquid methane propulsion systems: Fully-integrated initial hot-fire test results," AIAA Journal, 2016.
- [28] J. Joseph, G. Agrawal, D. K. Agarwal, and S. S. Kumar, "Analytical study on effect of ullage temperature and helium concentration on cryogenic tank pressure during sloshing," Journal of Cryogenics, 2021.
- [29] V. I. Naoumov, V. G. Krioukov, A. L. Abdullin, and A. V. Demin, Chemical Kinetics in Combustion and Reactive Flows: Modeling Tools and Applications. Cambridge University Press, 2019.
- [30] W. Lei, L. Yanzhong, J. Yonghua, and M. Yuan, "Experimental investigation on pressurization performance of cryogenic tank during high-temperature helium pressurization process," Institute of Refrigeration and Cryogenics, Xi'an Jiaotong University, 2014.
- [31] R. L. Morehead, M. J. Atwell, E. A. Hurlbert, and J. Melcher, "Cold helium gas pressurization for spacecraft cryogenic propulsion systems," NASA Johnson Space Center, Houston, TX, 77058 United States, 2016.
- [32] R. L. Morehead, M. J. Atwell, E. A. Hurlbert, and J. Melcher, "Cold helium gas pressurization for spacecraft cryogenic propulsion systems," NASA Johnson Space Center, Houston, TX, 77058, United States, 2016.

- [33] C. J. Kaplan, "Selection of a pressurization system for a storable liquid propellant rocket engine," Kocketydyne Div., North American Aviation, Inc., Canoga Park, Calif.
- [34] L. D. Quay, "Validated prediction of pressurant gas requirements in cryogenic run tanks at subcritical and supercritical pressures," Dissertation - Open Access, Mississippi State University, 2009.
- [35] W. M. Rohsenow, J. R. Hartnett, and Y. I. Cho, Eds., Handbook of Heat Transfer, Third. McGraw-Hill, 2000, Department of Mechanical Engineering, Massachusetts Institute of Technology; Energy Resources Center, University of Illinois at Chicago; Department of Mechanical Engineering and Mechanics, Drexel University.
- [36] J. Fu, B. Sunden, and X. Chen, "Influence of wall ribs on the thermal stratification and self-pressurization in a cryogenic liquid tank," Applied Thermal Engineering, vol. 73, pp. 1180–1192, 2014. doi: 10.1016/j.applthermaleng.2014.05.086.
- [37] K.-J. Cho, Y.-s. Jung, S.-H. Oh, et al., "The way of determining the optimal parameters of the propellant tank pressurization gas in the feeding system for liquid rocket engine," Journal of the Korean Society of Propulsion Engineers, 2005.
- [38] D. A. Day, Not a bang, but a whimper, <https://www.thespacereview.com/article/1326/1>, Accessed: 2024-08-12, 2009.
- [39] D. K. Huzel and D. H. Huang, Modern Engineering for Design of Liquid-Propellant Rocket Engines. American Institute of Aeronautics and Astronautics, 1992.
- [40] R. Mabboux, "Optimization of the pressurization system of the themis reusable rocket first stage demonstrator," TRITA-ITM-EX-2021:542, Approved 2021-09-01, Master of Science Thesis, Department of Energy Technology, KTH Royal Institute of Technology, Stockholm, Sweden, Sep. 2020.
- [41] I. Dincer and Y. Bicer, "Integrated energy systems for multigeneration," in Elsevier Inc., 2020, ch. Chapter 2: Fundamentals of energy systems, pp. 61–62.
- [42] N. T. V. Dresar, Liquid Oxygen Thermodynamic Vent System Testing with Helium Pressurization. National Aeronautics and Space Administration Glenn Research, 2020.
- [43] R. Hermsen, "Cryogenic propellant tank pressurization: Practical investigation on the tank collapse factor for small, high-pressure, cryogenic rocket propellant tanks," M.S. thesis, TU Delft, 2017.
- [44] Pink, "Centaur space vehicle pressurized propellant feed system tests," Lewis Research Center Cleveland, Ohio 44135 - National Aeronautics and Space Administration, Tech. Rep., 1972.

- [45] H. V. Nguyen, "Ground prepressurization by helium bubbling for cryogenic upper stages," 37th AIAA/ASME/SAE/ASEE Joint Propulsion Conference & Exhibit, 2001, AIAA 2001 -3833.
- [46] Pressurization Systems for liquid Rockets. NASA, OCTOBER 1975.
- [47] A. Manimaran and S. S. Hiremath, "Dynamic modeling, simulation and experimental investigation on cryogenic tank pressurization system," International Journal of Modelling and Simulation, 2019, issn: 0228-6203. doi: 10.1080/02286203.2019.1606009. [Online]. Available: <https://www.tandfonline.com/loi/tjms20>.
- [48] J. Bailey, Skartvedt, and Vandekoppel, "Predicting fluid thermal stratification in closed tanks," 1963.
- [49] R. L. DeWitt and T. O. McIntire, "Pressurant requirements for discharge of liquid methane from a 1.52-meter-(5-ft-) diameter spherical tank being static," Lewis Research Center, National Aeronautics and Space Administration, Cleveland, Ohio, Tech. Rep. NASA TN D-7638, 1974, Sponsoring Agency: National Aeronautics and Space Administration, Washington, D.C. 20546.
- [50] C. Lin and M. Hasan, "Self-pressurization of a spherical liquid hydrogen storage tank in a microgravity environment," Unknown Journal, 1992, Unknown note.
- [51] S. Barsi and M. Kassemi, "Investigation of tank pressurization and pressure control—part i: Experimental study," Journal of Thermophysics and Heat Transfer, 2013.
- [52] S. Barsi and M. Kassemi, "Investigation of tank pressurization and pressure control—part ii: Numerical modeling," Journal of Thermophysics and Heat Transfer, 2013.
- [53] Z. Liu, Y. Li, L. Wang, and Y. Jin, "Evaporation calculation and pressurization process research of on-orbit cryogenic liquid hydrogen storage tank," Cryogenics, 2015.
- [54] Z. Liu, Y. Li, and L. Wang, "Research on cryogenic propellant thermal stratification," Journal of Thermophysics and Heat Transfer, 2015.
- [55] J. Fu, B. Sunden, and X. Chen, "Influence of wall ribs on the thermal stratification and self-pressurization in a cryogenic liquid tank," International Journal of Heat and Mass Transfer, 2014.
- [56] J. Fu, B. Sunden, X. Chen, and Y. Huang, "Influence of phase change on self-pressurization in cryogenic tanks under microgravity," International Journal of Heat and Mass Transfer, 2015.

- [57] S. Roh, G. Son, G. Song, and J. Bae, "Numerical study of transient natural convection in a pressurized lng storage tank," Journal of Thermophysics and Heat Transfer, 2013.
- [58] L. Wang, Y. Li, C. Li, and Z. Zhao, "Cfd investigation of thermal and pressurization performance in lh2 tank during discharge," Journal of Thermophysics and Heat Transfer, 2013.
- [59] C. Ludwig and M. Dreyer, "Investigations on thermodynamic phenomena of the active-pressurization process of a cryogenic propellant tank," Cryogenics, 2014.
- [60] P. Chai and A. Wilhite, "Cryogenic thermal system analysis for orbital propellant depot," Journal of Spacecraft and Rockets, 2014.
- [61] J. Aydelott, "Normal gravity self-pressurization of 9-in. (23 cm) diameter spherical liquid hydrogen tankage," 1967.
- [62] L. Wang, Y. Li, Z. Zhao, and Z. Liu, "Transient thermal and pressurization performance of lo2 tank during helium pressurization combined with outside aerodynamic heating," Journal of Thermophysics and Heat Transfer, 2013.
- [63] G. Gary, L. Alfredo, C. Frank, H. Leon, H. Ali, and B. James, "Cfd modeling of helium pressurant effects on cryogenic tank pressure rise rates in normal gravity," Cryogenics, 2007.
- [64] L. Alfredo, G. Gary, C. Frank, H. Leon, and H. Ali, "Cryogenic pressure control modeling for ellipsoidal space tanks in reduced gravity," Journal of Thermophysics and Heat Transfer,
- [65] L. Wang, Y. Li, Z. Zhao, and J. Zheng, "Numerical investigation of pressurization performance in cryogenic tank of new-style launch vehicle," School of Energy and Power Engineering, Xi'an Jiaotong University, Xi'an 710049, China,
- [66] R. Hermsen and B. Zandbergen, "Pressurization system for a cryogenic propellant tank in a pressure-fed high-altitude rocket," 7th European Conference for Aeronautics and Aerospace Sciences (EUCASS), 2017.
- [67] M. E. Nein and J. F. Thompson, "Experimental and analytical studies of cryogenic propellant tank pressurant requirements," George C. Marshall Space Flight Center, Huntsville, Alabama, Tech. Rep., 1966, National Aeronautics and Space Administration Washington, D.C.
- [68] A. K. Majumdar, A. C. LeClair, and A. Hedayat, "Analytic modeling of pressurization and cryogenic propellant conditions for liquid rocket based vehicle designs," 2022.

- [69] A. Bandyopadhyay, A. K. Majumdar, A. C. Leclair, and J. G. Valenzuela, “Multi-node modeling of cryogenic tank pressurization system using generalized fluid system simulation program,” Journal of Propulsion and Power, 2022, Department of Electrical Engineering and Computer Science, Alabama A & M University, Normal, AL 35762, and Propulsion System Department, NASA Marshall Space Center, Huntsville, AL 35812.